TESIS DOCTORAL

NEW INSIGHTS INTO THE CHEMISTRY OF LASER-INDUCED PLASMAS. CUTTING EDGE STRATEGIES FOR SENSING AND CHARACTERIZATION OF MOLECULAR SOLIDS

Jorge Serrano Rojas

Directores: José Javier Laserna Vázquez and Javier Moros Portolés

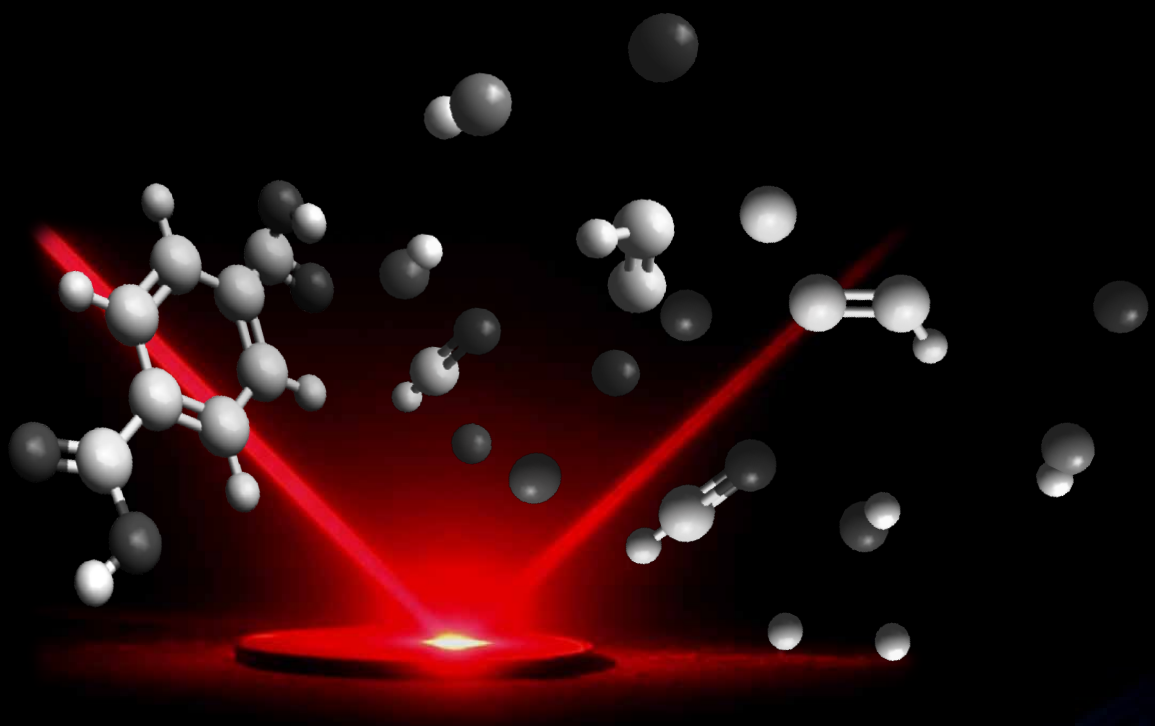

UNIVERSIDAD DE MÁLAGA

Facultad de Ciencias

Programa de doctorado: Láseres y Aplicaciones en Química

Málaga, 2016

AUTOR: Jorge Serrano Rojas

http://orcid.org/0000-0002-3778-7885

EDITA: Publicaciones y Divulgación Científica. Universidad de Málaga

Doctoral Thesis

UNIVERSIDAD
DE MÁLAGA

NEW INSIGHTS INTO THE CHEMISTRY OF LASER-INDUCED PLASMAS.

CUTTING EDGE STRATEGIES FOR SENSING

AND CHARACTERIZATION OF MOLECULAR SOLIDS

by

JORGE SERRANO ROJAS

THESIS SUBMITTED IN PARTIAL FULFILMENT OF THE REQUIREMENTS
TO APPLY FOR THE DEGREE OF DOCTOR

Departamento de Química Analítica
Facultad de Ciencias
Universidad de Málaga

Málaga, 2016

NEW INSIGHTS INTO THE CHEMISTRY OF LASER-INDUCED PLASMAS. CUTTING EDGE STRATEGIES FOR SENSING AND CHARACTERIZATION OF MOLECULAR SOLIDS

por **JORGE SERRANO ROJAS**

José Javier Laserna Vázquez
Catedrático de Universidad
Departamento de Química Analítica
Universidad de Málaga

Javier Moros Portolés
Investigador postdoctoral
Departamento de Química Analítica
Universidad de Málaga

Memoria de Tesis presentada para optar al grado de Doctor

Jorge Serrano Rojas

Málaga, Junio de 2016

JOSÉ JAVIER LASERNA VÁZQUEZ, Catedrático de Química Analítica de la Universidad de Málaga, y **JAVIER MOROS PORTOLÉS**, Investigador Postdoctoral del Departamento de Química Analítica de la Universidad de Málaga

CERTIFICAN

Que **JORGE SERRANO ROJAS** ha realizado bajo su dirección la presente Tesis Doctoral titulada "**NEW INSIGHTS INTO THE CHEMISTRY OF LASER-INDUCED PLASMAS. CUTTING EDGE STRATEGIES FOR SENSING AND CHARACTERIZATION OF MOLECULAR SOLIDS**" en el Laboratorio Láser del Departamento de Química Analítica de la Universidad de Málaga, y que el conjunto de publicaciones aportadas para avalar el trabajo científico no han sido utilizadas en Tesis anteriores, reuniendo a nuestro juicio los requisitos necesarios y autorizando, por ello, su presentación para optar al grado de Doctor.

Y para que así conste a los efectos oportunos firman la presente, en Málaga, a 14 de Junio de 2016.

Prof. José Javier Laserna Vázquez

Dr. Javier Moros Portolés

TESIS DOCTORAL POR COMPENDIO DE PUBLICACIONES

En cumplimento con los requisitos especificados en el Reglamento de Doctorado de la Universidad de Málaga, la presente Tesis Doctoral ha sido autorizada por los Directores de Tesis y el Órgano Responsable del Programa de Doctorado para ser presentada en el formato de "compendio de publicaciones".

Las referencias de los artículos en los que el doctorando figura como primer o segundo autor y que avalan la presente Tesis Doctoral se detallan a continuación de acuerdo a su orden cronológico de publicación:

- J. Moros, **J. Serrano**, C. Sánchez, J. Macías, J. J. Laserna, *New chemometrics in laser-induced breakdown spectroscopy for recognizing explosive residues*, J. Anal. At. Spectrom. 27 (2012) 2111–2122.

- J. Moros, **J. Serrano**, F.J. Gallego, J. Macías, J. J. Laserna, *Recognition of explosives fingerprints on objects for courier services using machine learning methods and laser-induced breakdown spectroscopy*, Talanta 110 (2013) 108–117.

- **J. Serrano**, J. Moros, C. Sánchez, J. Macías, J. J. Laserna, *Advanced recognition of explosives in traces on polymer surfaces using LIBS and supervised learning classifiers*, Anal. Chim. Acta 806 (2014) 107–116.

- **J. Serrano**, L.M. Cabalín, J. Moros, J.J. Laserna, *Potential of laser-induced breakdown spectroscopy for discrimination of nano-sized carbon materials. Insights on the optical characterization of graphene*, Spectrochim. Acta Part B 97 (2014) 105–112.

- **J. Serrano**, J. Moros, J.J. Laserna, *Sensing signatures mediated by chemical structure of molecular solids in laser-induced plasmas*, Anal. Chem. 87 (2015) 2794–2801.

- **J. Serrano**, J. Moros, J.J. Laserna, *Exploring the formation routes of diatomic hydrogenated radicals using femtosecond laser-induced breakdown spectroscopy of deuterated molecular solids*, J. Anal. At. Spectrom. 30 (2015) 2343–2352.

- **J. Serrano**, J. Moros, J.J. Laserna, *Molecular signatures in femtosecond laser-induced organic plasmas: comparison with nanosecond laser ablation*, Phys. Chem. Chem. Phys. 18 (2016) 2398–2408.

Málaga, 14 de Junio 2016

Prof. José Javier Laserna Vázquez

Dr. Javier Moros Portolés

AGRADECIMIENTOS

Quiero dar las gracias a todas las personas con las que he podido compartir esta etapa como estudiante de doctorado y que han contribuido de algún modo a que la realización de esta Tesis Doctoral haya sido posible.

En primer lugar, quiero agradecer a Javier Laserna el haber depositado en mí su confianza para desarrollar esta Tesis Doctoral dentro del Laboratorio Láser de la Universidad de Málaga. Él ha sabido como transmitirme sus conocimientos para fomentar mi aprendizaje y mi formación como científico. Además, siempre he podido contar con su ayuda para la resolución de los distintos problemas surgidos de la investigación.

Otra gran parte de mis agradecimientos van dirigidos a mi codirector, Javier Moros, por su generosa dedicación en la realización de esta Tesis Doctoral y su gran implicación en todos los estudios experimentales que la conforman. También por brindarme su amistad, haciendo que el trabajo en común fuera mucho más sencillo. Sin duda, ha sido una gran suerte contar con él para que condujera este trabajo.

A todos mis compañeros de laboratorio, gracias por hacerme sentir un miembro más del grupo desde el primer momento y por el aprecio que me habéis demostrado durante todos estos años. En especial, le estoy muy agradecido a Inma por su amistad, por permitirme compartir con ella mis preocupaciones y por el gran apoyo demostrado. A Tomás y Ángel, les agradezco sus consejos y los buenos momentos que hemos pasado juntos, dentro y fuera del laboratorio. A Fran y Salva, su gran compañerismo y su disponibilidad para echarme una mano en cualquier ocasión. A Marina, su afecto y la ayuda prestada en mis últimos experimentos. A Gabriel, Irene, Samara, Pablo y Diana, también les agradezco los buenos ratos compartidos y su apoyo. A José Miguel, Luisa, Patricia y Javier, les estoy muy agradecido por haberme ayudado en numerosas ocasiones y por surtirme de buenos consejos que han contribuido con seguridad a

la mejora de este trabajo. Finalmente, darle las gracias a Carmen y Mari Carmen por todas las veces que me han prestado su ayuda para solucionar algún problema.

También quiero agradecer a Jorge, Carlos y Javi, del Departamento de Análisis Matemático de la Universidad de Málaga, su notable contribución en varios de los trabajos de investigación incluidos en esta tesis.

Al profesor Jin Yu, de la Universidad Claude Bernard Lyon 1, le agradezco el haberme permitido realizar mi estancia predoctoral en su grupo de investigación y su dedicación en este periodo. Además, le doy las gracias a Tian Ye por su ayuda en la realización de mis experimentos y por su amistad. A Michelle y Adrián, gracias por vuestra amistad y por hacer que guarde un magnífico recuerdo de mi estancia en Lyon.

Por otra parte, agradecer la beca de investigación recibida del contrato SEDUCE, entre Indra Sistemas, S. A. y la Universidad de Málaga, y el soporte económico aportado por varios proyectos de investigación: Proyecto de Excelencia P07-FQM-03308 de la Secretaría General de Universidades, Investigación y Tecnología, Consejería de Innovación, Ciencia y Empresa de la Junta de Andalucía, y Proyecto CTQ11-24433 del Ministerio de Economía y Competitividad, Secretaría de Estado de Investigación, y Desarrollo e Innovación de España.

Naturalmente, quiero hacer patente mi gratitud hacia mis padres y hermanos por el esfuerzo realizado desde que comenzara mis estudios universitarios y su apoyo incondicional durante estos años de doctorado. En especial, a mi madre, por ser el pilar fundamental de mi vida. Y por supuesto, a mis sobrinos, por hacerme feliz siempre que comparto un rato con ellos.

A Lydia le agradezco de todo corazón el haberme acompañado durante todo este camino, el saber comprenderme, sus palabras de ánimo en los momentos más difíciles, y simplemente, el ser la primera persona en estar ahí de forma incondicional siempre que la he necesitado.

CONTENTS

RESUMEN

Dado que la presente memoria de Tesis Doctoral está redactada en inglés, en cumplimiento del Reglamento de Doctorado de la Universidad de Málaga, se incluye un resumen de la misma en español.

Desde su origen, la espectroscopia de plasmas inducidos por láser, más conocida por su acrónimo inglés LIBS (*Laser-induced breakdown spectroscopy*) ha sido empleada principalmente para la detección y cuantificación multielemental en el análisis de materiales inorgánicos. Sin embargo, su aplicación al análisis y caracterización de sólidos moleculares ha ido creciendo en popularidad debido a las atractivas características que dicha técnica ofrece. Entre ellas, se pueden destacar su potencial para realizar análisis *in-situ* de todo tipo de muestras (sólidos, líquidos y gases) sin necesidad de llevar a cabo una preparación previa de las mismas, su capacidad de detección simultánea y multielemental, su alta velocidad de análisis, y la posibilidad de su implementación en equipos portátiles y de detección a distancias remotas.

En lo concerniente al análisis de compuestos orgánicos mediante LIBS, las investigaciones desarrolladas han sido abordadas desde dos vertientes. De un lado, se han realizado exploraciones fundamentales destinadas a la comprensión de los fenómenos de ablación en este tipo de

compuestos, de los mecanismos de ruptura de dichas moléculas y de la química de los plasmas inducidos por láser, principalmente, en la formación de las distintas especies responsables de las respuestas de emisión óptica. De forma paralela, y desde un punto de vista analítico, la técnica LIBS ha sido empleada para la caracterización e identificación de compuestos orgánicos en distintos campos de aplicación. En este contexto, el primer bloque de la presente Tesis Doctoral se centra en las investigaciones desarrolladas para la obtención de un mayor conocimiento de los procesos físico-químicos que tienen lugar desde la generación del plasma hasta su extinción. También se evalúa la influencia de las distintas propiedades del pulso láser (energía, longitud de onda y duración) sobre estos procesos, y en consecuencia, en los patrones de emisión resultantes. Además, se han llevado a cabo exploraciones para intentar descifrar algún tipo de relación entre los patrones de emisión óptica de sólidos moleculares y su estructura química. El segundo bloque de la presente Tesis Doctoral se ha encaminado más a la implementación de la técnica LIBS en distintas aplicaciones que demandan la evaluación de sólidos moleculares. Así, se valoró la capacidad de LIBS como herramienta para la caracterización de materiales nanométricos de carbono en un estudio dirigido a la caracterización de grafeno, así como su potencial en el reconocimiento de compuestos explosivos.

A continuación se resumen los resultados más relevantes de la investigación desarrollada, diferenciándose los dos bloques de contenidos anteriormente mencionados.

1. Química de los plasmas inducidos por láser en sólidos moleculares

Durante el proceso de ablación láser, las moléculas pueden experimentar una atomización total de los enlaces químicos presentes o bien sufrir una fragmentación parcial. Aunque generalmente se produce una coexistencia de ambos procesos, la estructura molecular de los compuestos orgánicos y las condiciones operacionales empleadas en la ablación láser van a determinar la predominancia de cada uno de ellos. De esto se deduce que los plasmas de compuestos orgánicos pueden estar poblados, además de por electrones, por cantidades distintas y variables de átomos, iones y diferentes fragmentos moleculares. Además, las numerosas reacciones químicas que pueden acontecer en el seno del plasma entre las especies originales liberadas –y también con especies procedentes de la atmósfera que rodea al plasma– conducen a la generación de nuevas especies moleculares. Por lo tanto, cualquier relación entre las emisiones ópticas del plasma de un sólido molecular y su estructura química puede verse notablemente desvirtuada, poniendo así de manifiesto la complejidad existente para la exacta interpretación de su espectroscopia.

Típicamente, los espectros LIBS de sólidos moleculares se caracterizan por su alta similitud ya que el número de señales espectrales manifestadas está limitado a líneas atómicas e iónicas de emisión (típicamente, C, H, O y N) y a algunas bandas moleculares de emisión asociadas a pequeños radicales excitados (CN, C_2, CH, OH y NH). Además, como se adelantaba, cuando los plasmas son generados en atmósfera de aire se produce una participación activa de sus constituyentes mayoritarios (N_2, O_2, y vapor de H_2O) en la química de la pluma. De este modo, el proceso conocido como *ionización secundaria del aire* puede conducir a emisiones de H, O y N, y distorsionar la relación de estas emisiones con respecto a la composición química del compuesto analizado. A su vez estas especies atmosféricas pueden reaccionar con especies nativas y dar lugar a la generación de pequeñas moléculas.

Teniendo en cuenta estas dificultades a la hora de interpretar la espectroscopia de plasmas inducidos por láser de compuestos orgánicos, la presente memoria de Tesis Doctoral pretende proporcionar un mayor conocimiento y compresión de la química estos plasmas, así como justificar sus patrones de emisión LIBS y tratar de esclarecer cualquier vínculo con sus estructuras moleculares.

– Efectos de la estructura química de sólidos moleculares en los patrones de emisión LIBS

Distintos autores han demostrado la capacidad de LIBS para la caracterización de sólidos moleculares mediante el uso de las intensidades de emisión asociadas a distintas especies atómicas o radicales moleculares. Sin embargo, existe una carencia de estudios sobre la influencia que la estructura molecular de los compuestos orgánicos puede tener en sus respuestas ópticas de emisión. Una de las publicaciones incluidas en la presente memoria de Tesis Doctoral se centra en evaluar que efectos originan las distintas estructuras moleculares de los materiales orgánicos en las respuestas de emisión a través del análisis de un amplio conjunto de compuestos estratégicamente seleccionados por sus particularidades estructurales. Así, las variaciones observadas en los patrones ópticos de emisión debidas a la variación en la naturaleza, el número, y la posición de grupos funcionales han sido investigadas. Entre los compuestos analizados en este estudio se incluyen tres hidrocarburos policíclicos aromáticos, dos polímeros, una serie homóloga de bencenos para-disustituidos y dos conjuntos de isómeros de dinitrobenceno (DNB) y dinitrotolueno (DNT). Estos materiales fueron analizados en forma de pastillas, a excepción de los polímeros que se analizaron en su formato original (láminas planas). Los experimentos se desarrollaron en atmósfera de aire y se utilizó como fuente de excitación para la formación de plasmas un láser de Nd:YAG trabajando en su segundo harmónico (longitud de onda de 532 nm). Para evaluar el efecto de la longitud de onda de irradiación también se utilizaron el modo fundamental (λ = 1064 nm) y el cuarto harmónico (λ = 266 nm) de dicho láser. Para el desarrollo de los análisis se ajustaron el diámetro del

haz láser y su energía sobre la muestra para emplear una irradiancia constante de 3,3 $GW \cdot cm^{-2}$. Los parámetros temporales de adquisición de las señales ópticas se establecieron en un tiempo de retraso tras la incidencia del pulso láser de 1,28 μs, y un tiempo de integración de 1,1 ms, permitiendo así integrar la mayor parte del tiempo de vida del plasma. A continuación se detallan los resultados más relevantes de este estudio.

Influencia de la estructura aromática de un compuesto orgánico. El análisis LIBS de tres compuestos aromáticos policíclicos –naftaleno ($C_{10}H_8$), antraceno ($C_{14}H_{10}$) y pireno ($C_{16}H_{10}$)– permitió evaluar la influencia de la aromaticidad sobre los patrones de ablación y las emisiones ópticas resultantes. Bajo condiciones operacionales bien definidas, los espectros ópticos de emisión manifestaron señales de C, H, N, O, CN y C_2. Las emisiones de N y O, elementos no presentes en las muestras, indicaron la ocurrencia del proceso de ionización secundaria del aire. Mediante este proceso las moléculas de N_2 y O_2 del aire son disociadas y posteriormente excitadas debido a los mecanismos de interacción láser-plasma y plasma-aire. A su vez, las emisiones CN ponen de manifiesto la participación del nitrógeno ambiental (a nivel atómico o molecular) en la química del plasma. Tal y como se detalla a continuación, son varias las reacciones que pueden conducir a la generación de estos radicales diatómicos.

A partir de carbono atómico: $C + N \rightarrow CN$ ó $C + N_2 \rightarrow CN + N$

A partir de dímeros de carbono: $C_2 + N \rightarrow CN + C$ ó $C_2 + N_2 \rightarrow 2CN$

Por otra parte, las emisiones de C_2 tienen su origen en los dímeros de carbono liberados directamente de la molécula o bien en procesos de recombinación de átomos de C. Si bien la ocurrencia de ambas rutas va ligada a las condiciones operacionales –principalmente, a la intensidad de la excitación–, la presencia de enlaces carbono-carbono en los compuestos orgánicos se relaciona con mayores emisiones de C_2. Teniendo esto en cuenta, la relación de intensidades de

emisión CN a C_2 (en adelante expresada como CN/C_2) se estableció como un evaluador estadístico de la contribución de los procesos de atomización y fragmentación parcial de las moléculas ablacionadas. Así, valores elevados de CN/C_2 indican una mayor atomización del compuesto, mientras que valores bajos de este cociente revelan una mayor fragmentación de las moléculas. Además, se observó una conexión entre este estadístico y la estabilidad de la estructura cíclica de los compuestos conferida por la disposición de los electrones π con los orbitales p de los anillos. Se consideraron tres índices de medida de la aromaticidad: la escala efectiva de deslocalización electrónica (*ESED*), el índice total del modelo del oscilador armónico de aromaticidad (*HOMA*) y la energía de resonancia de Dewar (*DRE*). Los resultados revelaron un incremento de CN/C_2 de acuerdo con el carácter aromático y la energía de resonancia de las moléculas según la serie $C_{10}H_8$ > $C_{14}H_{10}$ > $C_{16}H_{10}$. Esta circunstancia sugiere que un incremento en la deslocalización electrónica da lugar a una menor generación de fragmentos C_2. Al mismo tiempo, estas deducciones esbozan que los dímeros de carbono proceden, en mayor medida, de la fragmentación parcial de las moléculas, mientras que los radicales CN son generados por recombinación atómica.

Fuerzas de los enlaces de carbono: *efectos inductivos*. Para evaluar la influencia de los efectos inductivos en las emisiones ópticas se analizaron dos polímeros: polietileno y politetrafluoroetileno, con fórmulas químicas $(CH_4)_n$ y $(CF_4)_n$, respectivamente. Ambos polímeros presentan una similar longitud y topología de los enlaces C=C. Sin embargo, la elevada electronegatividad de los átomos de F genera una fuerte polarización que debilita los enlaces σ. De este modo, la energía del enlace C=C en el fluoroetileno es aproximadamente la mitad de la que posee el enlace C-F, estando favorecida la ruptura de dicho doble enlace. Contrariamente, en el etileno el enlace C=C es más fuerte que el C-H. En consecuencia, ambos monómeros presentan distintos patrones de ablación, produciéndose la ruptura del fluoroetileno por el enlace C=C y en el etileno por el enlace C-H. Estas diferencias se reflejan en la liberación de fragmentos de C_2 y, por

tanto, en el evaluador estadístico CN/C_2, siendo mucho menor para el polietileno (2,2) en comparación con el valor para el politetrafluoroetileno (12,2). En definitiva, el efecto inductivo causado por el heteroátomo causa una mayor atomización de las moléculas de politetrafluoroetileno.

Efectos inducidos por los grupos funcionales. La influencia de distintos grupos funcionales en las respuestas de emisión óptica se evaluó a partir de una serie de nitrobencenos para-sustituidos ($R{-}C_6H_4{-}NO_2$, R = $-CH_3$, $-NH_2$, $-OH$, $-NO_2$). Los efectos resonantes generados en las moléculas como consecuencia de la presencia de estos sustituyentes conllevan la transmisión de densidad electrónica a través del sistema π del anillo bencénico. Esta transferencia de carga depende del efecto polar del grupo sustituyente, es decir, de su tendencia a retirar electrones del anillo debido a su electronegatividad. Para este conjunto de compuestos el evaluador estadístico CN/C_2 se comparó con los valores de la electronegatividad relativa inherente de Pauling de cada uno de los grupos funcionales, siguiendo ambos una tendencia creciente de acuerdo con la secuencia $-CH_3 < -NH_2 < -OH < -NO_2$. De este modo, la menor electronegatividad del grupo metilo (grupo electrón-donante) en el p-nitrotolueno se ve manifestada por un menor valor para CN/C_2. En dicha molécula la transferencia de electrones estabiliza una configuración en la que se alternan enlaces simples y dobles; una circunstancia que favorece la liberación de fragmentos C_2 frente a la atomización. En los casos de la p-nitroanilina y el p-nitrofenol los pares de electrones desapareados de los grupos −NH y −OH se deslocalizan en el anillo, favoreciendo que se mantenga el sistema electrónico π y, en consecuencia, la atomización de estos compuestos se ve beneficiada frente a su fragmentación. Por último, en el dinitrobenceno el fuerte poder electrón-atrayente de los 2 grupos nitro en posición para- debilita su estructura, potenciándose mucho más el proceso de atomización y dando lugar a una mayor generación de radicales CN.

Por otra parte, se analizaron los regioisómeros orto-, meta- y para- del dinitrobenceno. Aquí se observó como las emisiones ópticas mostraban cierta sensibilidad a la variación en la posición de los grupos funcionales. Cabe destacar que el orto-dinitrobenceno manifestó un valor para CN/C_2 significativamente menor que el de los otros dos isómeros. En dicho compuesto, las mayores repulsiones estéricas entre los grupos funcionales rigen una pérdida de conjugación del sistema π, que repercute en una mayor fragmentación parcial de la molécula, en detrimento de su atomización.

Efectos de la longitud de onda de irradiación. Para evaluar el efecto de la longitud de onda de irradiación sobre las emisiones ópticas se analizaron los isómeros 2,3-, 2,4-, y 2,6-dinitrotolueno empleando radiaciones de excitación de 266 nm (ultravioleta), 532 nm (visible) y 1064 nm (infrarroja). Aunque con el empleo de radiación visible las diferencias en los valores de CN/C_2 para los distintos isómeros no fueron excesivas, se obtuvo un valor ligeramente superior en el caso del isómero 2,4-DNT. Esta circunstancia se atribuye a los menores efectos estéricos para esta disposición de los grupos funcionales y, por tanto, a la menor modificación en la conjugación del sistema π con respecto a los otros dos isómeros. Por el contrario, el empleo de radiación láser de 266 nm dejó al descubierto mayores diferencias entre las respuestas ópticas debido a que las longitudes máximas de absorción de luz de estos compuestos se sitúan en esa región del espectro electromagnético. Un valor de CN/C_2 notablemente mayor se manifestó para el isómero 2,4-DNT dado que su máximo de absorción óptica se sitúa más próximo a 266 nm y, en consecuencia, la molécula sufre una mayor atomización.

La distinta distribución electrónica en las moléculas también condiciona sus propiedades termodinámicas, como por ejemplo las correspondientes energías relativas de estabilización asociadas a sus estructuras optimizadas. Con el empleo de pulsos láser de 1064 nm se observó un decrecimiento para CN/C_2 de acuerdo con la serie 2,4-DNT < 2,6-DNT < 2,3-DNT que, a su vez, conviene con un incremento de la energía relativa de estabilización. Valores bajos de esta energía,

que indican mayor movilidad de los electrones π, van ligados a una mayor atomización de la molécula. En definitiva, aunque los procesos dominantes derivados de la interacción láser–muestra puedan depender de la longitud de onda de irradiación, estos resultados ponen de manifiesto que la distribución electrónica en la molécula juega un rol crucial en los patrones de emisión resultantes.

– Rutas de formación de radicales hidrogenados en plasmas de sólidos moleculares deuterados inducidos con pulsos láser de femtosegundos

Desde que la espectroscopia de plasmas inducidos por láser comenzara a aplicarse al análisis de compuestos orgánicos, una gran parte de las investigaciones se ha centrado en el estudio de las rutas de formación de los radicales CN y C_2. Sin embargo, las vías de generación de otras especies moleculares diatómicas también presentes en los plasmas de compuestos orgánicos apenas han sido exploradas. Uno de los capítulos incluidos en la presente memoria de Tesis Doctoral evalúa los posibles orígenes de los radicales hidrogenados NH, CH y OH en plasmas inducidos mediante excitación con pulsos láseres ultracortos. Con este fin, junto con la espectroscopia de emisión óptica, se emplea como herramienta para el trazado de las rutas de reacción el marcado isotópico selectivo de compuestos orgánicos con átomos de deuterio. Este estudio se beneficia de los mayores desplazamientos isotópicos en las longitudes de onda de emisión experimentados por las bandas moleculares en comparación con los desplazamientos de líneas de emisión de átomos o iones. Mientras que la diferencia de masa entre isótopos tiene un efecto bastante pequeño en las transiciones electrónicas de los átomos, los niveles de energía rotacionales y vibracionales en las moléculas se ven afectados en mayor medida. Esto significa que con el uso de espectrómetros con un poder de resolución medio pueden monitorizarse simultáneamente las emisiones de isotopólogos.

En este estudio se empleó un láser de Ti:Zafiro como fuente de excitación que proporciona pulsos de 60 *fs* centrados a una longitud de onda de 800 nm. Bajo las condiciones experimentales empleadas se pudieron observar los desplazamientos ópticos de las principales transiciones electrónicas de los radicales ND, CD y OD con respecto a sus isotopólogos hidrogenados. Aunque las emisiones de ND y CD habían sido previamente caracterizadas mediante espectroscopia de fotólisis de destellos o de descarga eléctrica, por primera vez las emisiones de estos radicales deuterados han sido caracterizadas mediante LIBS. Además, los desplazamientos isotópicos observados en las emisiones ópticas de estas tres especies coinciden con los reportados en la bibliografía.

Con objeto de dilucidar las principales rutas de formación de los citados radicales se llevó a cabo el análisis LIBS de tres compuestos deuterados: urea $-CO(ND_2)_2-$, ácido tereftálico $-C_6D_4(COOH)_2-$, y antraceno $-C_{14}D_{10}$. De igual modo se analizaron sus isotopólogos no deuterados. Todas las muestras fueron analizadas en forma de pastillas. Los resultados más relevantes del presente estudio se detallan a continuación.

Formación de radicales NH. Las observaciones de las respuestas ópticas experimentales de los distintos isotopólogos sugirieron que la generación de la especie NH tiene como uno de sus principales orígenes la liberación directa de fragmentos desde las moléculas ablacionadas cuando éstas poseen enlaces N−H. Como ejemplo, la urea $-CO(NH_2)_2-$ puede liberar grupos amino y dar lugar a la formación de radicales NH tras la salida de un H. Esto justificaría las altas emisiones de NH manifestadas por este compuesto en comparación con los compuestos que carecen de enlaces N−H. Por otra parte, los espectros de urea deuterada $-CO(ND_2)_2-$ evidenciaron una mínima contribución de emisiones NH solapada con la banda de emisión dominante de ND, en torno a 337 nm. Esta circunstancia sugiere que el fenómeno de ionización secundaria del aire apenas se produce cuando se emplean pulsos de femtosegundos como fuente excitación, dejando entrever

que el H procedente de la humedad ambiental apenas contribuye a la formación de este radical. Por otra parte, debe indicarse que las respuestas espectrales de compuestos sin nitrógeno también manifestaron emisiones de NH. Estos resultados dejan patente que la generación de la especie NH a partir de la recombinación a nivel atómico de H nativo y N atmosférico también es una ruta factible. No obstante, el hecho de que las emisiones en estos casos fueran menos intensas que en el caso de la urea sugiere que es una ruta poco favorecida, lo que se justifica por la mayor afinidad de los átomos de N por los átomos de C. Con ánimo de indagar más sobre la formación de esta especie, se realizó un estudio de la evolución temporal de las emisiones NH y ND en plasmas del ácido tereftálico parcialmente deuterado. Se observó un crecimiento temporal de la relación de intensidades ND/NH durante los primeros microsegundos de vida del plasma. De acuerdo con esta tendencia, se propuso un patrón de ruptura del compuesto según el cual los átomos de H de los grupos hidroxilos se liberarían en primer lugar y reaccionarían con el N para generar NH. Posteriormente, los átomos de D serían liberados del anillo aromático y contribuirían a la generación de radicales ND mediante su reacción con el N atmosférico.

Formación de radicales CH. Las observaciones de las respuestas ópticas experimentales de los distintos isotopólogos sugirieron que la generación de la especie CH se encuentra supeditada a la manifestación de emisiones de C_2. Mientras que el ácido tereftálico y el antraceno revelaron emisiones de CH y C_2, la urea (carente de enlaces C-H y C-C) no manifestó emisiones asociadas a dicha especie. Por otra parte, el antraceno deuterado exhibió emisiones intensas de CD y despreciables de CH. De nuevo se evidenció la mínima contribución del hidrógeno de la humedad ambiental a la química de los plasmas inducidos con pulsos de *fs*. En particular, el espectro LIBS del ácido tereftálico deuterado manifestó una mezcla de emisiones de CD y CH lo que señala la participación de especies nativas de H o D en la rutas de reacción. De acuerdo con lo posibles patrones de ruptura de las moléculas, las principales rutas de generación de CH postuladas

involucran reacciones entre fragmentos C_2 y/o C_2H y especies oxigenadas de origen ambiental o nativo (O_2, O y OH).

Formación de radicales OH. La manifestación de emisiones OD en los espectros de compuestos totalmente deuterados y ausencia de características espectrales OH corroboró de nuevo la prácticamente nula contribución de la humedad ambiental a las rutas de formación de estas especies hidrogenadas. Por el contrario, el oxígeno atmosférico si tiene una participación activa en la generación de OH. Esto se deduce de las emisiones de OH en plasmas de antraceno (compuesto carente de átomos de oxígeno en su fórmula química). Se postularon como rutas principales la reacción entre átomos de H liberados de la molécula y oxígeno atmosférico, ya sea molecular o atómico. Cabe también decir que no se observó ninguna relación directa entre la intensidad de las emisiones de OH y la presencia de grupos hidroxilo en los compuestos.

Los resultados de este trabajo, de los que se deducen las rutas de formación más probables para la generación de especies diatómicas y de los que se extraen potenciales relaciones entre las emisiones moleculares y la estructura química de los sólidos analizados, apuntan al uso de LIBS como una herramienta selectiva para la caracterización de compuestos orgánicos. Tal y como se describirá más adelante, la técnica LIBS es una valiosa herramienta en aplicaciones como, por ejemplo, la detección de materiales explosivos y la caracterización de materiales poliméricos.

– Emisiones moleculares en plasmas orgánicos inducidos por láser de femtosegundos: comparativa con el régimen de excitación de nanosegundos

Hasta la fecha se han publicado numerosos trabajos enfocados al estudio de las emisiones moleculares de plasmas orgánicos inducidos con pulsos láser de nanosegundos. Sin embargo, el análisis LIBS de materiales orgánicos mediante excitación con pulsos ultracortos apenas ha sido explorado. Este trabajo evalúa la influencia de la duración del pulso láser en la generación de radicales diatómicos y en las resultantes emisiones moleculares en los regímenes de ablación de femtosegundos y nanosegundos. Los resultados obtenidos indican que la ruptura parcial de las moléculas ablacionadas y la posterior liberación de fragmentos es el principal origen de las emisiones moleculares cuando se emplean pulsos ultracortos. Contrariamente, en el régimen de nanosegundos las reacciones de recombinación atómica y de desplazamiento simple –intercambio de un átomo en una especie diatómica– se postulan como las principales rutas de generación de radicales diatómicos. Las diferencias encontradas en las respuestas espectrales obtenidas para cada régimen de excitación determinan una mejor correlación entre las emisiones ópticas y las estructuras moleculares de los compuestos cuando se emplean pulsos de *fs*. Por lo tanto, el uso de pulsos láser de *fs* proporciona una mejora de la selectividad en el análisis de sólidos moleculares mediante LIBS.

En este trabajo se diseñaron dos configuraciones experimentales prácticamente idénticas para llevar a cabo el estudio comparativo entre *fs*-LIBS y *ns*-LIBS. La única diferencia entre ellas radicaba en las fuentes de excitación consideradas. Un sistema láser de Ti:Zafiro (ancho de pulso 60 *fs*, longitud de onda 800 nm) y un láser de Nd:YAG (ancho de pulso 8 ns, longitud de onda 1064 nm) para los experimentos de *fs*-LIBS y *ns*-LIBS, respectivamente.

En relación a las muestras empleadas, se analizaron un total de siete sólidos moleculares: urea, ácidos tereftálico y L-ascórbico, melamina, cafeína, p-nitroanilina y pentaeritritol. La composición y las particularidades estructurales de estos compuestos permitieron evaluar las

probables rutas de formación de los radicales diatómicos y su relación con las estructuras moleculares. Al igual que en los trabajos descritos anteriormente, los compuestos sólidos fueron analizados en forma de pastillas.

Efectos de la duración del pulso láser en las emisiones de radicales diatómicos. Con objeto de estudiar la influencia de la duración del pulso láser en las emisiones ópticas se computaron las relaciones de intensidades de las emisiones moleculares con respecto a la señal de C atómico a 247 nm (CN/C, CH/C, C_2/C, NH/C, OH/C). Estas relaciones sirven como evaluador estadístico para reflejar el grado de generación de fragmentos moleculares con respecto a la atomización del sólido tras la ablación láser. Tomando como modelo la molécula de melamina ($C_3H_6N_6$), se observaron valores de estos estadísticos considerablemente mayores en el caso de *fs*-LIBS, lo que sugiere un predominio de los procesos de fragmentación sobre la atomización. Sin embargo, en *ns*-LIBS los valores bajos de estos cocientes proponen la atomización de molécula y posteriores reacciones de recombinación como procesos dominantes. Con independencia de la duración del pulso, en moléculas con enlaces C-N –como es el caso de la melamina– la generación de radicales CN puede producirse no sólo por la liberación directa del fragmento sino también por la reacción del C atómico con N atmosférico o nativo. Sin embargo, el mayor valor del cociente CN/C en *fs*-LIBS en comparación con el obtenido para *ns*-LIBS sugiere que la proliferación del radical CN ocurre principalmente por liberación directa tras la fragmentación parcial del compuesto. De forma análoga, el valor elevado del estadístico NH/C en el caso de *fs*-LIBS, también apunta a que la salida de fragmentos NH de los grupos amino es el principal origen de estos radicales en plasmas inducidos con pulsos láser ultracortos.

Influencia de la estructura molecular en la generación de radicales diatómicos. Se compararon los perfiles de emisión de los siete compuestos analizados en los regímenes de ablación de *fs* y *ns*. Por una parte, se analizaron las emisiones relativas de las especies de carbono (expresadas como tanto por uno de las emisiones totales de C, C_2, CH y CN). En *fs*-LIBS se observaron ciertas tendencias en los perfiles de emisión, probablemente ligadas a la estructura molecular de los compuestos. Las emisiones más intensas de CN fueron evidenciadas en plasmas de melamina, cafeína y p-nitroanilina, compuestos que presentan N en sus estructuras de carbono. De forma opuesta, los compuestos carentes de N manifestaron emisiones de CN ligeramente más débiles. Esta circunstancia corrobora el predominio de la liberación directa como ruta de formación, al tiempo que refleja la distinción entre sólidos moleculares según contengan o no el enlace C-N en su estructura. Por el contrario, en *ns*-LIBS la correlación de las emisiones de CN con la estructura molecular del compuesto se ve desvirtuada. Esta hecho se debe, en parte, a la mayor atomización sufrida por las moléculas y a la mayor interacción entre la atmósfera circundante y la pluma del plasma que equipara las emisiones de CN, independientemente de que los compuestos contengan o no N en su estructura molecular.

En cuanto a las emisiones de C_2, éstas fueron más intensas en *fs*-LIBS debido a la ya comentada menor atomización que experimentan las moléculas en este régimen de ablación y la mayor liberación fragmentos nativos. Aunque la producción de esto fragmentos va ligada a la presencia de dobles enlaces nativos entre átomos de C, no se observó una conexión directa entre el nivel de estas emisiones y el número de enlaces C=C presentes en cada compuesto. La reducida abundancia relativa de C_2 en plasmas generados con pulsos de *ns* es de nuevo atribuida al mayor grado de atomización y a la mayor afinidad del C para recombinarse con N atmosférico y generar CN. Finalmente, la existencia de emisiones de C_2 en la melamina (molécula sin enlaces C=C) evidenció la existencia de rutas alternativas a la liberación directa para la generación de este radical.

De igual modo, las emisiones relativas de CH también fueron más intensas en *fs*-LIBS. El análisis exhaustivo de las respuestas ópticas expuso que la intensidad de la señal de CH parece ser una combinación de la abundancia de fragmentos C_2 y la presencia de grupos OH en los compuestos, más allá de relacionarse directamente con la presencia de enlaces nativos C-H. Por tanto, parece razonable pensar que la reacción química radicales C_2 y OH pueda ser la principal ruta responsable de la producción de CH.

Además, se evaluaron y propusieron las posibles rutas para la generación de radicales NH y OH. De nuevo se computaron las emisiones relativas respecto al total de las emisiones de radicales hidrogenados (CH, NH y OH). Atendiendo a las señales ópticas de plasmas inducidos con pulsos de *fs*, se observaron emisiones de NH más elevadas en los compuestos con N y, especialmente, en aquellos con enlaces N-H. Las emisiones de NH en compuestos sin N fueron vinculadas a la reacción entre el N atmosférico y el H liberado de los sólidos ablacionados. Estas emisiones resultaron bastante menos intensas, no sólo por la ausencia de N en las moléculas, sino principalmente por la mayor afinidad del N atmosférico por los átomos de C liberados para formar CN. De forma análoga, también se observó una relación directa entre la presencia de grupos hidroxilo en los sólidos moleculares y la intensidad de las emisiones de OH (por ejemplo, para el pentaeritritol y para el ácido L-ascórbico). Por el contrario, al igual que ocurre con los otros radicales diatómicos, el mayor grado de atomización en *ns*-LIBS hace que las posibles relaciones entre las emisiones ópticas y la estructura molecular de los compuestos resulte mucho menos evidente.

Los resultados demuestran que las emisiones ópticas derivadas de la ablación láser con pulsos ultracortos reflejan mejor la estructura de los sólidos moleculares que las emanadas de la excitación con pulsos de *ns*. Esta mejor correspondencia se debe a un efecto combinado de dos fenómenos como son la menor atomización de los compuestos y la baja interferencia de la atmósfera circundante. Por lo tanto, *fs*-LIBS puede considerarse como una herramienta mucho más selectiva para el análisis de sólidos moleculares, en comparación con *ns*-LIBS.

2. Aplicaciones de LIBS al análisis y caracterización de sólidos moleculares

– Discriminación de materiales nanométricos de carbono. Caracterización óptica de grafeno

Desde el descubrimiento del grafeno en 2004, la comunidad científica ha realizado grandes esfuerzos en la mejora de los procesos para su fabricación y en la implantación de métodos para su caracterización físico-química. El grafeno, que es descrito como una capa grafítica monocristalina estable en condiciones ambiente, posee excepcionales propiedades: rigidez mecánica, dureza y elasticidad, una gran área superficial, alta conductividad térmica y eléctrica, una baja absorción óptica y una gran capacidad para su funcionalización química. Todas estas características lo convierten en un material muy atractivo para la fabricación de nuevos dispositivos así como para mejorar las cualidades de infinidad de productos fotónicos y electrónicos. Es por ello que el control de la calidad del grafeno, como componente esencial de dichos dispositivos, es un aspecto fundamental a controlar que precisa de técnicas analíticas capaces de diferenciar entre los productos de partida y los productos finales.

El uso de LIBS para esta aplicación se sustenta en los recientes progresos experimentados por la técnica en la caracterización de compuestos de carbono con similar composición química. En este trabajo las emisiones ópticas de plasmas de 3 compuestos de carbono puro (grafito, grafeno multicapa y grafeno de pocas capas) y de un material de partida en la síntesis de grafeno como es el óxido de grafeno han sido estudiadas en profundidad. Las muestras empleadas, originariamente en forma de polvo o copos, fueron prensadas y analizadas mediante LIBS empelando una configuración experimental en modo local y una excitación con pulsos láser de *ns*.

En cuanto a los resultados experimentales, las respuestas ópticas de todos los compuestos manifestaron líneas atómicas de emisión de C, H, O y N, así como señales asociadas a los sistemas moleculares CN y C_2. Las emisiones de H, O, N y CN en los plasmas de materiales con una composición del 100% de átomos de carbono son consecuencia de la interacción entre los plasmas

y su atmósfera circundante. En el caso del óxido de grafeno, se observaron altas emisiones de H que fueron atribuidas a la presencia de algunos grupos funcionales, tales como –OH y –COOH, en dicho material. Además, dichos grupos funcionales también justifican las emisiones intermedias de O exhibidas por este material, que difieren de las bajas emisiones para el resto de compuestos debidas únicamente a la contribución del aire. Por otra parte, la presencia de los grupos funcionales también repercute en otras emisiones remitidas por los plasmas de óxido de grafeno. La inclusión de grupos funcionales genera una mezcla de hibridaciones sp^2- y sp^3- de los átomos de C, disminuyendo el número enlaces dobles de C y por tanto la generación de dímeros de carbono por fragmentación directa. Como consecuencia de este cambio de estructura del plano base del material se detectan intensidades despreciables para las emisiones de C_2.

Una de las principales diferencias observadas en el proceso de ablación láser de los materiales en cuestión fue los distintos valores para los umbrales de formación de sus plasmas. Los resultados revelaron un incremento de dichos umbrales en función del número de capas de grafeno que conforman el material. Este hecho puede justificarse de acuerdo con los valores de difusividad térmica y área específica de los materiales, que también aumentan con el número de capas grafíticas. Por tanto, es posible concluir que el número de capas de grafeno que conforman cada material, así como su distinta disposición, afecta directamente al proceso de ablación.

También se llevó a cabo una evaluación del efecto de la fluencia láser (en el rango comprendido entre 10 $J \cdot cm^{-2}$ y 250 $J \cdot cm^{-2}$) en los patrones de emisión de estas muestras empleando parámetros temporales fijos para la adquisición de la señal LIBS (un tiempo de retraso de 1,5 μs y un tiempo de integración de 0,5 μs). Más allá de un incremento de la intensidad de la señal al aumentar la dosis de energía dispensada como consecuencia de su proporcionalidad con la tasa de ablación, las respuestas ópticas de los distintos compuestos no manifestaron diferencias significativas. Debe señalarse que las intensidades de algunas señales de emisión para el óxido de

grafeno se apartaban de las del resto de compuestos, por las diferencias estequiométricas anteriormente comentadas.

Por el contrario, la monitorización del progreso temporal de las señales moleculares permitió identificar distintas pautas de emisión para los 4 materiales analizados. Entre ellas, la más destacable es la significativa diferencia en la velocidad de extinción de las emisiones moleculares, principalmente de C_2, cuando los plasmas son inducidos con una alta fluencia láser (aprox. 250 $J \cdot cm^{-2}$). Mientras que en el óxido de grafeno estas emisiones experimentan una tendencia decreciente desde los primeros instantes posteriores a la formación del plasma, las intensidades de señal para el resto de materiales de carbono puro manifiestan un decaimiento mucho más sostenido. En estos materiales, el decaimiento de las señales moleculares parece ir acorde con el tipo de fragmentos de carbono (C_n) liberados durante su ablación. De este modo el grafito y el grafeno multicapa revelan un decaimiento más rápido de sus señales moleculares en comparación con el grafeno de pocas capas. Esta circunstancia se justifica por sus menores umbrales de ablación, que facilitan una mayor atomización y por tanto una liberación de fragmentos de carbono de menor tamaño que son disociados más rápidamente. De hecho, las diferencias entre estos materiales en la velocidad de extinción de la señal de C_2 son más acentuadas en comparación con las reportadas a partir del comportamiento temporal del radical CN. Esta conducta temporal no sólo permite corroborar que las emisiones de C_2 están directamente relacionadas con el grado de fragmentación de las estructuras grafíticas, sino que además puede actuar como un testigo marcador en la discriminación de materiales grafíticos con distinto número de capas.

En resumen, los resultados han demostrado que los umbrales de formación de plasma son distintos como consecuencia de diferentes propiedades de las estructuras de carbono, tales como su número de capas y la presencia de grupos funcionales. A su vez, estos umbrales de ablación de los materiales de carbono son los que definen el patrón de ruptura de dichas estructuras que,

posteriormente, repercuten directamente en el comportamiento temporal de las emisiones moleculares, permitiendo así la diferenciación de estos materiales.

– Nuevas estrategias quimiométricas aplicadas al reconocimiento de residuos explosivos

El desarrollo de la tecnología LIBS para la detección de residuos explosivos en el escenario de una posible amenaza terrorista viene motivado por la necesidad de disponer de una herramienta analítica que proporcione sensibilidad y fiabilidad suficientes en la interrogación rápida de objetos sospechosos. Sin duda, la capacidad para detectar e identificar la presencia de sustancias explosivas es vital para poder prevenir cualquier acto terrorista.

En este contexto, se incluyen en la presente Tesis Doctoral tres trabajos de investigación en los que las respuestas espectrales proporcionadas por la tecnología LIBS se han sometido a un tratamiento con potentes métodos quimiométricos para el reconocimiento de residuos explosivos. Aunque los trabajos han sido realizados a escala de laboratorio, pretenden abordar situaciones de riesgo en escenarios reales. Por ello, más allá del análisis de estos materiales a granel, se afronta la problemática de la detección de restos explosivos localizados a nivel de trazas sobre superficies de distinta naturaleza como consecuencia de su manipulación. Los tres estudios experimentales desarrollados comparten la metodología analítica y la herramienta quimiométrica, el aprendizaje de máquinas supervisado (*supervised machine learning*). Se pretende de esta forma obtener el máximo rendimiento de la limitada información proporcionada por la técnica LIBS, mejorando la sensibilidad y selectividad del método en el reconocimiento de residuos explosivos. La metodología consiste en el diseño y entrenamiento de un modelo de clasificación a partir de un conjunto de datos previamente conocidos (espectros LIBS de residuos de naturaleza conocida) para la posterior identificación y asignación de datos desconocidos (espectro LIBS de un residuo desconocido) a una determinada clase (residuo explosivo o residuo inocuo).

El equipo LIBS experimental empleado en estos tres trabajos de investigación fue el mismo, manteniéndose incluso las mismas condiciones operacionales (energía del pulso láser, condiciones focales, parámetros temporales de adquisición de la señal, etc.). Cabe destacar el uso de un láser pulsado de nanosegundos de Nd:YAG y un espectrómetro *Czerny-Turner* miniaturizado de cuatro canales.

A) Detección de residuos explosivos de naturaleza orgánica sobre soportes de aluminio

En este primer trabajo se abordó la situación más sencilla que puede encontrarse en el análisis LIBS de residuos en una superficie, esto es, cuando la composición elemental del residuo difiere de la composición de la superficie. Se realizó en primer lugar un estudio en profundidad de las emisiones ópticas de los plasmas de 9 compuestos orgánicos depositados como residuo sobre superficies de aluminio. Como residuos explosivos se consideró el conjunto formado por dinitrotolueno (*DNT*), trinitrotolueno (*TNT*), ciclotrimetilentrinitramina o hexógeno (*RDX*) y pentaeritritol tetranitrato (*PETN*). Como residuos inocuos también de naturaleza orgánica, cuya composición elemental y patrones de emisión son muy similares a los de las muestras explosivas, y que pueden actuar como potenciales confusantes se optó por materiales como la mantequilla, el aceite de oliva, el aceite de motor, la gasolina y la crema de manos. Una vez obtenido un volumen considerable de datos espectroscópicos de todos estos residuos localizados sobre superficies de aluminio, se procedió al tratamiento quimiométrico de la información LIBS. El método empleado se basó en la proyección de las intensidades de emisión de las señales espectrales más relevantes –C, CN, C_2, H, N y O– en distintos subespacios bidimensionales con el ánimo de identificar las características espectrales que proporcionaban la mejor distinción entre los dos tipos de residuos. Para poder examinar de una forma rápida todos los gráficos de dispersión construidos, se calculó un parámetro numérico denominado *Región Discriminante Residual –RDR–* definido por la siguiente ecuación:

$$\boldsymbol{RDR} = \frac{\boldsymbol{A_{solapamiento}}}{\boldsymbol{A_{explosivos}}} + \frac{\boldsymbol{A_{solapamiento}}}{\boldsymbol{A_{confusantes}}}$$

Este parámetro se fundamenta en el grado de solapamiento que existe entre el área ocupada por la nube de dispersión proyectada por los residuos explosivos –definida por la envolvente convexa de todos los datos que la constituyen– y el área ocupada por la nube de dispersión generada por los residuos inocuos. El valor que puede tomar dicho parámetro oscila entre 0 y 2. Así, un valor de 2 para el RDR indica que las dos nubes de datos se encuentran totalmente solapadas, de tal modo que las dos características espectrales involucradas en dicho subespacio bidimensional no permiten diferenciar entre los dos tipos de residuos. Por el contrario, un valor para *RDR* de 0, revela la mejor diferenciación entre residuos explosivos e inocuos.

Una vez identificado el gráfico más eficaz para la distinción de residuos de acuerdo con su naturaleza, se procedió a diseñar, construir y entrenar distintos algoritmos –*clasificadores*- basados en distintos principios estadísticos y matemáticos. Entre los modelos utilizados para hacer frente a la clasificación destacan los basados en densidades normales y en la regla del vecino más cercano, los basados en la estimación por núcleos o ventanas de *Parzen*, y los fundamentados en modelos de mezcla de funciones gaussianas y en las máquinas de vectores soporte. En el caso particular del reconocimiento de residuos depositados sobre aluminio se identificaron 3 diagramas que proporcionaron una adecuada separación entre clases de residuos. Se trataba de lo gráficos que involucraban la emisión atómica de C, N u O frente a la señal de H_α. Cabe señalar aquí que las emisiones de H, N y O pueden tener origen nativo o bien venir derivadas del proceso de ionización secundaria de aire. Esta circunstancia dificulta poder establecer si los residuos se diferencian directamente por su distinta estequiometria o bien por su estado físico y el distinto comportamiento de sus correspondientes plasmas con la atmósfera que los rodea.

Pese a que las señales moleculares CN y C_2 han servido en estudios previos como activos útiles para la detección de explosivos, en este caso no mostraron tener utilidad en la clasificación de los residuos. En particular, las emisiones de C_2 resultaban inservibles ya que en el rango espectral donde se manifiestan (desde 450 nm hasta 550 nm) también se exhibe el sistema de bandas de emisión del AlO, generado por la reacción del Al procedente de la muestra con el oxígeno ambiental, produciéndose un solapamiento entre ellas.

Atendiendo a las estadísticas de clasificación reportadas por los diferentes clasificadores diseñados y entrenados en los 3 gráficos anteriormente mencionados, los resultados determinaron que el clasificador construido en base a la estimación por ventanas de *Parzen* sobre el gráfico que proyectaba las intensidades de emisión de las señales de O y H_α resultó ser el más adecuado, proporcionando las tasas de falsos positivos y de falsos negativos más bajas, inferiores al 5 %.

Finalmente, se procedió a evaluar la sensibilidad de la metodología en el reconocimiento de estos residuos explosivos. En este caso particular, más allá de establecer la sensibilidad como el límite de detección (*LOD*) de acuerdo a la definición 3σ de la IUPAC –concentración de un elemento capaz de proporcionar una señal de emisión neta de al menos 3 veces la desviación estándar del fondo espectral– se trató de identificar cual era la mínima intensidad de señal a partir de la cual se podía acometer la distinción entre los dos tipos de residuos. Para ello se propuso un parámetro alternativo basado en el establecimiento de unas coordenadas espaciales (x, y) de las variables involucradas en los gráficos de dispersión como límites de corte para la identificación correcta de los residuos. De este modo, las respuestas espectrales de aquellos residuos interrogados que proporcionen unas valores de intensidad para las señales O y H_α superiores a los valores (x, y) establecidos permiten su correcta identificación. En caso contrario, esto es, si los valores de intensidad se encuentran por debajo existen dudas acerca de la fiabilidad en el reconocimiento. Para una mejor interpretación de los resultados las coordenadas se normalizaron a la máxima respuesta del detector. En particular para el gráfico *O vs* H_α, se obtuvieron unos valores para las

coordenadas muy próximos a (0, 0). Dichos valores mínimos para el límite de corte indicaban prácticamente una sensibilidad máxima en la distinción de ambos tipos de residuos. En definitiva, el clasificador diseñado puede asignar a la clase correspondiente con suficiente exactitud cualquier residuo cuya respuesta espectral ofrezca una mínima intensidad para las señales de oxígeno e hidrógeno.

Los hallazgos de esta investigación ponen de relieve la capacidad de LIBS en conjunción con el uso de máquinas de aprendizaje supervisado para el reconocimiento de residuos explosivos bajo condiciones experimentales definidas, esto es, localizados sobre soportes de aluminio. Por ello, el siguiente paso relacionado con esta línea de investigación consistió en evaluar la validez de esta misma estrategia en distintas situaciones –idénticos residuos pero emplazados en otro tipo de superficies–, tal y como se describe a continuación.

B) Detección de residuos explosivos de naturaleza orgánica depositados en superficies poliméricas

La identificación de trazas de explosivos orgánicos depositados sobre superficies poliméricas mediante LIBS es un problema mucho más complejo que el ejemplo descrito con anterioridad. En esta situación, el sustrato tiene la misma composición química que el residuo y ambos contribuyen a los patrones finales de emisión con idénticas señales (C, H, O, N, CN y C_2). Desafortunadamente, éste era un importante escollo a superar para el uso de esta tecnología en futuras aplicaciones reales. No obstante, el uso de métodos quimiométricos para el tratamiento de datos multivariables ha contribuido a superar este obstáculo. Mediante su uso es posible desvelar las mínimas diferencias existentes entre los espectros de emisión óptica de materiales explosivos e inocuos, pese a la dificultad añadida por la contribución de emisiones relativas al sustrato.

En este trabajo se consideraron los mismos nueve residuos empleados en el estudio realizado con las láminas de aluminio –DNT, TNT, RDX y PETN, como explosivos, y mantequilla,

aceite de oliva, aceite de motor, gasolina y crema de manos, como confusantes. Estos residuos fueron depositados sobre tres soportes poliméricos –*teflón, nylon* y *polietileno*– por lo que resultaron un total de 27 muestras binarias.

Para la selección de las variables espectrales que proporcionaban la mejor distinción de los residuos según su clase (es decir, el/los mejor/es diagrama/s de dispersión *2D*) se computó el correspondiente valor del parámetro *RDR* descrito anteriormente. Los resultados revelaron que, independientemente del soporte sobre el que se localizara el residuo, los diagramas que involucraban CN y C_2 como variables discriminatorias eran los más adecuados para la distinción entre tipos de residuos por proporcionar los valores más bajos de *RDR*. De acuerdo con la dispersión de las nubes de datos en estos gráficos, los residuos explosivos manifestaban mayores emisiones de CN y menores señales de C_2 en comparación con los residuos inocuos.

Para tratar de acrecentar la capacidad de discriminación, se evaluó el rendimiento de gráficos tridimensionales, añadiendo una tercera dimensión a los anteriores diagramas de dispersión. En estos diagramas *3D*, el cálculo del parámetro *RDR* involucraba los valores del volumen ocupado por las nubes de dispersión en lugar de su área. Dichos volúmenes fueron también definidos a partir de las correspondientes envolventes convexas de las nubes de datos. El análisis de los resultados desveló menores valores de *RDR* para los diagramas de dispersión *3D* en comparación con los reportados por los gráficos *2D*, justificando así el uso de los primeros al proporcionar una mejor separación entre residuos explosivos e inocuos, en particular diagramas *3D* formados por combinaciones de las intensidades de emisión de CN, C_2, H y O. Cabe resaltar que las emisiones ópticas de los plasmas inducidos a partir de los diferentes residuos mostraron un comportamiento similar para los distintos soportes. Por ello se consideró la construcción de un clasificador global a partir del mismo diagrama de dispersión *3D* para la detección de residuos con independencia del sustrato (es decir, válido para residuos depositados en *teflón, nylon* o *polietileno*). Si bien al agrupar las tres situaciones el gráfico construido reportaba un valor de *RDR* ligeramente

superior al proporcionado por cada gráfico independiente, la capacidad discriminatoria continuaba siendo suficiente como para identificar el tipo de residuo sobre cualquier sustrato polimérico mediante el empleo de un único algoritmo.

Además de los clasificadores ensayados en el trabajo anterior, en esta ocasión se incluyeron modelos adicionales de clasificación basados en el empleo de redes neuronales entrenadas por retro-propagación, según la regla de *Levenberg-Marquardt*, o mediante el uso del perceptrón lineal. Los resultados revelaron que el clasificador basado en el uso de redes neuronales entrenadas de acuerdo con la regla de *Levenberg–Marquardt* era el modelo que permitía el reconocimiento de residuos con mayor sensibilidad y especificidad. En particular, este clasificador construido a partir de un diagrama de dispersión involucrando combinaciones lineales de las intensidades de emisión de señales moleculares y atómicas (*CN/C_2 vs CN+C_2 vs O/H*) permitió obtener tasas de falsos negativos y fasos positivos de 2% y 1%, respectivamente.

En esta ocasión también se procedió a la evaluación de la sensibilidad del método en el reconocimiento de explosivos. De nuevo, no fue operable calcular un límite de detección de acuerdo a su definición clásica, no sólo por no haber materializado la cuantificación del residuo depositado sino también por la incerteza en la correspondencia exclusiva de la intensidad de cualquiera de las señales de emisión al propio residuo. De forma alternativa, se establecieron límites para la detección en base a las coordenadas espaciales de las variables involucradas a partir de las cuales se puede realizar la detección de residuos explosivos con un nivel de confianza del 95%. De acuerdo con esta condición, los resultados revelaron que la sensibilidad para la identificación de residuos explosivos crece según la secuencia DNT < RDX < TNT < PETN. La menor sensibilidad en la detección de DNT ($C_7H_6N_2O_4$) se atribuyó a una relación de intensidades O/H mucho más similar a la de los compuestos inocuos. El mayor contenido en O y las bajas emisiones de C_2 en el caso del TNT ($C_7H_5N_3O_6$) así como la ausencia de señal de C_2 en RDX ($C_5H_8N_4O_{12}$) y PETN ($C_3H_6N_6O_6$),

probablemente debido a la carencia de enlaces C=C en sus estructuras, podrían ser los factores que justifican su discriminación favorecida frente al resto de residuos inocuos.

En resumen, la estrategia quimiométrica diseñada permite diagnosticar en tiempo real a partir de las respuestas de emisión óptica la naturaleza explosiva de un conjunto acotado de residuos orgánicos depositados sobre soportes poliméricos, reportando tasas de falsos positivos y falsos negativos inferiores al 5%.

C) Detección de huellas dactilares de explosivos depositadas sobre objetos de mensajería

En este trabajo se desarrollaron algoritmos quimiométricos para la identificación de residuos depositados sobre distintos sustratos derivados de objetos de mensajería: una caja de embalaje de cartón, un sobre de papel marrón acolchado y un sobre de uso común de papel blanco. Se trata así de evaluar el rendimiento de la técnica LIBS y los algoritmos quimiométricos para afrontar una posible situación real de amenaza terrorista. En este escenario, residuos explosivos pueden quedar depositados en la superficie de un objeto cotidiano por manipulación tras la preparación de un artefacto explosivo improvisado o *IED* (del inglés, *improvised explosive device*). Por tanto, los residuos fueron dispuestos, en este caso, a nivel de huella dactilar. Además, el conjunto de compuestos explosivos y confusantes fue ampliado respecto al considerado en las anteriores investigaciones. Además de los explosivos orgánicos evaluados con anterioridad, se incluyeron dos materiales explosivos compuestos como la cloratita (preparados a partir de $NaClO_3$ y/o $KClO_3$, azufre y azúcar) y el amonal (resultado de la mezcla de NH_4NO_3 y polvo de aluminio). De igual modo, también se amplió la lista de potenciales confusantes. Junto con las sustancias utilizadas con anterioridad, también se emplearon otros compuestos orgánicos como un nuevo tipo de aceite de motor, gasóleo, jabón, azúcar y edulcorante, así como algunas sales inorgánicas como KCl, $KClO_3$,

NaCl, $NaClO_3$, NH_4NO_3 y azufre que podían enmascarar la detección de los nuevos explosivos considerados.

En términos generales, la estrategia seguida en esta ocasión para la discriminación de las huellas dactilares no difería a la de los trabajos anteriores. Sin embargo, dada la mayor complejidad del problema por contemplar residuos de muy distinta naturaleza química, en este caso se dispuso un algoritmo o árbol de decisión de varias etapas para acometer de forma secuencial la identificación de los mismos. Dicho algoritmo estaba integrado por 3 clasificadores basados en el empleo de redes neuronales entrenadas de acuerdo con la regla de *Levenberg–Marquardt*. El primero de los clasificadores fue construido a partir de un diagrama de dispersión *3D* que involucra las variables *Na vs K vs S*. Este clasificador es el encargado de identificar cualquier residuo de cloratita, en el supuesto de que se encontrara presente en el objeto. Mientras las dimensiones que implican las intensidades de emisión de las líneas atómicas de Na y K favorecen la distinción entre cloratita y azufre puro, la dimensión asociada a las intensidades de la línea de emisión de S permite discriminar entre el explosivo y las sales puras, los cloruros y cloratos de sodio y potasio. Los ensayos llevados a cabo con este clasificador revelaron una elevada efectividad, proporcionando sólo una falsa alarma en la identificación de las distintas huellas dactilares evaluadas. Una vez evaluada la información espectral asociada a la huella dactilar con este clasificador, si ésta no ha sido identificada como cloratita, se procede a su diagnóstico con un segundo clasificador diseñado a partir de un nuevo diagrama de dispersión *3D* que implica las dimensiones *O vs H vs Al*. Este clasificador trata de identificar la posible pertenencia de la huella al explosivo amonal –NH_4NO_3 y polvo de aluminio. Para aumentar la sensibilidad del reconocimiento, tras haber detectado la presencia de emisiones de Al durante el análisis de los soportes en ausencia de residuo, se decidió hacer uso en la construcción del clasificador de las intensidades de una línea de emisión de Al poco intensa. De este modo, sólo aquellos soportes en los que se encontraba una huella dactilar de amonal reportaban una señal óptica con una intensidad significativa de esta línea, pudiéndose

reducir así el número de falsos positivos en la detección de amonal. Si bien es la línea de Al la dimensión que aporta el mayor peso al modelo de clasificación, la inclusión de las emisiones de H y O mejoran la selectividad del clasificador. De este modo, los ensayos llevados a cabo con este clasificador revelaron unas tasas del 0% para los falsos negativos y los falsos positivos.

De nuevo, una vez diagnosticada la información espectral asociada a la huella dactilar con este segundo clasificador, si ésta no ha sido identificada como amonal, se ejecuta finalmente su evaluación con el tercero de los clasificadores, construido a partir de un gráfico de dispersión *3D* que involucra las señales *CN vs* C_2 *vs H* y se encarga de etiquetar la huella dactilar si se trata de un explosivo orgánico. En este diagrama de dispersión las nubes de datos asociadas a huellas de residuos explosivos e inocuos mostraron disposiciones diferenciadas a lo largo del eje que contempla las intensidades de la señal de H. No obstante, la distinción entre clases se acomete esencialmente por las mayores intensidades para las emisiones de CN y las menores lecturas para las señales de C_2 asociadas a huellas de explosivos. Pese a ello, existen una serie de valores de estas intensidades muy parejos para ambos tipos de residuos, explosivos e inocuos, dando lugar a una zona de solapamiento de los dos conjuntos de datos en la que se ve debilitada la exactitud del clasificador para su identificación. Como consecuencia, el rendimiento de este clasificador da lugar a unas tasas de falsos negativos elevada en el reconocimiento de residuos, esto es, alerta de la presencia de un residuo explosivo ante algunas huellas dactilares de productos inocuos. El problema radica principalmente en la elevada similitud entre las respuestas ópticas de los explosivos orgánicos y las de algunos productos confusantes como el azúcar y el edulcorante. No obstante, también repercute negativamente la elevada variabilidad entre las respuestas ópticas de un mismo residuo como consecuencia de su distribución poco uniforme cuando se deposita en forma de huella dactilar.

De igual modo que en el proceso de identificación de residuos sobre superficies poliméricas, se planteó la posibilidad de utilizar un algoritmo de decisión único para la exploración de huellas

dactilares en el conjunto de los tres sustratos considerados, en lugar de un árbol de decisión particular en función del sustrato donde se pretendiera reconocer la huella. Los resultados obtenidos con este modo de operación fueron ligeramente mejores a los conseguidos mediante el empleo de un algoritmo de decisión particular específico para cada soporte. Esto se vio reflejado en un descenso significativo de la tasas de falsos positivos, es decir, ninguna huella dactilar de sustancias explosivas pasaba inadvertida para el algoritmo.

En definitiva, los hallazgos de esta investigación han puesto de manifiesto que el escrutinio de la información LIBS a través de un árbol de decisión conformado por 3 clasificadores basados en el empleo de redes neuronales entrenadas de acuerdo con la regla de *Levenberg–Marquardt* permite afrontar el reconocimiento de huellas dactilares de residuos explosivos localizadas en la superficie de objetos de mensajería con unas tasas de error globales próximas a un 10%.

En resumen, todas las investigaciones englobadas en la presente memoria de Tesis Doctoral suponen no sólo un avance en el conocimiento acerca de las causas y los orígenes de la respuesta de emisión óptica de una técnica de análisis multielemental en la exploración de sólidos moleculares sino que también atestiguan el notable potencial de la tecnología LIBS para numerosas aplicaciones en las que se ven involucrados este tipo de compuestos.

OBJECTIVES

In the last two decades, research in laser-induced breakdown spectroscopy (LIBS) has undergone unprecedented growth.[1] Amongst the features that define the identity of this multi-elemental analytical technique, as its ability to offer a rapid real-time analysis of countless samples without any previous preparation whatever the state of the matter, it is worth mentioning also its field deployability as well as its readiness to perform remote analysis. In summary, a number of positive innovative attributes that have motivated the use of LIBS in a wide variety of applications.[2] Nonetheless, as in the rest of analytical techniques, some limitations remain, in particular as regards the analysis of organic samples. In this particular case, LIBS does not offer a good selectivity due to the high similarity of the optical emission outcomes from those compounds that share analogous elemental compositions.[3] LIBS is rigorously considered as an atomic technique since optical emissions from those elements composing the ablated sample are spectroscopically featured. Nevertheless, it may also provide molecular information of the sample through molecular emissions from some excited diatomic radicals present in plasmas. This is reason by which a more extensive use of technique is currently progressing towards molecular sensing applications. However, while at present this proposal is mainly intended to cope with the identification or recognition of organic materials, work is ongoing to step towards its use for quantification purposes in the near future.

Therefore, the applied research that will be conducted during the development of the present Doctoral Thesis is aimed at shedding light on the chemistry of laser-induced plasmas of molecular solids as well as the design and implementation of new strategies to exploit molecular excited assets for sensing and characterization of organic materials in real-world applications. So, quite a few particular goals shall be pursued to cope with these broad objectives.

Firstly, to complement the already existing knowledge on chemistry of organic plasmas, the origin and the potential routes leading to the generation of less investigated molecular species must be unveiled. To date, research has shown a particular concern on disclosing the origins of CN and C_2 radicals, which are normally the most representative molecular emissions in plasmas of organics. Thus, for moving forward, the disclosure of origins and formation pathways of hydrogenated radicals (OH, NH and CH), which have been scarcely explored in laser-induced plasmas, will be pursued. Since the vast majority of LIBS applications are performed in air at atmospheric pressure, our interests will be focused in the applicability of LIBS to atmospheric conditions to meet general analytical challenges.

Another important aspect to be considered with regard to selectivity and specificity of LIBS from organic plasmas are the likely relationships between the final optical emission patterns and the chemical structure of organics. The knowledge and identification of the spectral features which are truly representative of the structure of the compounds is of prime importance to exploit the use of LIBS as identification tool of organic samples. Although several studies have dealt with the analysis of organics by LIBS, there are not conclusive findings concerning the influence of the molecular structures of organics on their optical emission patterns. In this connection, it will be the subject of a systematic research within the development of the present Doctoral Thesis the diagnostics of laser-induced plasmas of a wide set of organic compounds with structural and compositional particularities, in order to reveal possible relations between the different molecular emissions –CN, C_2, OH, NH and CH– and the chemical structure of organic compounds.

It is well known that operational parameters in LIBS, such as the excitation wavelength, the laser pulse length and the laser pulse energy, significantly affect the ablation process, the generation of the subsequent plasma and, hence, the optical emission signals displayed.[4] Therefore, another goal that is raised for this Doctoral Thesis is the judgment of the effects of operational conditions on the emission spectroscopy of molecular solids. Since LIBS applications in many disciplines use nanosecond lasers for driving the ablation sampling process, our interests will be focused on scrutinizing the influence of different radiation wavelengths to the molecular emissions. At the same time, since the use of femtosecond lasers is now much more widespread, the potential effects on sensing and characterizing molecular solids by LIBS attributed to the laser pulse duration shall be evaluated.

In addition to all these fundamental studies on plasmas of organic compounds, some investigations in the present Doctoral Thesis must be routed to the exploitation of this background knowledge towards different LIBS applications. Currently, LIBS technology is implemented in a wide range of real-world applications that benefit from its attractive features. Notwithstanding this, research in the present Doctoral Thesis will attempt to address the most cutting edge applications involving organic materials.

On the one hand, the functionality of LIBS to the scrutiny of graphene –a material with exceptional properties and multiple applications that has been set to revolutionize the material world– and other nano-sized carbon materials will be evaluated. This investigation is motivated by the growing interest in the production of graphene and the need of analytical tools to control the quality of the materials involved in its manufacturing process.[5] The optical characterization of graphene and its differentiation from other carbon-based materials with similar chemical composition is the first step for a future implementation of LIBS in this application field.

Additionally, another field of study that has generated much interest in the use of LIBS is the detection of energetic materials. Certainly, investigations aimed at developing LIBS for security

applications have been encouraged by the increasing number of terrorist attacks during the last decades.[6] The detection of explosives by LIBS provides the possibility of real-time and in-situ analysis of potential threats also minimizing the risk for the operator when using remote or standoff sensors. For this reason, the application of LIBS in the area of homeland security and in potential military field operations must be addressed.

While some research has proved the potential use of LIBS for the detection of explosive materials, some pre-existing limitations of the technique have been also exposed. The main hindrance when applying LIBS for the recognition of organic explosives (typical chemical formula $C_CH_HN_NO_O$) lies in a biased loss of the molecular information of the target after laser ablation. Furthermore, emission signals that draw the optical fingerprint of explosive substances are not only scarce but also identical to those of innocuous organic materials. Hence, the efficiency of LIBS as analytical tool for the detection of explosive materials needs to be increased. To attain this, the design and implementation of advanced chemometric strategies to extract as much as possible information from this type of LIBS data shall be conducted. The main purpose of this research is the development of a fast, sensitive and reliable methodology providing the most accurate distinction between explosives and harmless compounds. Since the end-use of this methodology is intended to application in a real scenario of terrorist threat, the performance of the approach shall be tested to label minimal contaminations of explosive materials during recognition of traces deposited on solid surfaces.

REFERENCES

1 L. Radziemski, D. Cremers, *A brief history of laser-induced breakdown spectroscopy: From the concept of atoms to LIBS 2012*, Spectrochim. Acta Part B 87 (2013) 3–10.

2 F. J. Fortes, J. Moros, P. Lucena, L. M. Cabalín, J. J. Laserna, *Laser-induced breakdown spectroscopy*, Anal. Chem. 85 (2013) 640–669.

3 J. M. Anzano, I. B. Gornushkin, B. W. Smith, J. D. Winefordner, *Laser-induced plasma spectroscopy for plastic identification*, Polym. Eng. Sci. 40 (2000) 2423–2429.

4 A. Bogaerts, Z. Chen, *Effect of laser parameters on laser ablation and laser-induced plasma formation: A numerical modeling investigation*, Spectrochim. Acta Part B 60 (2005) 1280–1307.

5 W. Choi, I. Lahiri, R. Seelaboyina, Y. S. Kang, *Synthesis of graphene and its applications: a review*, Crit. Rev. Solid State 35 (2010) 52–71.

6 J. L. Gottfried, F. C. DeLucia Jr., C. A. Munson, A. W. Miziolek, *Laser-induced breakdown spectroscopy for detection of explosives residues: a review of recent advances, challenges, and future prospects*, Anal. Bioanal. Chem. 395 (2009) 283–300.

INTRODUCTION

1. An overview of laser-induced breakdown spectroscopy

The laser-induced breakdown spectroscopy (LIBS) is a technique based on the detection and analysis of the spectrally resolved optical emissions of atoms, ions and small molecules present in plasmas generated by the pulsed laser ablation of samples.[1] This technique exhibits several distinctive capabilities that have contributed to its fast expansion in numerous areas of applied chemistry and physics. Notable among them are, the potential to examine raw –without any previous preparation– samples, its flexibility to analyze any state of the matter –solids, liquids, and gases–, the potential to perform a simultaneous multielemental detection, its suitability for real-time monitoring of the elemental composition of samples, the potential for fast analysis, its adaptability upon field deployable instruments, and its handiness to operate at remote distances.[2]

The origin of LIBS dates from 1962, a couple of years after the pulsed ruby laser was invented by *Maiman*,[3] when the first publication revealing laser-induced plasmas as a spectral source was presented by *Brech* and *Cross*.[4] Shortly after, the technique was first used in the field of surface analysis[5] and to examine metallic samples by pulsed Q-switched ruby laser as unique excitation source.[6] Furthermore, during the sixties, optically induced breakdown when monopulse

ruby laser radiation was focused in air[7] and in water[8] was observed. Unfortunately, despite its promising start, the expansion of LIBS as analytical technique was slowed down over many years because of its limitations as quantitative method. It was not until the 1980s that, with the introduction of time-integrated and time-resolved spectroscopic measurements by *Loore* and *Radziemski*,[9,10] the scientific community again focused attention and reactivated investigations in LIBS. Since then, LIBS has not stopped growing, not only in obtaining more knowledge about its performance but also addressing a lot of real analytical challenges. A substantial part of the research interests has been focused on improving the sensitivity and selectivity of the technique. To this end, the application of different experimental approaches for the excitation, as the use of a double-pulse (*DP-LIBS*),[11] the handling of a scheme based on the tuning of the laser radiation of a pulse to the wavelength of a resonant atomic transition of the matrix atoms of the plasma (resonance-enhanced LIBS, *RE-LIBS*),[12-14] the delivering of multi-pulses (*MP-LIBS*),[15] and the operation with ultrashort laser pulses[16] has been considered.

On the other hand, improvements in LIBS instrumentation have allowed the development of field-deployable sensors which may be used in a wide variety of applications.[17] In this connection, standoff sensors have been constructed with the goal of analyzing distant targets in environments where physical access is not possible or may present a risk to the operator.[18] In the last years, the design of remote instruments based on a fiber optic cable to operate in aquatic media for analyzing submerged archaeological findings in sea is also a clear indicative fact of the progress and the potential of LIBS.[19] Lastly, the effective deployment and implementation as crowning of the technology has been evidenced with its flexibility and adaptability to a new environment as the surface of Mars for geochemistry exploration in this planet.[20]

Nowadays, LIBS has become a very trendy analytical technique expanding to numerous application fields such as industry,[21] homeland security,[22,23] geology,[24,25] biomedicine,[26] cultural heritage,[27] and planetary exploration.[28,29] However, the current research in LIBS is not only focused

towards the starting-up and the development of laser-based analytical applications[30] but also on the knowing, the understanding, and the unveiling of the fundamental aspects of the ablation physical process and the chemistry of the plasma.[31]

Particularly, a broad diversity of chemical reactions may occur in plasmas generated from the laser ablation of molecular solids. In this regard, the elucidation of the routes leading to the generation of diatomic radicals, and the emitting key species involved, are being, in recent years, subjects of interest for several research groups.[32-39] This is because the knowledge on origins of molecular emissions and connection of these with the molecular structure of the ablated compounds is a key factor to implement LIBS as characterization tool of molecular solids.

2. Fundamentals of LIBS

Laser-induced plasmas are non-stationary bodies whose stages of generation, evolution, and extinction are framed within a defined temporal scale. Figure 1 illustrates a simple sketch of the progress of plasmas generated with nanosecond (*ns*) laser pulses under air atmosphere at atmospheric pressure. It all begins with the delivering of a pulsed laser beam that is tightly focused onto the target surface. As seen, during the first instants of the laser-surface interaction (only a few nanoseconds after its shock), a fraction of the delivered radiative energy enters the target. This absorbed radiation produces a high energy density at the focal point that leads to a heating and a vaporization of a very thin and slightly deep layer from the surface, followed by a mass removal process called ablation.[40] Several processes such as phase transitions and material ejection occur. If the energy provided by the incoming laser radiation is sufficiently high, heated material in the vicinity of the surface induces stress waves of sufficient magnitude to plastically deform it. Consequently, a thermal expansion at the surface occurs, and a weak plasma that propagates away from the target surface is generated; the plasma ignition has begun. Then, the arrival of the tailing part of the laser pulse contributes to various interaction-based phenomena such as electron capture, collisional excitation and ionization, recombination processes and fragmentation of higher clusters, occurring inside the plume.[41] Consequently, due to the absorption of that remaining energy, a plasma plume with elevated both temperature and electron density, and sown with electrons, ions, atoms as well as small molecules and clusters is created.

After the end of the laser pulse, the plasma plume continues its expansion into the surrounding atmosphere and interacts with it. A shock wave, which propagates along the direction of plasma expansion, is also created. As the plasma evolves its temperature decreases and the excited species relax producing spontaneous emission of radiation. The emitted light is spectrally and temporally resolved into a spectrograph providing analytical information of the constituent elements

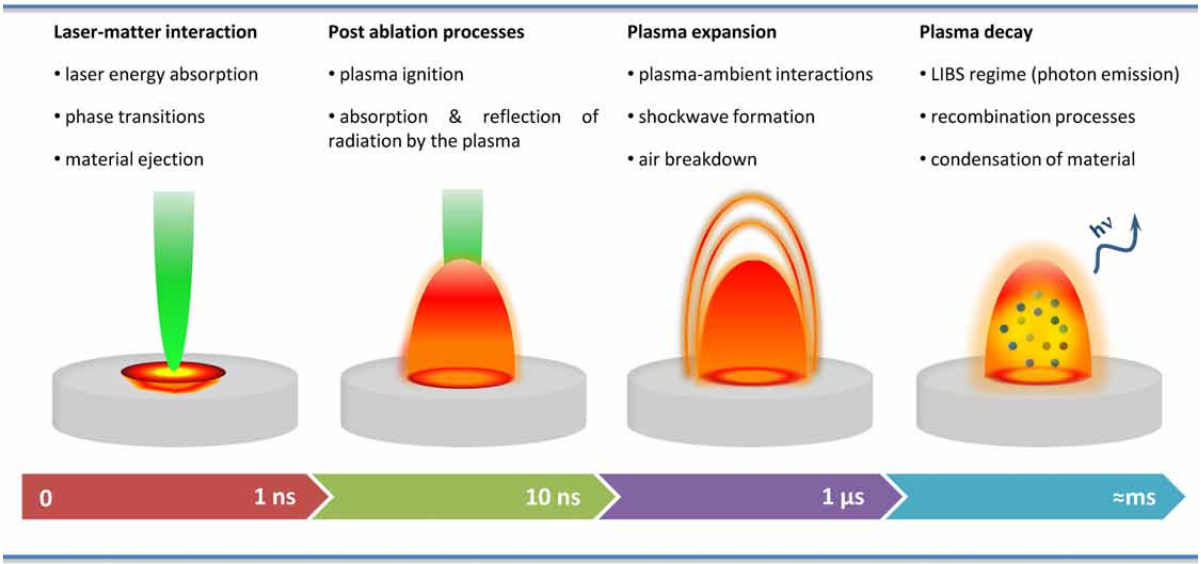

Figure 1. Representative time-scale for the evolution sequence of a plasma induced by a *ns* laser pulse.

of the ablated sample. Finally, the plasma condenses itself and disappears in the order of few milliseconds after the laser impact.[17,42,43]

A comprehensive description of all processes following the laser-matter interaction will be discussed in the next subsections. It must be noted that mechanisms will be described for the general case of *ns*-LIBS. The characteristics of ultrafast laser ablation will be discussed as a particular case since the time-scale for the ablation process and the plasma evolution differ from the *ns* regime.

2.1. Ablation process

In the context of spectroscopy, ablation is the process of mass removal following the absorption of laser radiation by a solid material.[40] Several mechanisms such as thermal diffusion, melting, and intense evaporation of the sample are involved in laser ablation. The process of mass ejection produces a crater on the sample surface. This crater is usually circular; however, its shape depends on the laser beam profile (commonly Gaussian or flat-top) and the focusing optics. In addition to the imprint of the laser impact other features can be distinguished on the crater

surroundings. Minute particles generated by condensation during the plasma cooling may drop in the form of deposits around the crater. If a melt phase is also present, splashes and droplets of liquid material may also solidify on the sample surface.[43]

Laser ablation can be described as a photothermal, a photochemical or a photophysical process. The occurrence of each process depends on the laser pulse characteristics −mainly radiation wavelength and pulse duration− as well as the type of material analyzed (i.e. metals, ceramics or organics). In photothermal ablation, the excited electrons due to photon absorption are slowed (thermalized) on the picoseconds scale. A heating of the sample occurs in the focal volume, thereby inducing the degradation of the lattice and the cleavage of chemical bonds if they exist. Conversely, in photochemical ablation, the direct absorption of more energetic photons is able to generate the lattice breaking without preheating. An intermediate situation exists when both the thermal and the non-thermal mechanisms contribute to the sample ablation. In this instance, the ablation process is guided by a photophysical mechanism.[44]

Several diagnostic techniques like fast imaging,[43,45-47] shadowgraph imaging[48-50] and light scattering[51] have been used to monitor the evolution of the ablation process following the laser impact on the sample. All these efforts have helped considerably to boost knowledge on laser ablation. However, a complete collection of all the involved mechanisms has not yet been faithfully established.

There are also two parameters that allow evaluating the aftermaths of the ablation process: the *ablation efficiency* and the *ablation rate*; frequently used to quantify the amount of material removed from the sample surface under the action of the laser pulse. The former may be defined as the ratio of the volume of matter ablated (cm^3) to the laser pulse energy (J) [52] or, equivalently, by the ratio of the crater depth (cm) to the laser fluence ($J\ cm^{-2}$).[53] Likewise, the *ablation rate* refers to mass ablated (g) per unit time (s) and per unit area (cm^2). Alternatively, this parameter may be defined as the ablated mass per pulse or ablated thickness per pulse.

2.2. Plasma ignition

The ignition of laser-initiated plasmas begins with the gas breakdown by the tightly focused laser pulse. The normal energy dosage needed for the plasma onset lies in the range between 10^8 and 10^{10} W cm^{-2} for solid samples.[2] The plasma formation begins by *multi-photon ionization* process (R.1.) whereby atoms and molecules absorb enough photons to ionize, while they release free electrons. From the incoming radiation the high density of generated electrons gains energy. Consequently, the transference of energy from electrons to other atoms from the sample occurs, and the process progresses by *avalanche ionization or cascade ionization* (R.2.). These sequences of events may be schematized as follows:

$$A + nh\nu \rightarrow A^+ + e^- \qquad \text{(R.1.)}$$

$$A + e^- \rightarrow A^+ + 2e^- \qquad \text{(R.2.)}$$

where n is the number of photons, h is the Planck´s constant, ν is the frequency of radiation, A is an atom and A^+ is a single charged atom.[54]

The possible participation of an additional mechanism called *Coulomb explosion*, must be also contemplated. After the detachment of electrons from the sample by multi-photon ionization, a surface charge grows and the ions in the lattice undergo a strong repulsion. If this electrostatic repulsion is able to overcome the lattice bonding energy, ions are ejected from the sample surface to recover neutrality. Due to the electrostatic nature of this process, its occurrence is unlikely to emerge during laser ablation of conductive materials.[55] In contrast, for dielectrics and semiconductors the contribution of such mechanism may be substantial.[56]

Although all the above mentioned mechanisms may coexist, a set of generalities may be pointed out according the nature of the samples and the properties of the radiation. The ablation of conductor materials is generally guided by thermal processes and the *cascade ionization* when long laser pulses and long wavelengths are used. Conversely, the happening of *multi-photon ionization*

and *Coulomb explosion* processes is more frequent in laser ablation of dielectric materials. Furthermore, both processes are usually linked to ultra-short pulses, high irradiances and short wavelengths.

2.3. Expansion of the plasma plume

Once the plasma plume has been created above the target surface, it expands preferentially forward into the surrounding ambient, in opposite direction to propagation of the laser pulses. When the emerging plasma interacts with the incoming laser radiation, a part of the pulse energy stimulates the heating and the ionization of the vapor, while the other fraction continues toward the sample surface.[43] The interaction between the plasma and the laser pulse during the initial stage of expansion leads to the so-called laser-supported absorption waves (*LSAWs*) that govern the propagation of the plume into the surrounding atmosphere. Depending on operational parameters such as the laser fluence and buffer gas conditions, three main types of *LSAWs* can be differentiated: *laser-supported combustion* waves (*LSCWs*), *laser-supported detonation* waves (*LSDWs*), and *laser-supported radiation* waves (*LSRWs*). Differences between them, featured by velocity, pressure and the effect of the radial expansion on the subsequent plasma evolution, arise from the different propagation mechanisms of absorbing front into the cool transparent atmosphere. Figure 2 schematically depicts these three main propagation mechanisms of *LSAWs* according to the amount of laser energy deposited per unit area –fluence. At low fluences, *LSCWs* frequently dominate the plasma expansion (Figure 2A). In this model, a zone of post-shock gas at constant pressure separates the precursor shock front, which is located ahead of the absorption zone that is attached to the plasma volume, which, in turn, is in contact with the target surface. Despite that the shock wave enlarges the gas density, pressure, and temperature, the region of post-shock gas continues to be transparent to the laser radiation. Hence, residual laser energy is efficiently absorbed by the front edge of the plasma while propagates into the shocked gas. The major mechanism

causing *LSC* wave propagation is radiative transfer from the hot plasma to the cool high-pressure gas created in the shock wave. At intermediate fluences, the propagation of plasma plume is governed by *LSDWs* (see Figure 2B). In this case, the post-shock gas zone is located slightly behind the shock front and also slightly ahead of the plasma volume, which is also detached from the target surface. In the *LSD* regime the laser energy is absorbed in the post-shock gas zone and the plasma volume is heated isometrically, that is, the absorption zone reaches a pressure, temperature, and density higher than the vapor gas placed just above the sample. Thereby, the shock front enhances efficiently and a great thrust is imparted to the target surface. Consequently, the expansion of the LSD wave is governed by such absorption mechanism. Finally, at very high fluences, *LSRWs* are produced (see Figure 2C). In this case, ultrafast expansion leads to the coupling of the plasma volume and the absorption zone but all significantly detached from the target surface. The generated plasma has very elevated both temperature and density. Then, extreme UV radiation emitted by such plasma heats and ionizes the ambient gas without any change in pressure and density. Consequently, a large fraction of the incident laser radiation is absorbed and prevented from being delivered to the target surface.[57]

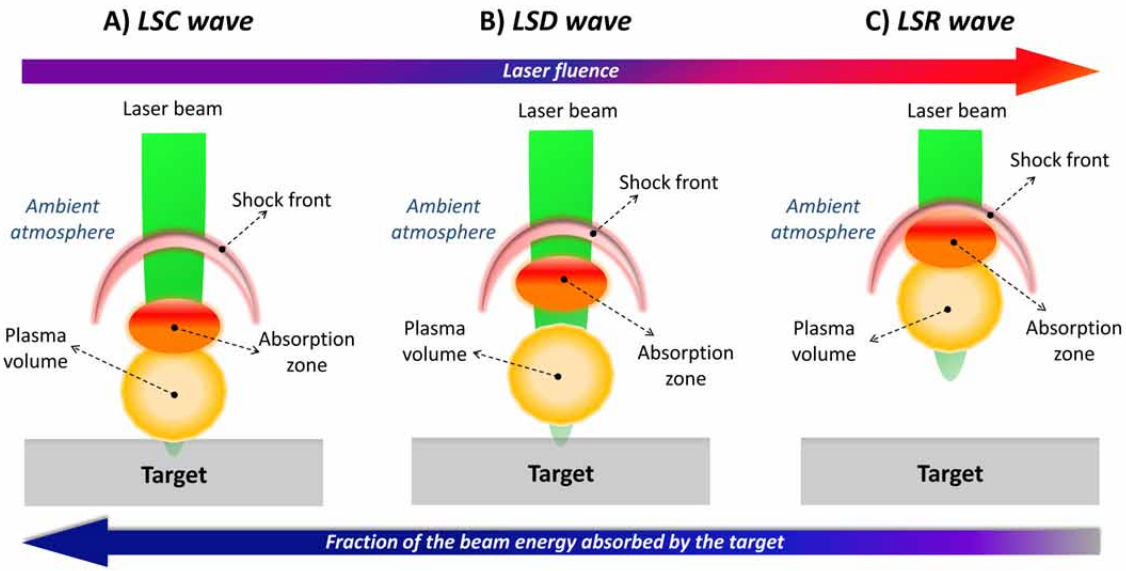

Figure 2. Schematic view of the structures of A) laser-supported combustion (*LSC*), B) laser-supported detonation (*LSD*), and C) laser-supported radiation (*LSR*) waves expanding into a surrounding ambient at atmospheric pressure. This figure has been adapted from similar one featured in the reference 58.

Furthermore, when a high power density is employed, optically dense plasma may be obtained. In such a situation, the surface of the plasma plume may be shielded, what prevents that the tailing part of the laser pulse reaches the sample. This phenomenon is known as *shielding effect.* It occurs when the plasma frequency (ν_p), which is defined by equation 2.1, becomes greater than the laser frequency (ν_l).

$$\nu_p = \left(\frac{4\,\pi\, n_e\, e^2}{m_e}\right)^{1/2} = 8.9 \cdot 10^3\ (n_e)^{1/2} \quad [\text{Eq. } 2.1]$$

where n_e is the plasma electron density (cm^{-3}), e is the electron charge, and m_e is the electron mass.

In terms of electron density, a critical value may be calculated through equation 2.2 for a specific laser wavelength (μm):[42]

$$n_c \sim \left(\frac{10^{21}}{\lambda^2}\right)\ \ cm^{-3}\ [\text{Eq. } 2.2]$$

where n_c is the critical electron density (cm^{-3}) and λ the excitation wavelength.

The plasma shielding reduces the amount of energy arriving at the target through both the partial absorption and the reflection of the laser beam. This event may revert in the saturation of the ablation rate with increasing laser fluences.[59] Its occurrence depends on several factors namely energy, duration and wavelength of the laser pulse, the surrounding atmosphere and the sample properties.

Three principal mechanisms that may contribute to the plasma shielding are *inverse bremsstrahlung (IB), photoionization (PI) and Mie absorption*[60]. The extent in which each mechanism affects the global absorption coefficient is conditioned by the excitation wavelength. *Rozman et al*. proposed equation 2.3 to calculate an overall plasma absorption coefficient (α_{plasma}) that includes these contributions:

$$\alpha_{plasma} = \alpha_{IB} + \alpha_{PI} + \alpha_{Mie}\ [\text{Eq. } 2.3]$$

The *IB* implies the absorption of photons by free electrons moving through the electric field of an ion or less likely by a neutral atom. Although this process is dominant in plasmas induced by IR radiation, its effect is significant when using UV radiation and high both electronic density and temperature of the plasma are reached. The *IB* absorption coefficient[61] via free electrons (α_{IB}) can be calculated by equation 2.4:

$$\alpha_{IB}(cm^{-1}) = 1.37 \cdot 10^{-35}\, \lambda^3\, n_e^2 T_e^{\frac{1}{2}} \quad \text{[Eq. 2.4]}$$

where λ is the laser excitation wavelength, n_e is the electron density and T_e is the electron temperature of the plasma.

On the other hand, the *PI* mechanism consists on the absorption of a photon into a neutral atom that is ionized. Its occurrence is more probable with UV excitation. The photoionization absorption-coefficient is obtained by summing up all the excited states whose ionization energies are smaller than the laser photon energy. This coefficient can be predicted with Kramer's formula:[62,63]

$$\alpha_{PI} = \sum_{n} 7.93 \cdot 10^{18} \left(\frac{E_n}{h\,\nu_l}\right)^3 \left(\frac{1}{E_n}\right)^{1/2} N_n \quad \text{[Eq. 2.5]}$$

where E_n and N_n are the ionization energy and number density of the excited state n, respectively; h is Plank's constant; and ν_l is laser frequency, being I is ionization potential of the ground state.

Finally, *Mie absorption*, which is caused by small particles or clusters, governs in low temperature plasmas. Thus, the contribution of this effect to the overall absorption coefficient is negligible in laser-induced plasmas.

Moreover, during the plasma expansion the interaction between the plume and the surrounding atmosphere results in emissions from the species composing the buffer gas. For instance, when plasmas are induced in air atmosphere, nitrogen, oxygen and water vapor molecules may be dissociated and emissions from excited atoms of hydrogen, oxygen and nitrogen are manifested. This process is referred as *secondary ionization* of the surrounding atmosphere.

2.4. Decay and emission of the plasma

Shortly after the end of the laser pulse the plasma possess an extremely high temperature and an elevated electron density. These conditions give rise to intense continuum emission which dominates the spectral response in the first instance. Hence, conventional spectral measurements are registered between some nanoseconds and few microseconds elapsed from the incidence of the laser pulse onto the target. As the plasma evolves, it cools off, the temperature and electron density decrease sufficiently, and ionic and atomic emission lines begin to be resolved within the spectral signal. While ionic lines are normally observed along just some hundreds of nanoseconds, the atomic signals have a larger life time and their emissions can be extended during a few microseconds. The prevalence of these emissions over time is closely tied to ablation conditions, since these influence the plasma properties and the density of its population species. At the later stages of the life time of the plasma, some emissions associated to small molecules, clusters and particles can also emerge. Some of the possible mechanisms leading to the formation of these species are molecular fragmentation, recombination processes, vapor condensation, liquid sample ejection, phase explosion (occurring when a material is heated beyond its limit of thermodynamic stability) and *spallation* (photomechanical fracture due to thermo-elastic stress wave).[64-67] Typically, the light emitted from the expanding plasma is dispersed using a spectrograph and subsequently gathered and analyzed. The spectroscopic analysis of all the optical emissions from the excited species enables identification of the elemental composition of the ablated material. Furthermore, the gathered emission spectrum provides information regarding the temperature and particle density of the plasma itself, as discussed below.

The temporal behavior of laser-induced emissions is exemplified by Figure 3. The time-resolved spectral signals of graphite plasmas generated in air at atmospheric pressure are depicted. Immediately following plasma ignition, that is a for a delay time below 0.5 μs, all emissions are entirely masked by the high continuum –spectrum not shown. As the plasma evolves, the emissions

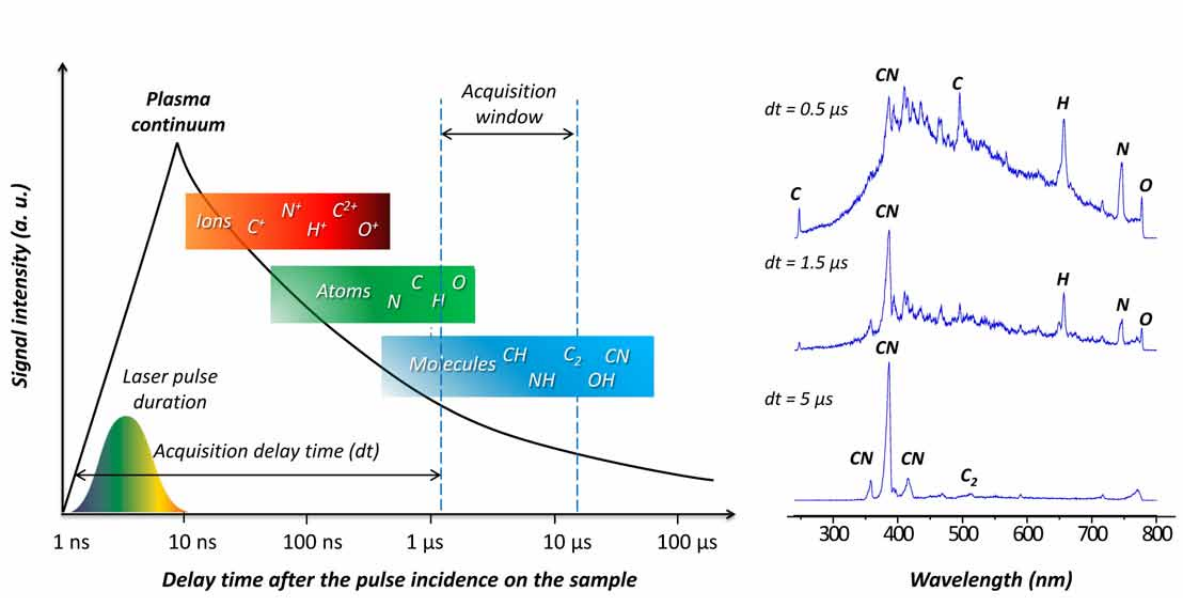

Figure 3. Temporal behavior of optical features in emission spectra gathered from graphite plasmas induced in ambient air at atmospheric pressure. This figure has been adapted from similar one featured in the reference 42.

associated to native C atoms from the sample, new formed species –CN–, as well as elements coming from the secondary ionization of the surrounding air (H, N and O) stick out above a broad nonspecific background. As seen, a gate delay of about 1.5 µs is required for almost entirely suppress such continuum emission. Later, as the plasma cools down, emissions of C, H, N and O become extinct while CN and C_2 molecular band systems dominates the spectrum.

2.5. Parameters for plasma characterization

As commented above, the plasma generated contains atoms and ions in different excited states, free electrons and radiation. Considering that properties of the plasma define emitted light, there is no question that such light constitutes a faithful reflection of the several species populating the plasma[68] and the different physical-chemical processes occurring.[69] In addition, the analysis of this light allows diagnostics of plasma properties through the computation of a pair of important plasma parameters from the LIBS spectra: the electron density (n_e) and the temperature (T). Brief comments on these parameters are provided below.

- *Electron density*

Electron density, in general, specifies the thermodynamic equilibrium states of the plasma.[70] Optical emission spectroscopy methods may be employed for its determination. One of the methods employed to calculate the electron density is based on the broadening of emission lines due to the *Stark effect* (collisions of the emitting atoms with electrons and ions). For non-hydrogenic ions, the Stark broadening is dominated by electron impact. Then, the full width at half maximum (FWHM) of lines, $\Delta\lambda_{1/2}$, is given by the following expression:

$$\Delta\lambda_{1/2} = 2W \times \left(\frac{n_e}{10^{16}}\right) nm \quad [\text{Eq. } 2.6]$$

where n_e is the electron number density (cm^{-3}) and the coefficient *W* is the electron impact parameter.

- *Plasma temperature*

Plasma temperature determines the strength of the different distribution functions describing the plasma state.[71] Several methods based on the line emission of neutral atoms and ions as well as on the line-to-continuum ratio are nowadays available to determine the temperature of plasmas (*T*). The requirements of local thermodynamic equilibrium (*LTE*) and optically thin plasmas have to be satisfied to apply the greater number of methods. However, alternative methods, which allow calculating the plasma temperature without making any *LTE* assumption, have been also proposed by several authors.[31] A general approach for temperature calculation is based on the use of Boltzmann plots[72]. For plasma in *LTE*, the Boltzmann's law relates the total density N(T) of a neutral atom or ion to the population of an excited level[73,74], as expressed in equation 2.7:

$$I_{mn} = -\frac{hc}{4\pi\lambda_{mn}}\frac{N(T)}{U(T)} g_m A_{mn} exp\left(-\frac{E_m}{k_B T}\right) \quad [\text{Eq. } 2.7]$$

where I_{mn} is the relative line intensity, λ_{mn} is the wavelength, A_{mn} is the transition probability, g_m is the statistical weight for the upper level; E_m is the energy of the excited level, T is the temperature, k_B and h are Boltzmann and Planck constants, repectively, and U(T) is the partition function.

Taking natural logarithm in the Boltzmann equation, such method allows calculating the excitation temperature by plotting $ln(I_{mn}/g_mA_{mn})$ *vs* E_m. Once known the slope of this plot, which is equal to $(1/k_BT)$, the plasma temperature (T) can be estimated. Although the range of plasma temperatures may broadly change depending on both the LIBS operational conditions and the sample nature, values from 6000 K to 15000 K are characteristically reached.[75,76] Commonly, plasma temperature is calculated within a specific integration window of the optical signal and an average value of such temperature is provided. However, the plasma temperature undergoes temporal variations. That is, it normally drops as the gate delay increases from the plasma formation until its extinction. These decay trends may also differ as a function of the operational conditions and gas environments.

On the other hand, the vibrational (T_{vib}) and rotational (T_{rot}) temperatures of excited radicals may be determined from their molecular emission bands. Several procedures such as the use of Boltzmann plots[75] and a fitting of experimental spectra[74] to synthetic ones may be employed. As an example, LIFBASE free software program may be used to simulate spectra of the OH, CH and CN radicals, among other species.[77]

- *Local thermodynamic equilibrium*

Meaningful application of theoretical Boltzmann–Maxwell and Saha–Eggert expressions that relate fundamental plasma parameters and concentration of species essentially requires the existence of local thermodynamic equilibrium (*LTE*) in the plasma.[78] Laser-induced plasmas are characterized by strong radiative losses and by high expansion velocities. As a result, these plasmas can be in strong non-equilibrium. When plasma is in thermodynamic equilibrium (*TE*), each process is balanced by its inverse process, which is known as the principle of detailed balancing. The system reaches a uniform steady state of thermodynamic equilibrium when there is an overall balance in the collision processes suffered by the particles. However, when the energy lost by radiative processes is smaller than that involved in collisions between species that govern transitions and chemical

reactions, the *LTE* is set.[76,79] For satisfying this condition a sufficiently high electron density has to be reached. The most popular criterion usually invoked as a proof of the existence of *LTE* in the plasma is the McWhirter criterion.[80] Even though this criterion is known to be a necessary but not a sufficient condition to insure *LTE*. The McWhirter criterion allows calculating the critical electron density (n_e) for which the plasma is within *LTE* using the following equation:

$$n_e \geq 1.6 \times 10^{12} T^{1/2} (\Delta E)^3 \ cm^{-3} \quad [\text{Eq. } 2.8]$$

where *T* is the plasma temperature (*K*) and *ΔE* is the higher energy difference (eV) of the levels whose populations are given by *LTE* conditions. This approach assumes that the collisional rates are at least ten times the radiative rates within the plasma. The critical electron density for LIBS plasmas is usually estimated in the range of 10^{15}–10^{16} cm^{-3}.

2.6. Influence of operational parameters in laser-induced plasmas

Without forgetting that nature and specific characteristics of laser-produced plasmas are closely tied to the type of material, the whole chain of possible events and processes occurring during plasma formation intimately depend on the radiative attributes, that is, laser pulse operating parameters like its energy (*E*), wavelength (*λ*), duration (*τ*) and shape. At the same time, the pressure and composition of the background atmosphere play an important role in the subsequent plasma evolution.[1] From a theoretical point of view, the ideal for attributing the changes observed on the ablation process and the optical spectra would be to have reliability that they are associated to the variation of one parameter. Unfortunately, the complex interplay between different processes generating the LIBS plume and the dominance of some over others as a function of the conditions makes difficult to ascertain which effects are most responsible for the observations. The following sections briefly encompass a discussion on the main effects when varying operational parameters in LIBS.

2.6.1. Laser pulse energy

Far beyond the absolute energy per pulse, two magnitudes are interchangeably used to describe the energetic regime for laser ablation: *fluence* (energy per unit area, J cm^{-2}) and *irradiance* (power per unit area, GW cm^{-2}). Both are referred to the total laser pulse energy deposited on the target surface per unit of area, therefore experimental diagnosis of these parameters requires a judicious estimation of the spot size over which the laser beam is focused. The disparity between the two terms is that *irradiance* contemplates the laser pulse duration whilst the *fluence* is a time-integrated measurement of the applied energy.

All processes occurring as a consequence of the laser-sample interactions such as heating, melting and vaporization of the sample are naturally influenced by the energy dosage provided.[81] As a general trend, increasing laser *fluence*/*irradiance* above the ablation threshold of the sample (minimal *fluence*/*irradiance* leading to a mass removal process) entails larger both crater depth and ablated mass. However, when laser energy input on the sample considerably exceeds such threshold, very high density plasmas are generated. Consequently, this density may partially or entirely shield the sample from the laser radiation; not the full energy is transferred from the laser pulse to the original material. Hence, a saturation of the ablation rate can be detected.[82,83]

The energetic regime in which ablation occurs also affects the geometrical aspect (size and shape), the dynamical behavior as well as the inherent properties (temperature and species number density) of expanding plasmas. Generally, the size and the expansion velocity of plasmas proportionally increase with the laser energy. With regard to the shape, at low irradiance, the expansion of plasma, containing little ablated matter and having low internal energy, prevails in a radial direction over that in a longitudinal one. Thus, the plume core remains "*attached*" to the sample surface, having a more disk-like shape. In contrast, at high irradiance, the plume is capable of pushing the surrounding air far enough in front of itself in order to expand into a hemispherical

shape because of the higher content of ablated matter and its larger internal energy.[84] In turn, an increase is detected for T and N_e with the raise of the irradiance.[85]

All these effects of laser irradiance also became evident on the surface morphology of the interrogated target. Disparity between plasmas produced from the same sample but at distinct irradiation regimes are considered to originate in the different mass removal mechanisms occurring, as identified through various kinds of structures such as ripples, cones, cavities, and waves like ridges, at the center and peripheral regions of the generated crater print.[86]

2.6.2. Laser pulse wavelength

Excitation laser wavelength (λ) also plays an important role on plasma generation, laser-plasma coupling, plasma expansion dynamics and confinement, plasma properties and crater generation.[87] The differential effects that laser pulse wavelengths cause on the generated plasmas have not been only evaluated experimentally[88-92] but also modeled theoretically.[81,93]

Typically, harmonics of different orders (λ = 532, 355, 266 and 213 nm) from the fundamental wavelength of a Nd:YAG laser (λ = 1064 nm) have been used to investigate the influence of the laser wavelength in LIBS experiments. The energy of incident photons affects the laser-target coupling and the ensuing laser-plasma interactions that, in turn, modify the morphology of the plasma plumes. In line with this, *Boueri et al.*[50] captured shadowgraph pictures of plasmas induced from Nylon. Spherical shape for the shock wave expansion of plasmas generated by UV radiation was observed. Conversely, a preferential propagation in the direction of the laser incidence resulted from IR excitation. In good agreement with this work, cylindrical plumes were observed following the laser ablation of aluminum with 1064 nm radiation. The cylindrical morphology of plumes denotes the dominance of *IB* absorption by plasmas at long laser wavelength.[87] Similarly, in the laser ablation of polymers, lower plasma thresholds and more intense emissions for IR excitation

than those for UV were observed. These results were attributed to higher plasma temperatures for the former case since absorption by the plasma due to *IB* increases with wavelength.[94]

Particularly, in the field of laser ablation of organics there is still an ongoing discussion about the variety of mechanisms for material removal that are active depending on the particular excitation wavelength, for example, whether in addition to *photothermal* processes, *photochemical* reactions or even *photophysical* and *mechanical* processes are relevant.[95] In a first step, it is generally recognized that for *ns* laser pulses, the energy of the laser photons is exploited for electronic excitation. The following steps are still under discussion. In *photochemical* processes, electronic excitation by the optical absorption of high energy photons results in direct bond breaking.[96-98] The molecules come into a dissociative electronic excited state since the chemical bonds breakdown due to the expulsive force between atoms. Hence, when the energy of the incident photons is higher than the energy of a specific bond, this may be directly broken by just absorbing one photon. For example, a typical C-N bond, with a dissociation energy of 3.04 eV, may be broken by absorbing one UV photon (λ = 266 nm) with an energy of 4.66 eV. However, when using IR radiation at 1064 nm (1.17 eV), a multiphoton absorption process would be required for the photodissociaton of this bond. In this case, *photothermal* processes are more probably to occur. The electronic excitation is thermalized on a picosecond (*ps*) timescale, and the progressive heating of the target results in thermal bond breaking.[99-101] Finally, if both thermal and non-thermal mechanisms significantly contribute to the overall processing rate, the process is denoted as *photophysical*. Two independent channels of bond breaking[102,103] or different bond breaking energies for ground-state and electronically excited-state chromophores[104,105] are supposed for this mechanism. Consequently, together with differences in the morphology of laser-produced plasmas, dissimilarities between the ablation craters printed as a function of the irradiation wavelength have been observed. Just for instance, the laser ablation of polyvinyl chloride with 266 nm excitation generated clear craters on the polymer surface, whereas with 355 nm wavelength larger thermal damage was produced on the

material; circumstances also denoting the dominance of photochemical and photothermal processes, respectively.[90]

2.6.3. Laser pulse duration

The pulse duration (τ) is often defined as a full width at half maximum (*FWHM*), that is, the width of the time interval within which the power is at least half the peak power. Any focused laser pulse, whatever its duration, meets the required conditions in ablation since usually the rate of energy deposition greatly exceeds the rate of energy redistribution and dissipation. As a result, extremely high temperatures are attained in those regions where energy absorption occurs. Since the mechanisms of energy dissipation are variable, changes in the temporal width of laser pulses lead to fundamental differences of the ablation process.[106] A differentiation between ultrashort (<1 *ps*) or short (>1 *ps*) ablation regimes is widely accepted. Similarly, the terms *ns*-LIBS and *fs*-LIBS are often found in literature.[107] In this section, a concise description of the main effects of the laser pulse duration in laser-induced plasmas will be accomplished.

Figure 4 shows a schematic illustration where the main features of *fs*-LIBS and *ns*-LIBS, at the different stages of the plasma evolution, are compared. Commercially available *fs* and *n*s lasers typically generate pulse durations of tens of *fs* and few *ns*, respectively. Hence, effects of laser pulse durations of 60 *fs* and 8 *ns* (18 μm and 2.4 m in length, respectively) have been discussed as hypothetical cases in this example. In a first stage, when incident light strikes the target surface, the photons of the laser pulse, regardless its length, are absorbed by the material. For *fs*-LIBS, the absorption of radiation and the material heating is extremely fast. Indeed, the thermal conduction from the laser-impact area to the lattice is minimized because the pulse duration is shorter than the timescale of photon-electron lattice interactions.[108] However, with *ns* excitation, there is a longer interaction time between the laser beam and the sample. Therefore, thermal effects generally take

places during the ablation process. As observed, at early times of plasma formation, the closing tail of the *ns* pulse may also interact with the expanding plasma and reheat it, thereby increasing its temperature and electron density. Conversely, laser-plasma interactions do not exist during ultrashort excitation since the *fs* pulse delivery finishes before the plasma onset. In this context, phenomena such as the reheating of the plasma and its shielding effect are expected to have negligible contributions.[50] In particular, reheating of the plasma is the responsible cause of the significantly higher intensity of continuum emission identified in *ns*-LIBS spectra as compared to that detected in *fs*-LIBS ones.[109,110]

Numerous studies have been conducted in the last years to assess the substantial differences between *ns* and *fs* laser-produced plasmas.[80,111-113] For instance, concerning plasma geometry, *ns* laser-induced plasmas typically show spherical expansion whereas *fs* excitation produces narrower plasmas, which preferentially expand normal to the sample surface. Furthermore, decay rates of electron density and temperature have been found faster in plasmas generated with *fs* pulses as compared to those obtained for *ns* laser-generated plasmas.

Finally, as indicated in Figure 4, substantial differences in shape as well as volume have been noticed in the morphology of craters formed by lasers with different pulse widths ($t = \infty$).[114]

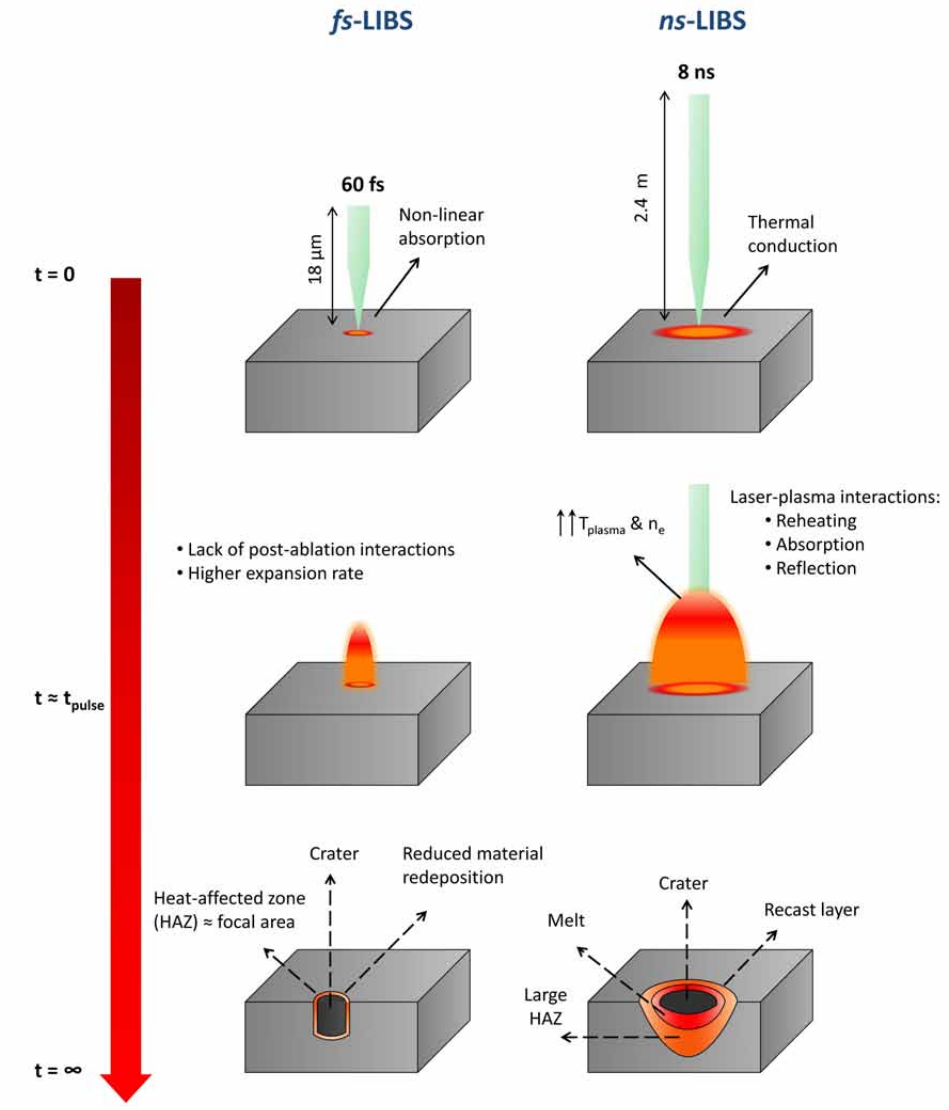

Figure 4. Schematic representation showing a comparison of main features of *fs*- and *ns*-LIBS

During *ns* irradiation the ablation proceeds via melt expulsion guided by the vapor pressure. This is an unstable process that generates a crater on the sample surface accompanied by a melt or recast layer. Hence, *ns* laser ablation craters usually show significant irregularities in the crater rims because of resolidification of splashed melt layers. A wide heat affected zone (*HAZ*) is also commonly observed. In contrast, when using ultrafast laser pulses, absorption, phase transformation and ablation processes happen in a short time scales (~ps), the heat load to the surrounding material is minimized. Thus, craters formed by *fs* laser ablation are cleaner and deeper with well-defined edges. In addition, a negligible *HAZ* is generated.[49]

In summary, differences in duration of laser pulses lead to completely different mechanisms of laser-target and laser-plasma interactions and plasma expansion processes, which dictate the plasma lifetime, plasma emission and analytical figures of merit attained under each excitation regime.[16,115]

2.6.4. Surrounding atmosphere

Although LIBS is classically conducted under standard Earth atmosphere, there are is growing interest in performing experiments under atmospheres with distinct chemical composition and gas pressure. The properties of the surrounding media critically influence the expansion dynamics of plasmas and their ensuing spectral features (e.g. emission lines intensity and broadening). General considerations on the impact of the ambient gas are pointed out in this subsection.[116]

- ***Effect of gas pressure***

As far as it is known because of the expansive nature of laser-produced plasmas, the background gas pressure may affect to the laser ablation of the sample, as well as to the expansion and emission of the plume.[117] Studies on the effects of ambient pressure have revealed that the processes of heating, melting and vaporization of the samples at various ambient pressures is very similar since generally pressure has a minute influence on the fraction of absorbed laser energy.[118]

Regarding the plasma dynamics, the general effect of the background gas is reported to be the spatial confinement and slowing down of the expanding plume. The increase in the pressure of the atmosphere, regardless its composition, maximizes the confinement of the plasma and reduces its expansion rate. Moreover, the recoiling of plasma may occur.[119] Consequently, at very low gas

pressure plasma plumes of larger size and with lower density of species and temperature as compared with those induced at higher pressures.

Variations in gas pressure involve changes in its density. Such a circumstance has also demonstrated to have an impact on the reactivity of the excited species that populate the plasmas because of alterations on their collision rates. An example of this is the recombination process in plasmas of organic samples of native C with atmospheric nitrogen to generate CN radicals. The increase of the N_2 density in the medium accelerates the kinetics of species, thereby raising the formation rates of that molecular radicals.[120]

Since the pressure of the bath gas influence the development and properties (e.g., *T* and N_e).of laser-produced plasmas, their effects on the analytical performance of LIBS for chemical analysis are particularly manifested in peak spectral resolution, emission signal intensity, signal-to-noise ratio (*SNR*) and amount of material ablated. In the initial stages (i.e., first few nanoseconds), plasmas at two different pressures behave very similar, thus, there is little to no gas effects during the initial plasma lifetime. However, gas pressure modifies the plasma confinement as it departs from the target surface. At high pressures, plasma energy is quickly lost to the surrounding atmosphere by collisional processes with the surrounding gas and therefore the plasma is short lived. In contrast, at low pressures the plasma expands much further into the ambient atmosphere but it is not cooled rapidly by the surrounding species. Hence, lifetime of the emitting species is long and the integrated emission volume becomes large. Consequently, more light from the laser plasma can be collected, and higher peak intensity of emission lines is observed. Notwithstanding this, there is a lower limit in the gas pressure (ca. 5^{-10} Torr) below which the plasma confinement seems to be insufficient. In this case, the collisions between the expanding plasma and the ambient gas decrease, thereby leading to a reduced collisional excitation. Consequently, the intensity of the emission signals may drop notably.[121]

In this context, because of the adiabatic expansion and free of plasma-ambient interactions, spectra gathered from plumes induced into vacuum exhibit a lower background emission –better *SNR*– and narrower peaks –better spectral resolution–, as compared to those acquired from plasmas at atmospheric pressure. Furthermore, at low pressures, the small electron density of the plume diminishes the occurrence of plasma shielding phenomenon. Consequently, the main portion of the pulse energy is delivered on the target and larger ablation rates and higher crater depth are attained as compared to excitation at atmospheric pressure.[122]

- ***Effect of gas composition***

While the majority of ablation studies are conducted in air, the requirements for improving fundamental knowledge and for coping with challenging novel applications have promoted investigation of LIBS operation under different gas compositions.[123] As with the pressure, effects of distinct background atmospheres on the dynamics of the generated plasmas, their properties –temperature and electron density–, emission intensity, peak widths and profiles as well as mass removal during LIBS have been broadly studied. Unlike the gas pressure that predominantly has repercussion on the plasma temperature, the chemical composition of the ambient gas mainly influences the electron density; associated to the Stark broadening.[124-126]

Thorough studies conducted on the effects of atmospheric Ar, He, and air on plasmas have revealed that Ar and He atmospheres are both effective for increasing LIBS spectral intensity compared to air.[127] Regarding to plasma properties, it is determined that high temperatures and electron densities are attained for plasmas in Ar ambient, whereas low temperatures and electron densities result in plasmas generated in He atmosphere. In this connection, through the study of temporal data, it was also found that Ar ambient led to slow decay of both electron density and plasma temperature, whereas He gas caused a fast decay in both parameters.[128] These differences between values and their ensuing decay of electron density and temperature of plasmas in Ar

compared to He is argued on the basis of the thermal conductivity, 15.76 eV and 24.58 eV, respectively.[129] The lower the ionization potential, the higher the electron density and the plasma temperature, and slower their corresponding decays.

Composition of the background gas has been shown also to influence the diameters and depths of craters and the amount of material ablated. Ablation craters are usually deeper and wider in He compared to those generated in an Ar atmosphere. The dominant mechanism for such improvement seems to be the plasma shielding since the heating of the background gas by inverse *Bremsstrahlung* is less effective for He, thereby leading to lowest plasma shielding and most amount of ablated material.[130] Despite this, the highest overall emission signal intensities are found to decrease in the order of Ar > He, which is largely due to higher plasma temperatures. In contrast, emission lines gathered from plasmas induced in Ar atmosphere manifest a higher Stark broadening than those collected from plasmas generated in He.[131] Furthermore, it should not be forgotten that the background gas may also enhance or quench particular emission lines –fractionation–, thereby causing that peak intensities in the spectrum do not reflect the stoichiometric abundances of the elements in the sample. Because of the proximity of their ionization potential, the behaviors of plasmas induced in air (15.6 eV), N_2 (15.58 eV) and O_2 (12.06 eV) are closer to those evolving in Ar atmosphere.

In summary, as evidenced, the judicious choice of pressure and gas composition dramatically modifies the ablation process and the subsequent LIBS spectra, particularly in terms of intensity and resolution of the spectral signals.

3. LIBS instrumentation

In general terms, LIBS uses instrumentation similar to that used by other atomic emission spectroscopy methods. The distinctiveness of LIBS lies on the use of a powerful excitation source for both the sampling process –ablation– and the later excitation of the constituent elements. In addition to the excitation source, the implementation of a typical LIBS experiment needs some basic instrumental components, which can be summarized as follows: the focusing optics, that is, an arrangement of mirrors and lenses to guide the laser beam to the sample; the light collection system; the spectral detection system; and the device for storing, processing and analysis of the acquired data. Although these basic elements are common to any LIBS setup, the technical requirements of these components must be adapted to the required applications. For illustrative purposes, Figure 5 shows diagrammatically a typical LIBS setup used in local scale lab analysis.

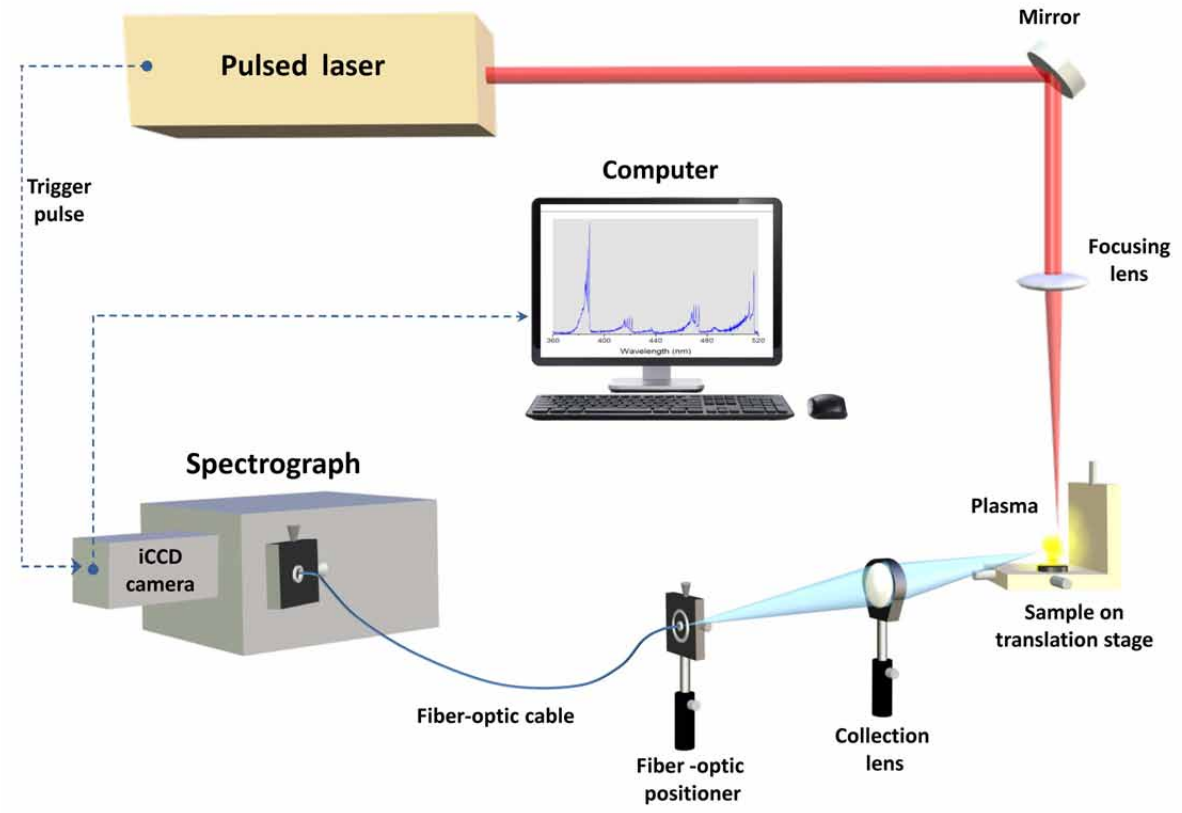

Figure 5. Diagram of a typical LIBS setup.

The main components are depicted: the pulsed laser that generates the powerful light packages used to produce the plasma plume; the optical system for delivering a focused laser pulse to the target sample, comprising a laser wavelength optical mirror and a focusing lens; the target holder; the optical system for collecting the light emitted by the created plasma and for guiding it towards the detection device, comprising a collecting lens and an optical fiber; the detection system consisting of a spectrograph to spectrally resolve the light and a detector –intensified charge-coupled device– to record the light; and the computer, with the specific control software, for acquisition and storage of the spectral information. The following sections encompass a brief description of these key pieces in a LIBS experiment.

3.1. Excitation source

A laser system of high energy as excitation source is the key component within the LIBS framework. In this section, basic principles of laser operation and different laser sources used in LIBS experiments will be briefly described.

The term "LASER" is an acronym for *Light Amplification by Stimulated Emission of Radiation*. The mechanism of stimulated emission produces photons with the same frequency, same phase, same sense of polarization and that propagates in the same direction. Figure 6 sketches the main elements of a laser system to describe the principle behind laser action. A laser basically consists of a *pumping source* that supplies energy to an *active medium* placed on an *optical resonator*. The *pumping source* perturbs the level population distribution in the *active medium* with transitions from the ground state level to the upper level that ultimately results in population inversion. Gas discharge laser lamps and direct-current arc lamps are routinely used as optical pump sources for solid state lasers, whereas gas lasing media is typically optically pumped using radiofrequency. Once the population inversion is reached, the spontaneous emission photons that are emitted along the *optical axis* of the *resonator* are responsible for initiating the formation of an amplified light wave. This wave is continuously reflected forward and backward between the two reflective mirror parallel surfaces that bound the *optical resonator*. For each round trip in the *optical resonator*, the light wave passes through the active medium twice and experiences amplification as long as the active medium exposes the population inversion. Furthermore, the shape and separation of these mirrors define the spatial distribution of the light wave inside the laser. However, while one of these mirrors reflects almost one hundred per cent of the light wave the other is partially transparent to allow its output. The light wave lost in the resonator that passes through the output coupler leads to produce the laser radiation.[132]

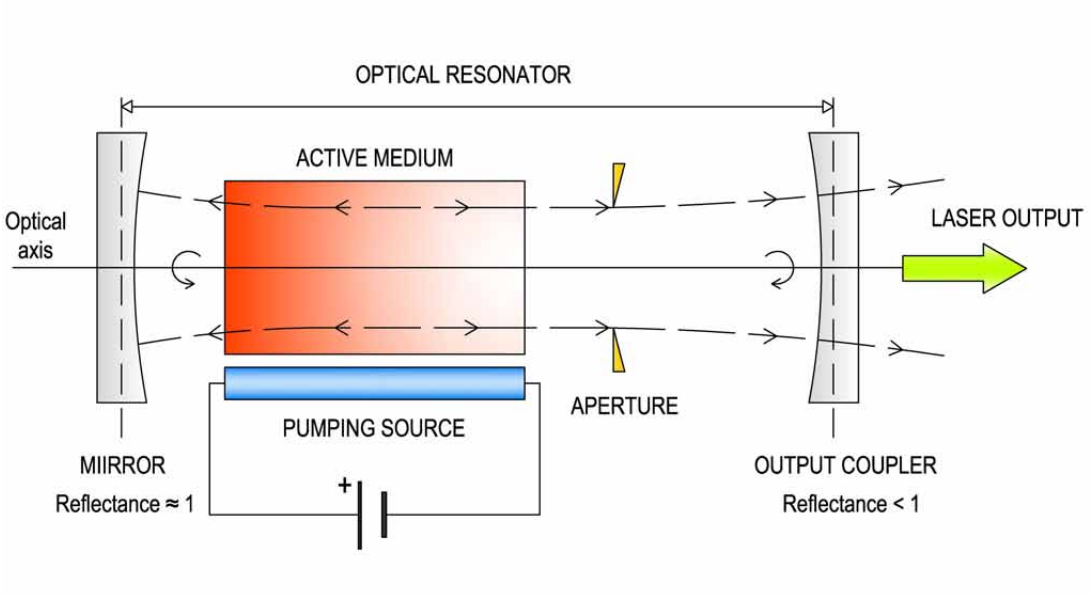

Figure 6. Schematic diagram of a typical pulsed laser system.

The distinctive properties that characterize laser radiation are the brightness, the tunability and high chromaticity, high directionality, temporal and spatial coherence, and controlled polarization.

A multitude of laser types with different wavelengths, energies, pulse durations, and light beam profiles are applied for laser ablation studies and LIBS applications, depending on the requirements of each research. The following paragraphs shortly outline the main lasers used in LIBS.

3.1.1. Nanosecond lasers

Nowadays, the most widespread excitation sources used for LIBS measurements are solid-state lasers, flash lamp-pumped, with Nd:YAG as laser medium and operated in the Q-switch mode to generate high-energy laser pulses with durations in the nanosecond range. These lasers are composed by an yttrium aluminum garnet crystal host ($Y_3Al_5O_{12}$) were neodymium atoms (triply ionized –Nd^{3+}–) are embedded to form the laser active medium. The Nd:YAG laser constitutes a four-level system. The pumping of the active medium, which is normally found rod-shaped, is accomplished by the action of Xe flash lamps, which are capable to produce microsecond to

millisecond duration pulses of broadband light of high radiant intensities at high repetition rates. The flash lamps may simply be arranged parallel to the rod. However, in the most common configuration the flash lamp is a tube located at one of the focus of a mirrored cavity, consisting of an elliptical cross-section perpendicular to the rod's axis, with the laser rod located at the other focus of the cavity. Under this configuration, the full emission from lamp is gathered by the rod. An alternative for pumping the Nd:YAG rod is the use of a semiconductor diode laser pumps (diode pumped solid-state –DPSS– laser). In these kind lasers, the pumping is done either by an array of diodes placed on the side the rod or by a fiber-coupled diode laser that illuminates the endface of the laser rod.[133]

At the same time, for obtaining short and high‐energy pulses, the most common operational manner for pulsed lasers is *Q-switched* mode. While the pumping action is continuous, the light is allowed to reflect in the mirrors only for a short time to achieve the laser action. Such short periodic intervals are controlled by an acousto–optic coupler. An oscillating electric signal drives a transducer to vibrate, which creates sound waves in the crystal, thereby causing it to act as a grating for the incoming light. Thus, when there is no density change along the light path through the crystal, the optical amplification occurs. In contrast, laser action is prevented if light is scattered. The Q-switching allows generating laser pulses of few nanoseconds (5-20 ns) with peak energies from 10 mJ to 1 J. Although the output laser wavelength for the normal operational mode of Nd:YAG laser is 1064 nm, additional output shorter wavelengths may be easily generated with a variety of non-linear conversion techniques – harmonics generation. Non-linear crystals (e.g. potassium dihydrogen phosphate –KDP– or Barium borate –BBO–) are used to frequency doubling (532 nm), to triple the frequency (355 nm), and to frequency quadruplicating (266 nm) of the laser output. Although some larger wavelengths may be tuned, this conversion leads to a notable decrease of the laser energy.[132]

3.1.2. Femtosecond lasers

While lasers with nanosecond pulse duration are the standard "workhorse" for a LIBS setup, the discovery of high fluence solid state materials like Ti:Sapphire together with the invention in the late 1980s of the chirped pulsed amplification (*CPA*) technique, which is based on the stretching in time of the laser pulses prior to their amplification, led to remarkable progress in the development of ultrahigh peak power lasers.[134,135] The basic operating scheme of *CPA* is illustrated in Figure 7. *CPA*-based *fs* laser systems consist of a seeding laser –also known as femtosecond oscillator–, a stretcher, an amplifier and a compressor, which act as detailed below:

(1) As a first building block, the seeding laser is the responsible component to generate *fs* pulses. Although in the past few years new laser materials that can produce *fs*-class pulses have emerged, the shortest laser pulses (<10 *fs*) are typically emitted by Ti:sapphire lasers through the most effective modern short-pulse generation mechanism –Kerr-lens-mode-locking (KLM).[136,137] These stable oscillators produce a train of *fs* pulses at a high repetition rate (ca. 10 MHz), necessary to support mode-locking, but with a limited energy per pulse of tens or hundreds of nanojoules. However, they are tunable over as much as 400 nm (680-1080 nm).

(2) The output of the megahertz-repetition-rate oscillator is then chirped. The chirping process consists on the pass of the ultrafast pulses through a dispersive medium (for example a tilted grating) to be stretched up to a longer duration –nanosecond pulse width– to avoid damage to the optical components of the amplifier stage caused by the high peak power. In summary, chirping process spreads the wavelengths in the pulse over a much longer interval, reducing the peak power before amplification.

(3) In the amplifier the laser pulse energy is enlarged to several milijoules. The bandwidth of the amplifier must be large enough to accommodate the full spectrum of the short pulse. The amplifier of course requires optical pumping to sustain gain and amplification.

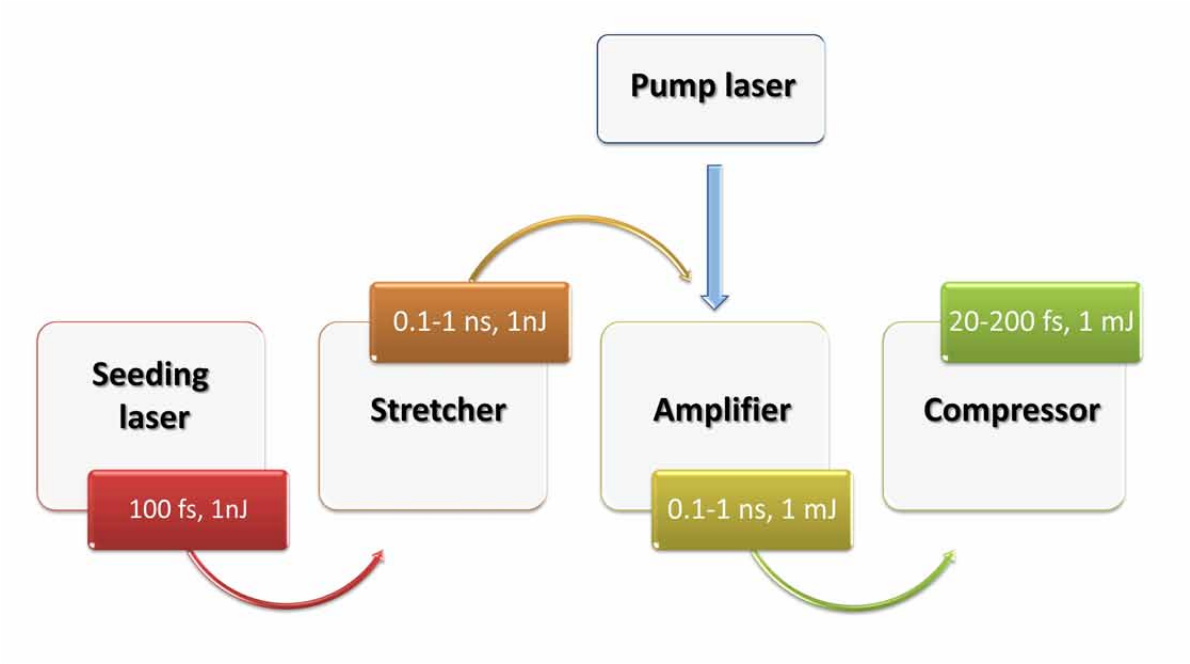

Figure 7. Concept of chirped pulse amplification (CPA) based laser.

(4) The pulses ejected from the amplification stage, usually via an electro-optical modulator, become recompressed close to the original pulse duration or less. The compressor unit reverses the dispersion process, squeezing the amplified light in time to recreate the ultrashort pulse, this time with much higher amplitude. Before *fs* laser pulses are used in any experiment, diagnostics in order to fully characterize their temporal profile and their spectral phase is routinely performed.[138] In order to gain better insight into the operation principle of *fs* lasers, the reader is referred now to the references 134-138.

The invention of the *CPA* technique in 1985 was a revolutionary breakthrough in femtosecond laser systems, resulting in the appearance of powerful femtosecond laser pulses and in the imminent availability of powerful commercial laser systems. Ultrashort pulse duration gave numerous benefits with respect to *ns*-LIBS: low ablation threshold, reduced sample damage, small ablated mass, improved spatial resolution, and absence of fractionation vaporization.[107] As discussed above (*Section 2.6.3*), the mechanisms leading to energy absorption and target ablation are entirely different for *ns*- and *fs*-LIBS. The *fs* laser pulses are so short that processes like ionization, sample heating, and vaporization all do not occur until the end or after the laser pulse. Hence, all laser

energy is deposited directly onto the sample before ablation occurs. The differences in laser-sample and laser-plasma interactions as well as in ablation mechanisms during interaction between ultrafast and nanosecond pulses with the sample lead to significant differences in crater shape and volume. *fs* lasers provide higher precision during ablation and minimized heat-affected zone on the material as compared to *ns* lasers. Disparities between expansion dynamics of generated plumes have been also detected. While *fs*-generated plasmas expand with a strong forward bias in direction normal to the sample surface, a spherical expansion is noticed for *ns*-produced plasmas. Such plasma expansion processes dictates distinct plasma lifetime, plasma emission and analytical figures of merit due to the distinctive duration of laser pulses. For all these reasons, *fs* laser pulses are predestined to providing a brighter future in numerous LIBS applications.

3.2. Optical system

The optical system comprises all active optical components used in a LIBS setup. Thus, all these optic components may be subdivided by their function, subject to the action during emission spectroscopy assisted by laser ablation in which they are involved. We refer to focusing optics, which is intended to guide and focus the laser pulses onto the matter, to produce the plasma plume; and to the collecting optics, responsible for gathering and conducting the emitted light from the plasma up to the detection device. The following sections encompass a brief description of this optical system in a LIBS experiment.

3.2.1. Focusing optics

Beyond some high-reflectivity mirrors to the laser-wavelength used to guide laser pulses along optical path from the laser to the sample, to attain and exceed the threshold for the plasma formation (typically greater than 10^8 $W \cdot cm^{-2}$) at the location of interaction with the sample, laser

pulses are usually focused down to a very small area by means of a single lens (in general a plane-convex lens and sometimes bi-convex or best form –spherical or cylindrical– lenses).

Each laser ablation setup usually contains a customized focusing lens in relation to the specific experiment requirements. Some critical features of this lens are transmission efficiency at the irradiation wavelength, the type of coating, the damage threshold, and the focal length. This last is particularly significant since it dictates the distance between the lens and the sample for which the laser pulse is focused to a highly small area.[139,140] Thus, when a *rectangular beam* with a *plane wavefront* of finite diameter D is focused by the lens onto a plane, the individual parts of the beam that pass through the lens converge and are imagined as point radiators of a new wave front. Since these radiators interfere with each other on the focal plane, constructive and destructive superpositions take place, and a distribution of the light energy with the central maximum containing about 86% of the total power in the beam is attained. The smallest focal diameter (d_{min}) limited by this diffraction phenomena of the wavefront, usually defined by the points where the intensity has fallen to ($1/e^2$) of the central value, is given by the equation 3.1.

$$d_{min} = (2 \cdot f \cdot \lambda)/D \quad \text{[Eq. 3.1]}$$

where f is the focal length of the lens, λ is the laser wavelength and D the diameter of the laser beam.

For a *plane front circular beam*, a correction factor of 1.22 is introduced and equation 3.2 becomes:

$$d_{min} = (2 \cdot 1.22 \cdot f \cdot \lambda)/D \quad \text{[Eq. 3.2]}$$

In the case of multimode laser beams the smallest focal diameter will be even larger since the beam comes from a cavity having several off-axis modes of vibration rather than from an apparent point source. This further correction for a multimode lasing regime considers transverse

electromagnetic modes of laser beam. However, since the number of radial zero fields, p, are more critical to the focal spot size than the number of angular zero fields, l, and that of longitudinal fields, q, a new part is introduced into the equation 3.3. The new expression reads as follows:

$$d_{min} = \frac{2 \cdot 1.22 \cdot f \cdot \lambda}{D} \cdot (2\,p\ \ + l\ \ + 1\,) \qquad [\text{Eq. } 3.3]$$

Although focal spot size is related to beam focus, wavelength, diameter and mode, there are other factors that affect focal spot diameter such as spherical aberration and thermal lensing effects.

In general, any lab bench LIBS setup uses a single focusing lens. However, in the case of field-deployable LIBS sensors, operating at standoff and remote configurations, for which the lens-to-sample distance may vary, optical arrangements composed by several lenses (e.g. beam expanders and telescopes) are used to adjust the laser beam focus.[42,140]

3.2.2. Collecting optics

With regard to the gathering of the radiation emitted from the plasma up to the detection device, several configurations can be considered in a LIBS experiment. In an illustrative way, Figure 8 sketches three optical layouts used in plasma light collection. Figure 8A shows the simplest scheme to gather plasma emission. A converging lens is placed orthogonal –possible option is also an angular arrangement–to the direction of laser incidence. Alternatively, Figure 8B depicts the simplest configuration in which the use of a single lens is exploited. The collection of light from the plasma materializes with the lens used to focus the laser beam. For this configuration a dichroic mirror is needed. As seen, this mirror allows passing the incident radiation wavelength but reflects the plasma light gathered by the lens. This configuration allows observing emission of the plasma shock front during its propagation, but it is not an arrangement to observe the axial and radial directions of the plasma expansion. Finally, Figure 8C shows optical layout using a spherical mirror

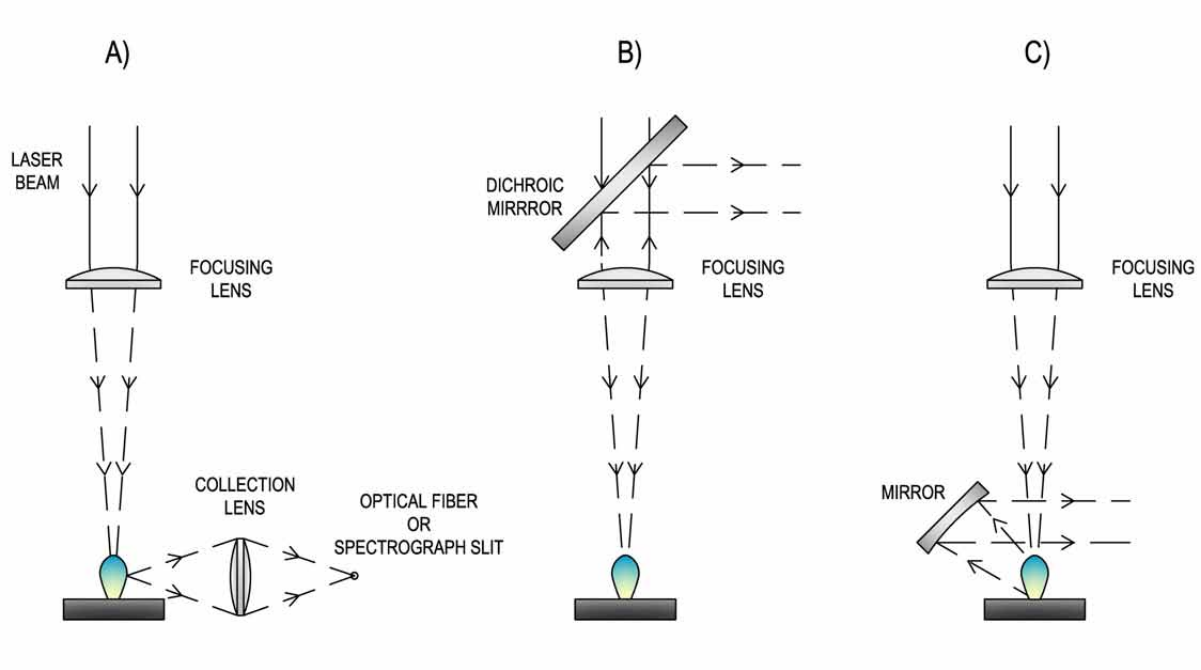

Figure 8. Frequent optical arrangements for plasma light collection in LIBS measurements.

instead of a lens to collect the plasma emission. Thus, all wavelengths emanating from the distant plasma that strike the mirror parallel to its principal axis are brought to a focus at the same convergence point. Accordingly, the use of this optic element suppresses any chromatic aberration.

Plasma light collected by using any of these configurations may be focused either directly on the entrance slit of a spectrograph or on the tip of an optical fiber.[42] Spectroscopic techniques extensively use optical fibers to pass radiation emitted to the detection device because of their excellent versatility. They are made of synthetic fused silica (amorphous silicon dioxide) and may be doped with trace elements to change their optical properties. A relatively large core and a high numerical aperture (*NA*) allow the fiber to gather the complete plasma volume. Core diameters of the optical fiber from 50 µm to 1000 µm are frequently used for LIBS measurements. Together with the size of the focused image of the plasma, the choice of the adequate optical fiber also involves to consider the wavelength range of interest. In this context, solarization resistant fibers are needed to observe deep-UV light (below 230 nm).

3.3. Light detection device

Once plasma light is collected, the radiation emitted is converted into an understandable format with a suitable device for allowing its ensuing analysis. This device is typically referred to as the spectrometer, and basically consists of a spectrograph that disperses polychromatic light into its spectral components and a detector that digitizes the optical signal as a function of wavelength. The most used spectrometers for LIBS measurements are based on *Czerny–Turner* spectrograph. Figure 9A illustrates its key components. As shown, the light collected from the plasma enters through a narrow slit placed at the input side, whose width may be fixed or variable. Then, light is collimated by a concave mirror and redirected towards the plane of a diffraction grating where polychromatic radiation is dispersed and spectrally resolved. This grating consists of a series of regularly spaced parallel grooves formed in a reflective coating deposited on an appropriate substrate. Their efficiency depends on the groove shape, angle of incidence and reflectance of the coating. Finally, a second concave mirror focuses the resolved light onto the plane of the detector coupled to the spectrograph. The spectral range covered by the spectrograph and its resolution is governed by the scratches on the surface of the diffraction grating (number of grooves per mm). Ideally, spectrometer used in LIBS measurements have to provide a wide spectral window with a high *resolving power* (R).[143] For a spectroscopic optical system this parameter is defined by equation 3.4:

$$R = \frac{\lambda}{\Delta\lambda} \quad [\text{Eq. } 3.4]$$

where Δλ is the spectral resolution which is defined as the smallest difference in wavelength that can be resolved at the wavelength λ. The spectral resolution provided by a spectrometer also depends on design parameters such as slit size, spectrometer focal length and properties of optical components. Regrettably, commercially available *Czerny-Turner* spectrographs are wavelength limited either in resolution or in the spectral coverage. The configuration of the system for a high resolution of the spectral features leads to a small range of the spectral window or, vice versa, a low

resolution within a broad spectral range. This fact may hinder the detection of specific emission lines due to their overlapping with close signals. In addition, when widely spaced signals within the electromagnetic spectrum need to be simultaneously monitored, several LIBS measurements may be performed to acquire different regions of the spectrum. Then, a broad band spectrum may be build by adding shorter spectral windows.

On the other hand, the use of *Echelle*-based spectrographs[141] has grown over the last years. The key design and performance of this spectrograph contrasts with that of the Czerny-Turner. Echelle spectrograph is designed to disperse the light in two orthogonal directions using two dispersion stages. Hence, a large spectral window (typically from 200 to 1000 nm) with a high spectral resolution can be simultaneously obtained.[42,142]

After the light has been spectrally dispersed by the spectrograph, its distinct components are registered in a detector. Basically, detectors are electro-optical devices converting the light into an electric signal. Photomultiplier tubes (*PMTs*), charged-coupled devices (*CDDs*) and intensified charged-coupled devices (*iCDDs*) are the most widespread detectors used in emission spectroscopy.[143]

- The *PMTs* permit performing time-resolved measurements and data acquisition at high frequency. Although these detectors may be used in large number of applications, they are frequently applied when high sensitivity in the visible region is demanded.
- *CCD* detectors contain an array of single photosensitive elements. Here electrons are generated due to the absorption of photons by a sensitive material. These electrons are stored in pixels arranged in rows and columns (silicon chip). The generated charge pattern is moved from the chip through a series of horizontal electrodes to be stored into a computer memory. This readout process implies the amplification of the charge on each pixel into a voltage (A/D conversion). Typical *CCD* has a fixed integration time of the signal (ca. 1 ms). However, some detector types allow working with integration less than 10 μs. The quantum efficiency (probability of an incident photon

generates a photoelectron) of the CCDs depends on the wavelength and on the direction of incoming light.

- *iCCD* detectors consist of a *CCD* and a microchannel plate (*MCP*) that act as intensifier. A sketch of an *iCCD* is shown in Figure 9B. The operating principle is based on the generation of free electrons in a photocathode following the incidence of photons. The application of an electric field accelerates the electrons toward the *MCP* which acts as electron multiplier. Then, electrons departing from the *MCP* strike a phosphor screen; an action that results in the generation of new photons. Lastly, the photons are guided by a fiber optic plate or, alternatively, by coupling a lens to the *CCD* array. Besides providing signal intensification, *iCCDs* are able to manage the timing acquisition parameters, that is, the delay time for the opening of the camera and the integration time of the optical signals (gate-open time of the intensified detector). Thus, such sensitivity and versatility are the reasons for which the *iCCDs* cameras are the more selected detectors for LIBS measurements.

For the convenience of the reader, the LIBS specific setups, which have been used in each one of the conducted experiments, are detailed in the particular chapters that constitute the scientific/technical part of the present Doctoral Thesis.

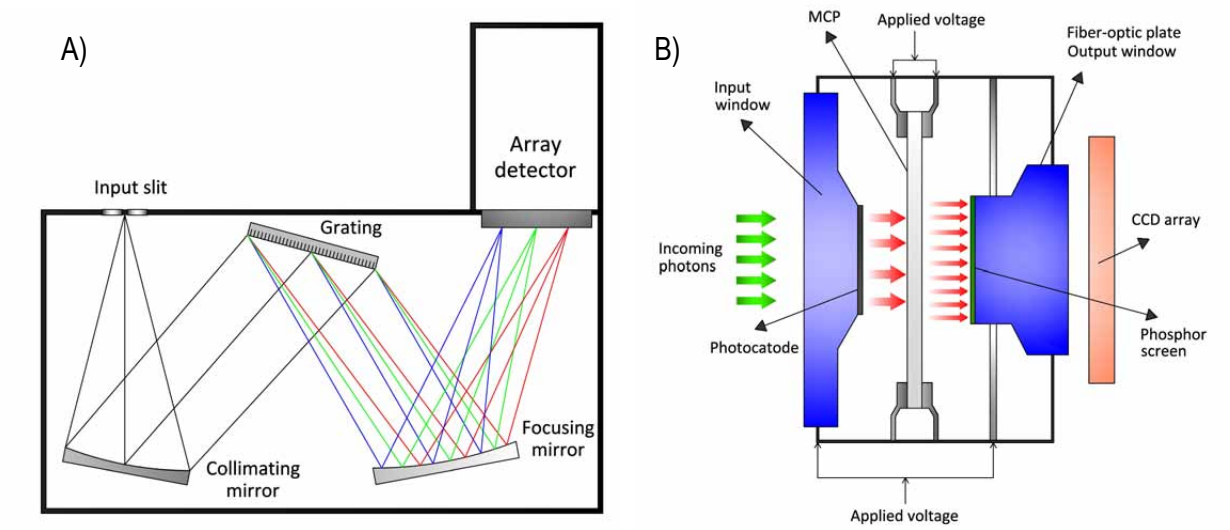

Figure 9. A) Design of a Czerny–Turner based spectrograph and B) Schematic view of an image intensifier structure.

4. Chemistry of laser-induced organic plasmas

Following its more than proved capability of multielemental analysis,[144-146] in the last years, LIBS has been uncovered as an appealing tool for the molecular analysis of organic compounds using optical emissions of small radicals existing inside plasmas. The analysis potential of the technique for molecular sensing have been explored in a wide range of applications such as the detection of energetic materials,[23] the sorting of polymers,[147] and the discrimination of bacteria.[148-152] Despite these accomplishments, the large similarity between the spectral fingerprints of the organic compounds remains an Achilles heel of LIBS towards the specificity on analysis. The high intricacy of the organic plasmas chemistry hampers the exploration and the ascertainment of concerns like the routes leading to the generation of excited molecular species as well as the linkage between the molecular emissions featured in LIBS spectra and the chemical structure of the analyzed compounds; key aspects to strengthening the figures of merit of LIBS.

The first studies on laser ablation of organics were developed by Srinivasan and Leigh who observed photochemical transformations in polyethylene terephthalate films after their interaction with UV radiation[153] However, in the context of optical emission spectroscopy, initial investigations were focused on the monitoring of molecular emissions from plasmas induced in graphite samples due to its simplicity as pure carbon material.[154] Most researches have been aimed at understanding the origins and formation mechanisms of small carbon clusters, mainly dicarbon (C_2) and cyano (CN) radicals. To this end, the temporal evolution and the spatial distribution of these emitting species have been studied by several authors.[32,115,155] Valuable researches on this line shed light on the effects of different core parameters in laser ablation, namely the laser pulse energy dosage,[41] the laser pulse duration,[115,156,157] and the surrounding atmosphere[41,155,157] to the formation of these molecular species.

Nevertheless, while information reported by these studies is very helpful, the analysis of molecular solids by LIBS is much more complex than the model case of pure carbon materials. A large variety of species are involved in a vast number of reactions occurring in plasmas of organics. Let me to mention only as an example the complex kinetic model proposed by *Babushok et al.* to describe the processes that lead to the electronically excited states of O, H and N atoms responsible for the emission lines in the LIBS plasmas of cyclotrimethylenetrinitramine (*RDX*). The kinetic model contains overall 137 species, with some decomposition products, excited radicals, and species coming from the background gas among them, participating in a total of 577 reactions; all this without including the excited C atom states.[33] Generally, although the assembled model cannot decipher all the processes involved in the plasma chemistry, it may help in understanding the ablation behavior of other C/H/N/O-containing materials and the why behind their optical emissions.

So far, a clear correspondence between the molecular structure of organics and their emission patterns has not been clearly established. Nevertheless, some investigations have tried to gain insight into this issue. To examine whether the resulting spectral fingerprint was related to the structure of molecular solids and could be used for their identification, *Portnov et al.*[158,159] explored the applicability of LIBS to organic compounds in ambient air by carrying out a survey of spectrally resolved emissions for nitrocompounds (*NCs*) and polycyclic aromatic hydrocarbons (*PAHs*). The computation of emission intensity ratios, C_2/CN and O/N, allowed differentiating between these varieties of carbon-containing aromatic samples. However, when plasmas are induced in air atmosphere, the complexity of plasma chemistry of the organic compounds is exacerbated by the contribution of the constituents of the Earth's atmosphere (O_2, N_2 and H_2O). Because of the energy deposited by the expanding plasma in the air and the collisional ionization processes occurring along the plasma ionized path in the background gas, O_2, N_2 and H_2O molecules can be dissociated and excited. As a result, H, N, O, and OH excited species not only may intervene in the chemical routes to the formation of new species (i.e. CN or NH radicals), but also can directly lead to their

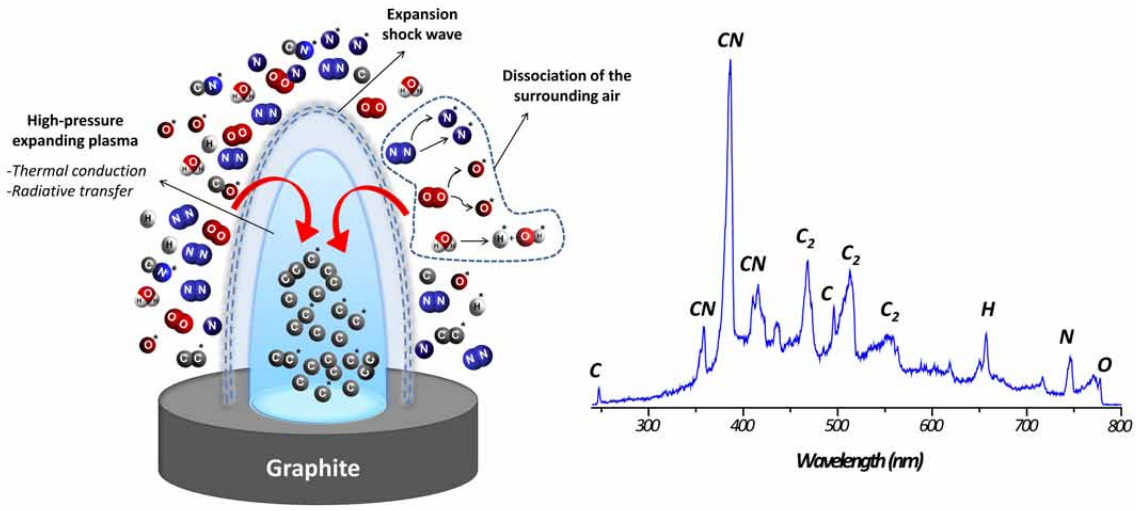

Figure 10. Representation of the secondary ionization process of the air in laser-induced plasmas together with a representative LIBS spectrum of graphite.

corresponding optical emissions, thereby altering those directly linked to the elemental composition of the organic compound. Consequently, a complete correspondence between the molecular structure of the organic compounds and the gathered emissions becomes much more difficult to observe. This phenomenon, referred as *secondary ionization* of the air, is schematized in Figure 10. The simple case of laser ablation of a pure graphite sample, which is formed by a 100 % of carbon atoms, is considered.

A priori, it would be reasonable to expect emissions from species containing only carbon – atoms and clusters– to feature within the LIBS spectrum of such sample. However, the occurrence of O, N, and H emissions can only be justified through an unequivocal contribution of air ionization. Likewise, optical emissions related to the CN radicals comes from the recombination process of the atmospheric nitrogen with the native carbon atoms seeding the plasma.[160]

By contrast, when the laser ablation progresses either under vacuum conditions or under an inert atmosphere (i.e. argon gas), any concurrence of the air atmosphere is blocked and, therefore a better matching between atomic emissions (C, H, N and O) and their elemental ratios in organic compounds is attained.[161]

4.1. Optical emissions in plasmas of molecular solids

The big challenge in the analysis of molecular solids by LIBS relies on the high similarity of the emission spectra gathered. Emission lines from atoms or ions of C, H, N and O as well as sequences of CN and C_2 molecular bands are the most representative signals featured in LIBS spectra of organic compounds. To put the discussion into context, Figure 11 depicts LIBS spectra of polyethylene (*PE*) and polytetrafluoroethylene (*PTFE*) induced with visible laser radiation (532 nm) under air atmosphere. As seen, despite that the two polymer materials have different elemental composition, the same emission signals are featured within their spectra. The differences observed between both spectral responses are basically slight changes in the relative intensities of the optical emissions. Such a circumstance suggests that differentiation between organic compounds by LIBS needs to be tackled using a comprehensive framework of relative emissions from atoms and small radicals rather than addressed from the simple detection of all these specific spectral features. Faced with this challenge, knowledge of all possible species that populate the plasma as well as the plausible formation routes from which they may arise; subjects that can significantly help to substantially improve selectivity of LIBS for sensing molecular solids. The main features of optical emission spectra of organics as well as the models proposed for the formation of diatomic radicals in laser-induced plasmas will be discussed in the following sections.

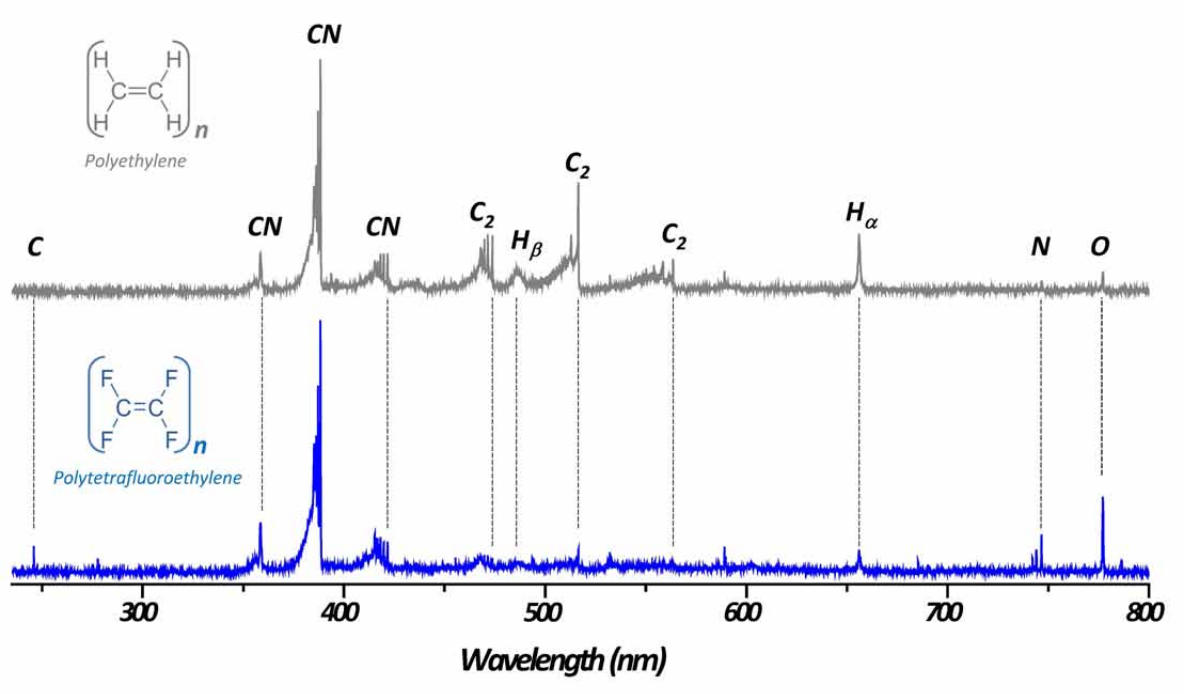

Figure 11. LIBS spectra of polyethylene (top) and polytetrafluoroethylene (bottom) from plasmas induced with ns pulses (λ=532 nm) in air atmosphere.

- ***Emissions of atoms and ions from organic compounds***

As already stated, optical emissions revealed by LIBS spectra of organic compounds are mainly associated to atoms and ions of carbon, hydrogen, nitrogen and oxygen.[161] The electron transitions and the associated wavelengths for the most sensitive emission lines of such species are listed in Table 1.

Table 1. Main electron transitions and the associated wavelengths for emission lines of C, H, N and O.

Specie	Transition	Wavelength (nm)
C (I)	$2s^2 2p3s \rightarrow 2s^2 2p^2$	193.09
C (I)	$2s^2 2p3s \rightarrow 2s^2 2p^2$	247.86
C (II)	$2s^2 4s \rightarrow 2s^2 3p$	392.07
C (II)	$2s^2 4f \rightarrow 2s^2 3d$	426.73
H_δ (I)	$2 \rightarrow 6$ ($n \rightarrow n$)	410.17
H_γ (I)	$2 \rightarrow 5$	434.05
H_β (I)	$2 \rightarrow 4$	486.14
H_α(I)	$2 \rightarrow 3$	656.28
N (I)	$2s^2 2p^2(^3P)3p \rightarrow 2s^2 2p^2(^3P)3s$	742.36 744.23 746.83
O(I)	$2s^2 2p^3(^4S°)3p \rightarrow 2s^2 2p^3(^4S°)3s$	777.19 777.42 777.54

Note: optical emissions from H corresponding to the Balmer series are identified as H-delta, H-gamma, H-beta and H-alpha (n, radial quantum number). (I) and (II) denotes atoms and single-ionized atoms, respectively.

Some molecular solids contain heteroatoms other than oxygen and nitrogen, like are phosphorus, sulfur, and the halogens –fluorine, chlorine and bromine. The ability of LIBS for the detection of such elements has been proved.[162-165] Notwithstanding this, since these elements have not been subject of study in the performed investigations, they are not emphasized in the present Doctoral Thesis.

- ***Emissions of diatomic species from organic compounds***

The most representative molecular emissions in LIBS are associated to C_2 and CN radicals. Concerning C_2 radicals, the laser ablation of the molecular solids may produce carbon dimers, often in an emissive excited state, through a variety of processes, being remarkable among them the direct release of native C=C bonds from the original molecule and a recombination of C atoms. While the C_2 molecule boasts seven triplet and six singlet electronic states giving rise to nine band

systems, which are spread over the entire range of the spectrum –from the vacuum ultraviolet, through the visible, up to the infrared spectral region–, the most easily excited of these band systems, and consequently with the most intense emissions, is the *Swan band system*, which arises from the $d^3\pi_g$–$a^3\pi_u$ transition and contains six sequences lying between 420 and 720 nm.[41,166-168] Within these band sequences ($\Delta\nu$, their specific vibrational transitions can be resolved depending on the ability of the detection system to distinguish between wavelength intervals. Even sometimes, the rotational transitions of each vibrational level are also exhibited. To graphically contextualize this, Figure 12 depicts the emission spectra, ranging from 430 nm to 570 nm, of four sequences ($\Delta\nu$= 2, 1, 0, -1) of C_2 *Swan system* from graphite plasmas according to the resolution ability of the detection system. As seen, in the low-resolution spectrum the vibrational transitions of each sequence are hardly distinguished, whereas the overall structural appearance of well-developed vibrational peaks is clearly discernible in the high-resolution optical response. Those spectra that feature all these transitions allow determining the rotational and vibrational temperatures (T_{rot} and T_{vib}) of the radical from the Boltzmann plot method[169] or calculating them by matching the strength of lines in optical spectra synthesized with semi-automatic program packages with those in the corresponding experimental ones.[170]

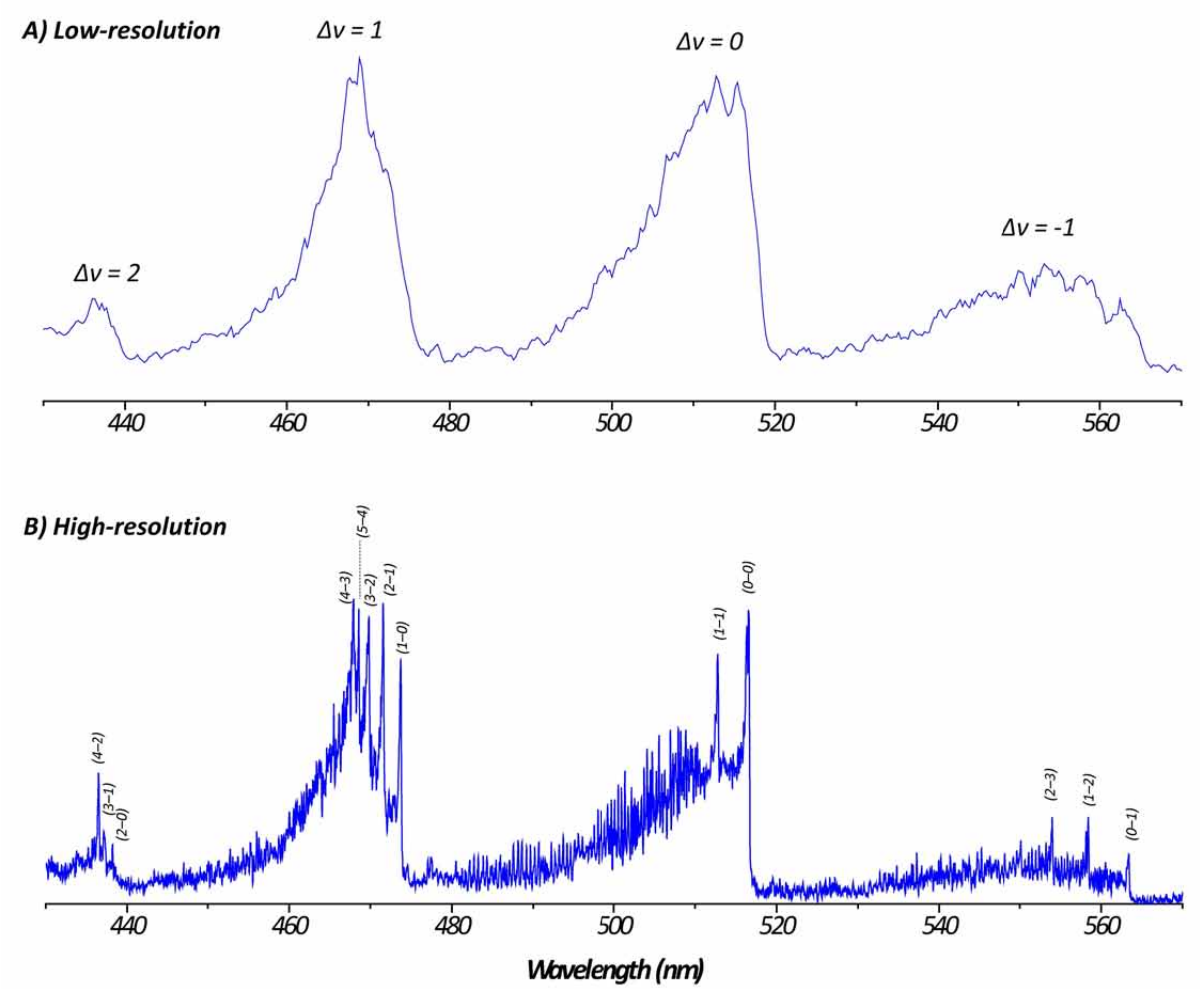

Figure 12. Optical responses of C_2 Swan Band System reached when graphite plasma emissions illuminate diffraction gratings with different total number of grooves on their surface, A) 150 grooves mm^{-1} and B) 1800 grooves mm^{-1}.

As far as cyano species is concerned, CN emissions are generally featured in LIBS of carbon-containing organic samples when plasmas are induced under air atmosphere. The *Violet system* associated to the $B^2\sum^+$-$X^2\sum^-$ transition, whose main sequences covers from ca. 350 to 430 nm, governs the spectrum. Figure 13 shows the spectral emission of the sequences $\Delta\nu$= +1, 0 and -1 for the CN species from plasmas of polyethylene. As observed, in general, under typical operational conditions for LIBS analysis the $\Delta\nu$= 0 band sequence is the most sensitive. As in the case of C_2, if all transitions are clearly resolved, the spectral analysis allows inferring of the rovibrational temperatures of CN radical that may be representative of the plume temperature if thermodynamic equilibrium exists.[171-173]

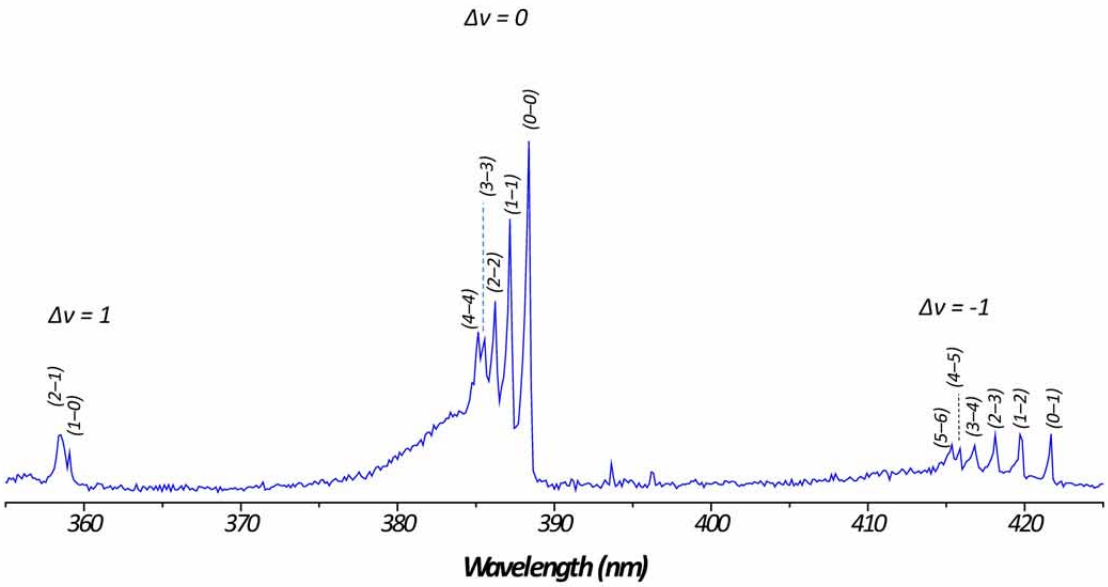

Figure 13. High resolution optical responses of CN Violet Band System from polyethylene plasma.

Together with CN and C_2 species, other diatomic molecules are present in the excited vapor. Depending on the ablation conditions, temporal settings and the instrumentation used for light detection, less sensitive emission bands associated to OH, CH, NH, N_2 and NO excited molecules may also be featured in LIBS spectra of organics.[120,174] Beyond these observable species, the existence of others radicals, which either do not emit in the UV-Vis-IR region of the electronic spectrum or are intermediate reaction products with extremely short lifetime, cannot be ruled out. Indeed, the combination of LIBS with mass spectrometry based techniques has allowed detecting a higher number of molecular fragments (e.g. C_2H^+, $C_2H_2^+$, C_3, CO^+, $HCNH^+$). Particularly, laser ionization mass spectrometry (LIMS)[175] and ion flow tube mass spectrometry (SIFT-MS)[33,176] have been successfully applied to study the fragmentation and recombination mechanisms in plasmas of organic explosives.

Table 2. Optical emissions for the band-heads of the sequences contained in the most intense electronic transitions of some diatomic molecules.[177]

Radical	System	Transition / Sequence		Wavelength (nm)
OH		$A^2\sum^+–X^2\pi$	(0–0) $\Delta\nu$= 0	308.9
NH		$A^3\pi–X^3\sum^-$	(0–0) $\Delta\nu$ = 0 (1–1) $\Delta\nu$ = 0	335.8 336.9
CH		$C^2\Sigma^+–X^2\Pi$ $B^2\Sigma^-–X^2\Pi$ $A^2\Delta–X^2\pi$	(0–0) $\Delta\nu$ = 0 (0–0) $\Delta\nu$ = 0 (0–0) $\Delta\nu$= 0	314.3 387.1 431.4
CN	Violet	$B^2\sum^+–^2X\sum^+$	(1–0) $\Delta\nu$ = 1 (0–0) $\Delta\nu$ = 0 (0–1) $\Delta\nu$ = -1	358.7 388.2 421.6
C_2	Swan	$d^3\pi_g–a^3\pi_u$	(2–0) $\Delta\nu$ = 2 (1–0) $\Delta\nu$ = 1 (0–0) $\Delta\nu$ = 0 (0–1) $\Delta\nu$ = -1 (0–2) $\Delta\nu$ = -2 (0–3) $\Delta\nu$ = -3	438.3 473.7 516.5 563.5 619.1 667.7

Notwithstanding this, investigations described in the present Doctoral Thesis focus only on the most regular diatomic species that exhibit optical response. Table 2 reports on emission wavelengths for labeling the band-heads of the sequences contained in the most intense electronic transitions of the emitting species concerned.

To show on paper the typical appearance of molecular emission fingerprint, Figure 14 depicts the *fs*-LIBS spectrum of terephthalic acid in which the spectral features of the most significant diatomic radicals that seed the laser-produced plasma are exhibited. As seen, alongside the most common CN and C_2 optical features, emissions associated to the OH, CH, and NH radicals also emerge in the spectral response. While the most plausible routes to produce CN and C_2 species in plasmas of molecular solids have been under active investigation and are practically elucidated,[178,179] the origins of hydrogenated species and their role within the plasma chemistry have

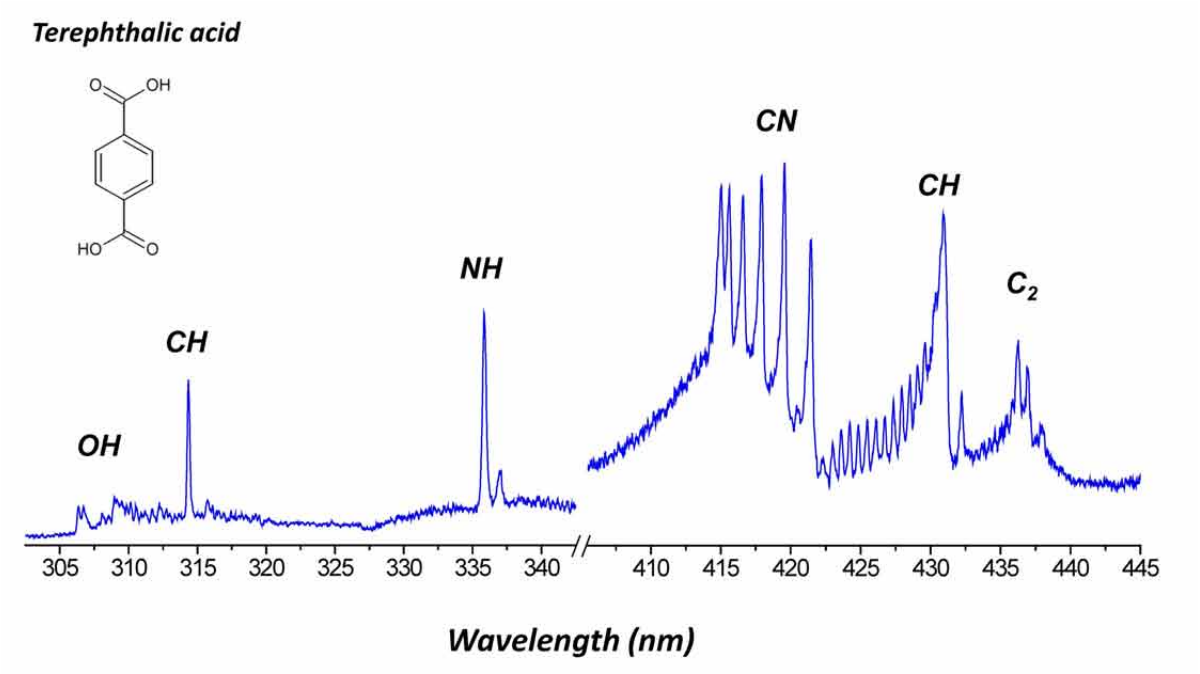

Figure 14. *fs*-LIBS spectrum from terephthalic acid plasma induced in air at atmospheric pressure.

been not addressed yet in depth. This circumstance has motivated the investigations in progress described in the Chapter 2 of the present Doctoral Thesis.

4.2. Formation pathways of excited diatomic radicals

Despite that the potential origins of excited diatomic species in LIBS organic plasmas have been studied in considerable depth, they continue to be debated still today. The direct release as fragments from the parent molecule and the occurrence of different chemical processes (recombination, substitution...) between species within the produced plasmas have been postulated as the feasible sources of such excited radicals. Furthermore, all these chemical routes tend to coexist rather to exclusively progress; while it is true that there is a whole series of factors influence that favor some mechanisms over others. Particularly, the ablation conditions, which define the primitive species that populate the plasma, cause chemical reactions to progress at a different extent. Some insights into this context are discussed below.

Regarding the C_2 radicals, its formation process has been studied according to the laser fluence used to ablate the sample. At low fluence, the laser energy delivered produces the partial fragmentation of the parent molecule. Then, molecular fragments with two or more carbon atoms follow a progressive dissociation as indicated in reaction 1:

$$C_n + M \rightarrow C_{n-2} + C_2 \qquad [R.\ 1]$$

In contrast, a larger atomization of the molecular solid occurs when increasing the laser energy. Then, recombination of carbon atoms to generate C_2 dimers becomes an important route by means of a three-body reaction [R.2]:[39,181]

$$C + C + M \rightarrow C_2 \qquad [R.\ 2]$$

Although itemizing all the reactions that may lead to the generation of carbon dimers is out of the scope of this section, some additional routes involving common species in organic plasmas for the generation of C_2 are reported. In this vein, the reactions 3 and 4, with CN and CH radicals as chemical precursors, have been also postulated to produce dicarbon radicals:[182,183]

$$CN + C \rightarrow C_2 + N \qquad [R.\ 3]$$

$$CH + CH \rightarrow C_2 + H + H \qquad [R.\ 4]$$

In general, the high excitation temperatures reached in laser-induced plasmas suggest a large atomization of the molecular solids.[184] However, the molecular structure of each compound certainly plays an important role in its mechanism of decomposition and therefore in the nature of the output species. Indeed, the nature of the C-to-C linkage (simple, double, triple, or aromatic) within the molecule probably affects the proliferation of C_2 fragments. Within this framework, some

Table 3. Mean bond enthalpies (kJ mol^{-1})

Chemical bond	Bond enthalpy (kJ mol^{-1})	Chemical bond	Bond enthalpy (kJ mol^{-1})
C–C	348	C–N	305
C=C	612	C=N	613
C≡C	837	C≡N	890
C–C (in benzene)	518	C–F	484
C–H	412	C–Cl	338

experimental results have revealed greater readings of C_2 emissions for unsaturated and aromatic compounds; outcomes that may correlate with the strength of the chemical bonds.[32,38] To contextualize the discussion, Table 3 displays the average bond dissociation energy –bond enthalpy– for the most usual carbon bonds in organic compounds.[185]

As seen, the dissociation energy of a double carbon bond is almost twice the strength of a simple bond. Hence, it seems rather likely that C_2 emissions observed from plasmas of unsaturated and aromatic compounds are mainly linked with the direct release of C-to-C double bonds from the parent molecule. In contrast, the easiest breakage of C-to-C simple bonds in saturated molecules suggests a recombination mechanism to produce C_2 species, if any. In summary, the dissociation energy of the chemical bond also influences on how and in what quantity the carbon dimers may be produced. However, the coexistence of the two processes to generate C_2 radicals should not be discarded.

In parallel, a great number of investigations have been focused on the possible sources of cyano radicals (CN). The CN radical is a very stable radical compared to other diatomic molecules, as can be deducted from information reported in Table 3, where bond dissociation energies of the most common diatomic species seeding organic plasmas are reported. As seen, CN molecule exhibits the highest dissociation energy. Such a circumstance underscores the large affinity between

Table 4. Bond dissociation energies in simple molecules.[186]

Molecule	Dissociation reaction	$\Delta H_{f\,298}$, kcal mol^{-1}	$\Delta H_{f\,298}$, kJ mol^{-1}
C_2	$C_2 \rightarrow C+C$	145	606.1
CN	$CN \rightarrow C+N$	175	731.5
OH	$OH \rightarrow O+H$	102.3	428.0
CH	$CH \rightarrow C+C$	80	334.4
NH	$NH \rightarrow N+H$	54	225.7
O_2	$O_2 \rightarrow O+O$	119	497.9
N_2	$N_2 \rightarrow N+N$	222	944.5
H_2	$H_2 \rightarrow H+H$	104	435.5

C and N atoms when they meet one another in the plasma, thereby justifying the prevalence of these emissions over those from other radicals in plasmas of carbon-containing organic samples induced in air atmosphere and under nitrogen-containing atmospheres, irrespective of the presence of nitrogen in the molecular formula of the sample.

This fact can be clearly observed in laser-induced plasmas of graphite. Since the sample is free of nitrogen, the formation of cyano radicals is necessarily due to recombination reactions of C atoms or higher molecular clusters (C_n, $n \geq 2$) with atmospheric nitrogen (either N or N_2).[187,188] Such processes for the generation of CN excited species can be itemized as follows:

$$C + N_2 \rightarrow CN + N \qquad [R.\ 5]$$

$$C + N \rightarrow CN \qquad [R.\ 6]$$

$$C_2 + N_2 \rightarrow CN + CN \qquad [R.\ 7]$$

When ablation is performed on nitrogen-containing organic compounds, the generation routes of CN radicals may also involve the native nitrogen. Likewise, cyano radicals may directly come from the direct release of a C-N bond of the parent molecule, if present. *Lucena et al.* found that intensities of CN emissions responded perfectly to the stoichiometry of three polysubstituted nitrotoluenes (mono–, di–, and tri–), when plasmas were induced in helium atmosphere, that is, when any kind of involvement of atmospheric nitrogen is avoided.[39] Alternatively, the use of ultrafast laser pulses (*fs*-LIBS) allows reducing the secondary ionization of air, which has been explained in a preceding section, thereby minimizing the contribution of nitrogen from air. Thus, a better correlation between the presence the C–N native bonds and the CN emissions featured within the emission response is attained. In this vein, this connection was evidenced by an exploration on the temporal evolution of CN emissions during *fs*-LIBS analysis of bacteria samples. The temporal behavior of CN emissions in plasmas of bacteria departed from the kinetic trend shown by CN signals gathered from graphite plasmas. In the case of graphite, CN emissions peaked after several hundreds of *ns* due to recombination processes, whereas CN intensity decayed rapidly for samples containing either native CN bonds or also nitrogen and carbon atoms as elementary constituents.[189]

On the other hand, the reaction routes leading to the generation of hydrogenated radicals such as OH, NH and CH has been scarcely explored. As in the case of C_2 and CN, it is expected that the formation processes of hydrogenated radicals may involve both native species and air constituents when ablation occurs in Earth atmosphere. In addition, such radicals may be produced from a direct release from the parent molecules following the laser ablation process. The likelihood of a direct detachment of diatomic fragments from the ablated compound and their prevalence in laser-induced plasmas depend on operational conditions such as the energy deposited on the target as well as on the wavelength and duration of the laser pulses. The reader is referred, in particular, to the Chapters 2 and 3 of the present Doctoral Thesis to "navigate" through the most plausible routes to form diatomic hydrogenated radicals in laser-induced plasmas of molecular solids. Furthermore,

within these chapters the description of reactions is intertwined with the influence of the laser pulse duration and the chemical structure of molecular solids on the ensuing emissions of such radicals; a matter which needs still to be looked into at more closely.

4.3. Laser ablation molecular isotopic spectrometry

Optical spectroscopic techniques for measuring isotope-resolved molecular emissions were developed long time ago. Initially, these techniques mainly employed radio-frequency discharges as excitation source of molecules in gas phase.[190,191] However, the capability to detect isotopic shifts in molecular emissions by LIBS was recently demonstrated by *Russo et al.*[192] This new method, which measures optical spectra of transient molecules produced in ablation plumes for the isotopic analysis of samples, is known as *laser ablation molecular isotopic spectrometry (LAMIS)*. The main advantage of *LAMIS* is that molecules present larger optical isotopic shifts as compared with those transitions in atoms. As can be deducted from values reported in Table 5, optical isotopic shifts for atomic species (C, N or O) are typically of the order of few pm; therefore far exceeding the resolution of a conventional LIBS spectrometer. Conversely, the spectral shifts between isotopomers of diatomic molecules (CN, C_2…) may reach values from hundreds of pm to few nm. Hence, these large shifts allows identifying simultaneously emissions from isotopomers by using an spectrometer with a low spectral resolution for isotopic detection.[193]

Among the potential abilities of *LAMIS* is worth to note the tracing of reaction routes in order to understand the chemical processes occurring in a laser-produced plasma[178,179,199] and the determination of isotopic elementary ratios in samples.[200,203-206] In the context of the present Doctoral Thesis, the LIBS analysis of isotopically labeled organic compounds is an interesting approach as a diagnostic tool to unveil and trace the dominant routes leading to the diatomic radicals in laser-induced plasmas.

Table 5. Isotopic shifts in optical emissions from atoms and molecules.

	Specie	Wavelength (nm)	Molecular band sequence	Isotope shift (nm)		Ref.
Atom	^{12}C	247.856 283.670	—	^{13}C to ^{12}C	0.001 0.005	194 195
	H	656.272 (H_α) 486.133 (H_β) 434.047 (H_γ)	—	D to H	- 0.179 - 0.133 - 0.119	196
	^{14}N	744.229 746.831	—	^{15}N to ^{14}N	0.003 0.003	197
	^{16}O	777.196 844.676	—	^{18}O to ^{16}O	- 0.004	198
Molecule	$^{12}C^{14}N$	421.6	$B^2\sum^+–^2X\sum^+$ // (0-1)	$^{13}C^{14}N$ to $^{12}C^{14}N$ $^{12}C^{15}N$ to $^{12}C^{14}N$	- 0.70 - 0.70	179
	$^{12}C^{12}C$	473.7	$d^3\pi_g–a^3\pi_u$ // (1-0)	$^{13}C^{12}C$ to $^{12}C^{12}C$ $^{13}C^{13}C$ to $^{12}C^{12}C$	0.75 1.52	199
	^{16}OH	306.40	$A^2\sum^+–X^2\pi$ // (0-0)	^{16}OD to ^{16}OH	0.123	200
	^{14}NH	335.99 337.70	$A^3\pi–X^3\sum^-$ // (0-0) $A^3\pi–X^3\sum^-$ // (1-1)	^{14}ND to ^{14}NH	- 0.32 - 0.71	201
	^{12}CH	430.99	$A^2\Delta–X^2\pi$ // (0-0) (1-1)	^{12}CD to ^{12}CH	- 0.61	202

To date, some recent studies have been mainly focused on elucidating the production routes of C_2 dimers and CN radicals. The formation processes of C_2 from laser ablation of a mixture of benzoic acid-^{12}C and amorphous carbon-^{13}C were firstly studied by *Dong et al.* Their results demonstrated the occurrence of a recombination process to create C_2 molecules since emissions associated to the species $^{12}C^{13}C$ were featured in LIBS spectra from the plasmas induced on such target.[199] Furthermore, spectral features from plasmas of benzoic acid-α-^{13}C (^{13}C-labeled terminus were explored. The computed $^{12}C^{12}C/^{13}C^{12}C$ intensity ratios pointed out also a direct release of C_2

molecules from the aromatic ring of the compound as an additional formation mechanism. Therefore, findings force to come to the realization that the progress of both formation routes coexists during plasma lifetime. Moreover, it was observed that isotopic ratios ($^{12}C/^{13}C$) derived from C_2 and CN exhibited opposite behaviors with respect to delay time. These opposite trends proved not only that the dissociation of chemical bonds in the plasma is incomplete and selective but also that any mechanism forming CN from C_2 species as precursors can be unambiguously ruled out.[178] In addition, the above described mechanisms for the formation of C_2 species perfectly match with findings reached by *Glaus et al.* who investigated in a temporally and spatially resolved manner the LIBS analysis of fumaric acid with a ^{13}C labeled double bond. Researchers observed that the recombination of atomized C dominates the generation of C_2 at early times following the plasma formation, whereas the incomplete breakage of C=C bonds (^{13}C labeled) was demonstrated to be a significant process at later times.[179] In parallel, the isotopic labeling of organics with ^{15}N also allowed inferring the contribution of ambient nitrogen to the formation mechanism of CN radicals. The larger amount of $^{12}C^{14}N$ emissions as compared with those of $^{12}C^{15}N$ derived from nanosecond laser-induced plasmas of $^{15}N_2$-urea samples in ^{14}N ambient gas indicated that the reaction of atmospheric N with C species is the preferential origin of CN radicals.[179] However, while the pronounced anisotropy of the $^{12}C^{15}N$ to $^{12}C^{14}N$ ratio detected in the early plasma pointed out a poor initial mixing of the plasma with the ambient gas, for later times of plasma (> 20 μs) the contributions from the sample and ambient nitrogen isotopes tend to balance.

Amongst the research that comprise the present Doctoral Thesis, the newest findings on evaluating the formation routes of hydrogenated radicals (OH, NH and CH) using similar approaches to those described are reported; specifically, from the analysis of several deuterated molecular solids. The reader is referred, in particular, to the Chapter 3 of the present document to find further detailed information on these investigations.

5. Applications of LIBS to the analysis of organic materials

In recent times, laser-induced breakdown spectroscopy has proved to be a versatile and effective tool for the analysis of organic materials in several application fields. Some examples of the most explored applications are illustrated in Figure 15. Among them, the detection of explosive compounds in homeland security and forensic science, and the sorting of plastics for recycling have acquired notable significance. Furthermore, other applications such as the identification of microbiological samples and the quality control in food and pharmaceutical industry are gathering greater importance over time.

As pointed out above, optical emission responses from laser-induced plasmas of organic compounds bear a great similarity between them; a circumstance that severely limits the selectivity and the specificity of the technique to this type of compounds. Generally, spectral features displayed

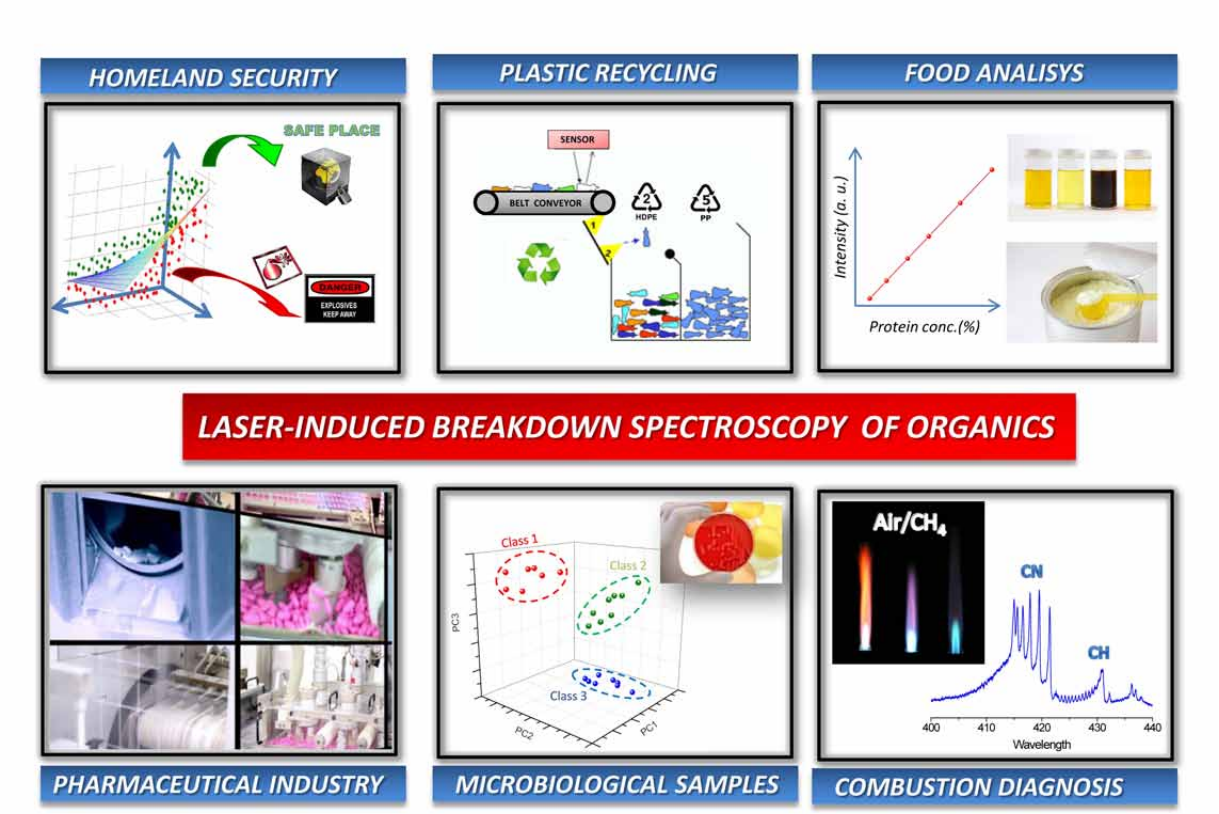

Figure 15. LIBS applications to organic materials.

by LIBS spectra of organic compounds are lines of C, H, O and N, and sequences of molecular bands, primarily of the CN and C_2 molecules. Therefore, it is spectral information that requires powerful data treatment tools to address the enormous detection and identification challenges being posed. As a solution, in almost the totally of the cases at hand, LIBS is coupled to chemometric techniques. Basically, chemometrics performs calculations on the emission measurements of chemical excited species using statistic principles, mathematical models and computational methods, thereby allowing extraction a larger amount of information from a raw data set.

The combination of chemometric methods with LIBS data has been mainly focused to the detection and identification of unknown targets. In this vein, ***pattern recognition*** methods that are based on the labeling of an input measurement (e.g. spectrum), are commonly used. When the models developed for classification are trained from previously labeled data, methods are referred as ***supervised learning*** techniques. Conversely, when classification models are trained from unlabeled data, techniques are termed as ***unsupervised learning*** methods.[207]

Regardless the statistical technique used, the same procedure is accomplished for predictive applications in the ***supervised pattern recognition*** technique. The framework of this approach is schematized in Fig. 16. First, LIBS information is acquired under fixed and well-defined operational conditions. This original data can be preprocessed, if applicable. For instance, spectral normalization, a background subtraction, or a signal smoothing are common processes to apply. In addition, in general, prior to the chemometric modeling, the data set acquired is reduced by removing non-informative variables. Thus, only those spectral features coherent with the specific chemical constituents of organic compounds are extracted to create a recognition classifier. To this end, supervised recognition method operates in two chronologically non-overlapping stages. First, a learning stage is applied to the information supplied by a labeled training data set. During this phase, the algorithm acquires the necessary knowledge to find a regularity in patterns of the training data set and to derive a rule that is able to differentiate among the regarded classes and, therefore, to

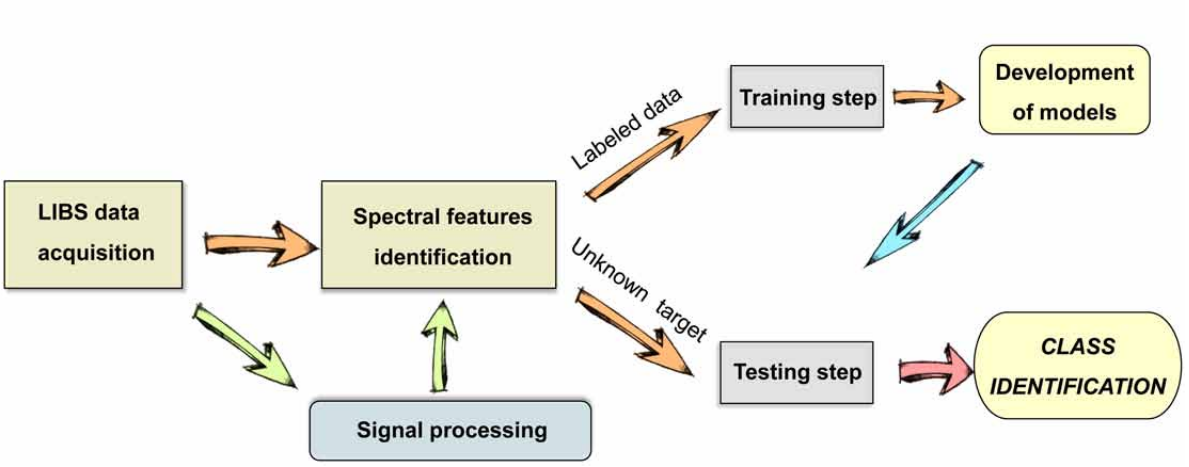

Figure 16. Schematic sequence for class identification by supervised pattern recognition.

assign, on future, any unknown sample to one of these classes. Once completed this phase, a testing stage starts. Without any attempts to acquire new knowledge, the algorithm proceeds to classify some known samples –labeled test data–, which had not initially been included in the training data set, as members of the considered classes. This step allows evaluating the classificatory abilities of the designed model. Once the performance is assured, the model may be routinely applied to future predictions.

A large variety of chemometric methods have been combined with LIBS to cope with classification of organic samples. Among them, the most outstanding are listed below:

- method of normalized coordinates (MNC)[208]
- principal components analysis (PCA)[209]
- linear discriminant analysis (LDA)[210]
- partial least squares-discriminant analysis (PLS-DA)[209,211]
- soft independent modeling of class analogy (SIMCA)[209,212] and
- neural networks (NN)[212,213]

Because it is not the subject of this Doctoral Thesis, the intricacies of all these chemometric techniques are not significantly detailed. For more detailed information, readers are referred to specific references.[214,215]

In contrast, in the focusing of the issue before us, the next sections, disaggregated by application fields, will provide a brief review to the state of the art in LIBS analysis of organic compounds.

5.1. Detection of explosive materials

Currently, the design of sensors and the development of techniques to detect an explosive material in real-time regardless its location, is of crucial importance due to the latent threat of a terrorist attack.[216] In this sense, LIBS disposes of a series of characteristics, which places it at the forefront of explosive sensing techniques, as compared to other analytical techniques. LIBS copes with difficult analytical challenges since hardly alters the target interrogated, has capability of operating in-situ (field-deployable sensors), in real time, and rapidly and with appropriate sensitivity. Furthermore, LIBS sensors may be miniaturized and designed to work in a contactless way at long distances, somewhat which minimizes the risk for the operator.[217]

Research in explosives detection by LIBS arose in 2006 when residues of organic explosives, located on aluminum supports, were detected at distances up to 45 m. In this work, the discrimination between organic explosives (TNT, RDX, PETN, Composition B and C4) and harmless compounds was accomplished by means of an algorithm based on intensity ratios of representative emission signals.[218] Since then, the capabilities of LIBS for the detection of energetic materials have been extensively explored.[23,219] In this field, LIBS has reached new heights with the detection of explosive residues from human fingerprints left on solid surfaces at distances up to 30 m.[220] Indeed,

LIBS sensors designed to this matter have become more robust, and currently, some of them offer a great number of features like target pointing, scanning and wide-ranging capabilities.[221]

Beyond the conventional operating mode, LIBS has also coped with the recognition of explosives materials under different configurations. The uses of double pulse configurations (*DP*-LIBS)[222-224] and ultrashort excitation (*fs*-LIBS)[225-227] have demonstrated to have several advantages, thereby reporting noteworthy results. *DP*-LIBS has proved an improvement on the selectivity to the explosives identification, since the contributions of atmospheric emissions, mainly O and N, on the final emission pattern are reduced. This is a crucial factor when O and N emission lines are used as discriminant variables in the chemometric models. Moreover, the sensitivity of the method gets better because emission intensities increase, probably, due to the thermal reheating of the plasma.[223]

Concerning the effect of ultrashort laser pulses in the recognition of explosives by LIBS, few studies have been done. Such a circumstance is justified on the complexity involved in working with *fs*-LIBS due to both the big size of femtosecond lasers as well as by their more restrictive operational conditions. All this hinders its assembling in portable sensors. In any case, several studies have evidenced possible advantages of *fs*-LIBS for the identification of organic explosives as compared to *ns*-LIBS. Some of them are a reduced interrogation of the substrate when explosive residues are investigated, the minimization of the background continuum within the optical responses, as well as, like in the case of *DP*-LIBS, a negligible atmospheric entrainment. However, these benefits tend to disappear for large laser fluences.[226] A comparison between *fs*- and *ns*-LIBS of trinitrotoluene (TNT) residues deposited on aluminum supports found larger molecular emissions (C_2 and CN), which can be considered as tracers for this explosive, in the case of the ultrashort pulse regime.[225] Moreover, the molecular formation dynamics of few explosives like NTO, HMX, and RDX in distinct atmospheres have been scrutinized[228] and emission signatures resulting from femtosecond and nanosecond laser-induced plasmas have been compared. Results revealed that the CN-to-C emission intensity ratio in these nitrogen-containing compounds was higher for ultrashort irradiation

as compared to that attained for the *ns* regime; a distinctive character that may be beneficial for identification purposes.[227]

In a real-world scenario of a terrorist attack, finding clues lies on the sensing of traces deposited on solid surfaces rather than detecting a bulk material in itself. This operational framework has guided the strategic focus in many of the research works to investigate laser ablation of binary samples instead of the laser sensing of pure explosives. Such binary targets raise several possibilities to occur. The explosive residues may be localized in a large variety of surfaces with widely varying properties, being the chemical composition, due to the subject that we are concerned with, the most relevant feature. Always depending on the thickness, in general, a thin layer of an explosive residue is ablated together with the support behind it. Hence, detection of organic traces located on the surface of a metallic surface is relatively straightforward. The spectrally-resolved emissions of the organic compound are easily traceable among those of the metallic species.[229] Indeed, the mere identification of carbon related emissions (e.g. C, CN and C_2) indicates the presence of the organic substance. Conversely, if the support and the residue have the same nature (i.e. both are organics) the detection of explosive traces becomes a more difficult task. As both of them exhibit an analogous elemental composition, they contribute with identical signals to the final emission spectrum. Spectral information is expected to differ only in the relative intensity of the observed emissions, regardless of whether the residue exists on the support or not.

Once residues have been detected, special case is the subsequent distinction between harmful and innocuous materials, whatever the binary target. The challenge lies on the differentiation between residues that share similar elemental composition; a problem that becomes worse when surface has a related chemical composition. Some solutions have been put forward in this regard. On the one hand, the choice of an appropriate set of experimental conditions, such as the irradiance level and a fine tuning of the focal conditions of the laser pulses, enlarges the sensitivity of a surface analysis, and hence allows a selective inspection of the residue by the absence of any contribution

from the support.[230] An alternative option is to tackle the differentiation with spectral data treatments and the chemometric techniques.

Since a significant number of investigations conducted during the development of the present Doctoral Thesis project are focused on the design and implementation of chemometric strategies to the LIBS information for recognizing explosive residues, the reader is urged to browse on the specific chapters 5, 6, and 7 for further detailed information. As a summary, it can be pointed out that ***supervised learning methods (SLMs)*** have been considered to address three distinct real-world situations: the recognition of organic explosives located on aluminum supports, the recognition of organic explosives located on polymeric substrates, and the recognition of explosive fingerprints on objects for courier services. It should be emphasized that performance of this chemometric framework has been very successfully tested, validated, and also transferred from a laboratory scale to a remote recognition of explosive fingerprints at the Laser Laboratory of University of Málaga.[231]

5.2. Sorting of polymers

The use of LIBS as analytical tool for the classification of polymers lies in the need of alternative methods for recovering plastic wastes within the first stage of a recycling process. As mentioned, the great speed in analysis, the nondestructive nature, and the ability for real-time monitoring of LIBS are features that bring also many benefits for the sorting process of plastics.[147] As in the case of explosives recognition, different strategies have been used to process the LIBS information in order to distinguish between polymers. Among them, the correlation with spectral libraries by the method of normalized coordinates (MNC),[208,232] the analysis of spectral emission ratios,[233.] the application of multivariate methods[234] and artificial neural networks (ANNs)[213,235] have been considered for identifying polymer samples. Polymers such as polyethylene terephthalate

(PET), polyethylene (PE), polypropylene (PP), and polystyrene (PS), which compose the most common objects that we use in our everyday, have been discriminated by means LIBS.

On the other hand, LIBS instruments implemented for in-line measurements have proven to effectively identify polymer wastes with high content in chlorine (e.g. polyvinyl chloride, PVC)[236] In the same way, emission lines of F have been used as tracers on the identification of fluorine containing polymers (e.g. polytetrafluoroethylene, PTFE).[237]

Despite that the determination of the elemental composition of polymers allows an efficient sorting of plastics, the waste management process for recycling also seeks to remove potentially toxic plastics. This challenging issue can be addressed through the examination of the particular composition of plastic additives. In this context, LIBS has been applied to analyze the content of toxic heavy metals involved in pigments (Pb, Cd, Hg …) of technical polymers[238] and of plastic parts of toys [239] as well as to identify flame retardants (Br, Cl …) in several plastics.[240]

In this line of enquiry, the most cutting-edge application of LIBS to plastic recycling processes lies on the classification of polymeric fragments from obsolete mobile phones. To this end, chemometric models for plastic samples classification have been designed on the basis of emission lines of elements representative of the coatings, like Si, Al, Ti, Na, K, and Ag, rather than on emission features related to organics.[241]

Undoubtedly, the feasibility of LIBS for the analysis of polymers seems more than evident in view of the numerous researches dealing with this issue. However, it is still far from being implemented as a reference method of analysis in an industrial environment.

5.3. Identification of microbiological samples

The identification of microbiological samples like bacterial spores, molds, pollens, and nerve agent simulants is an extended application of LIBS in the fields of food security, environmental

inspection and citizen security. The similar elemental composition of the samples is again the main challenge in the use of LIBS for the classification of biological species. Hence, on this occasion, researchers have also had recourse to the use of chemometric tools for deciphering spectral information to afford discrimination among the different biomaterials. From the mere use of several cumulative intensity ratios [149] up until implementation of sophisticated multivariate methods [242-244], including the application of simple principal-components analysis[245], have been considered to deal with the differentiation of several types of biomaterials simulants of a chemical warfare.

In parallel, the analysis of bacterial samples is important to ensure food safety and streamline the food-monitoring process. In this context, multivariate regression analysis of LIBS spectra has been employed to distinguish the live bacterial pathogens *Escherichia coli O157:H7* and *Salmonella enterica*, on various foods (eggshell, milk, bologna, ground beef, chicken, and lettuce) and food-processing surfaces (metal drain strainer and cutting board).[246] Also regarding issues relating to human security, neural networks have been used for the Identification and discrimination of bacterial strains of same species causing hospital acquired infections, as they exhibit resistance to antibiotics, through detection of the small changes in their atomic composition, as a result of their mutations and genetic variations.[152]

Beyond the development of the predictive models, some efforts have been also focused in the use of alternative operative conditions to deal with these issues. In this regard, bacterial samples (*Escherichia coli* and *Bacillus subtilis*) have been analyzed by LIBS using femtosecond laser pulses. Some specific features, like the negligible displaying of emissions of N and O from the excited surrounding air, the favored emissions of intramolecular bonds as compared to the atomic ones, and the different kinetic behavior of molecular band head intensities of native CN bonds released by sample and of new formed CN from carbon recombination with atmospheric nitrogen, have been attained using this ablation regime. All this converts *fs*-LIBS in a very attractive technique for analyzing biological samples, since the outputs provide valuable data that allows an unambiguous

distinction for a specific bacterium either from a natural environment or from other biological species.[112]

5.4. Food industry

LIBS has also demonstrated the potential to be a game changer in the food industry, which has also benefited from the product discrimination attainable with conventional LIBS sensors. In this context, LIBS combined with neural networks (NNs) has been applied to the identification, quality control, traceability, and adulteration detection of extra virgin olive oils with a certainty of more than 95%.[247] Furthermore, the level of C_2 emissions compared to atomic carbon emissions has been used to correlate the content of saturated fatty acids in oils in order to differentiate between palm oil and a group formed by corn, olive and sunflower oil.[248]

Another attractive application is the analysis of milk samples. LIBS measurements in low pressure He atmosphere allowed obtaining a good correlation between CN emission levels and the protein content in milk. Such emission feature was used to quantify the protein concentration in the samples tested.[249] In parallel, a qualitative analysis of the composition, including not only proteins but also trace elements, of maternal milk and commercial infant formulas was performed by *Z. Abdel-Salam et al*. The relative concentration of proteins was also related to CN and C_2 emissions.[250]

Finally, LIBS has been also employed to detect residues of pesticides (chlorpyrifos) located on fruit surfaces. In this case, P, S and Cl emission lines were used as main analytical assets to differentiate between clean and contaminated fruits.[251]

5.5. Pharmaceutical industry

While up until only a few years ago, LIBS was largely unfamiliar to the pharmaceutical industry, several research works have evidenced the possibility of using this technique for qualitative and quantitative analysis of pharmaceutical products that are mainly formed by an organic matrix. The capabilities of LIBS for a rapid quantitative analysis of multi-component pharmaceutical tablets was first illustrated using the atomic line emissions from some specific hetero-atoms such as phosphorus, chlorine, and fluorine contained in the pharmaceutical active ingredients of solid dosage form. Since none of these elements were present in the inactive matrix, they could conveniently be used to tag and quantify the drug content. It was also shown that using internal standardization of the corresponding atomic line emission with the C emission line at 247 nm the analytical performance of LIBS, namely in terms of sensitivity, linearity, precision and reduction of matrix effects was significantly improved. Furthermore, it was demonstrated that LIBS was able to measure the concentration of magnesium stearate (used as lubricant in some tablets); a task which had not been possible with High performance liquid chromatography technique –routinely used in the pharmaceutical industry.[252]

Concerning the organic analysis, several analgesic pills —paracetamol, ibuprofen, and acetylsalicylic acid— have been indentified based on the use of spectral libraries and intensity ratios involving C, C_2, H, N and O emissions.[253] In addition, conventional chemometric tools (SIMCA and PLS-DA) and a nonlinear classification method as support vector machines (SVM) have been applied to the discrimination of pharmaceutical samples.[254] A comparative study evidenced that the utilization of SVM provides important improvements over classical chemometric approaches for the discrimination of such samples in terms of accuracy and sensitivity.[255]

Beyond chemical analysis, LIBS has shown to be a valuable tool in this application field to cope with other type of essays to assess the quality of pharmaceutical products. In this context, even though it proceeds through evaluation of optical emissions from representative elements, LIBS has

been used for rapid determining the thickness of coating and the uniformity of the content in pharmaceutical tablets by a depth profile monitoring.[256,257]

5.6. Combustion diagnostics

Last but not least, LIBS has been also used as a diagnostic method for combustion systems. Measurements of gas composition in these systems are needed to recognize the gas mixing and to optimize the combustion process. Several works have addressed this issue. For instance, LIBS was used to analyze composition in reactants and in flames for different gas mixture fractions of C_3H_8, CH_4, and CO_2 in air. Atomic emission ratios including C, O, and N lines were used to predict the gas composition.[258]

Stavropoulos et al. used LIBS to determine the equivalence ratio of fuel-to-air inside combustion systems in laminar premixed methane–air Bunsen flames. Such equivalence ratio was quantitatively determined from the ratio of intensities hydrogen and oxygen lines,[259,260] or alternatively from the number densities ratio of such species.[261] In this line, an ungated miniature LIBS sensor for studying a methane/air flame has been also developed and used to measure the equivalence ratio of a CH_4/air flame by computing the intensity ratio of H_α and O emission lines.[262] Furthermore, emission intensity ratios of LIBS signals have been used to obtain quantitative measurements of the mixture fraction of natural gas-air in turbulent flames.[263]

Lastly, femtosecond lasers have been also employed for combustion diagnosis in some experimental studies. *Kotzagianni et al.* performed the in-situ determination of fuel content in methane-air combustible mixtures. A linear increase of CN intensity with the concentration of fuel was noticed. Thus, the use of CN signal was proposed to examine the fuel content in such combustion flames.[264,265]

In summary, the above described LIBS applications evidence that this technique does not clash with other analytical techniques for the analysis of organic materials. LIBS has demonstrated to be able for coping with some complicated goals beyond its multielemental atomic nature. However, there is still a long way to go and many challenges lie ahead for solving to reach the necessary maturity for its overall effectiveness to be assessed. In this sense, all the experimentation contained in the present Doctoral Thesis seeks to contribute a grain of sand for making progress towards the maturity and the exploitation of LIBS as a leading-edge analytical tool.

REFERENCES

1 F. J. Fortes, J. Moros, P. Lucena, L. M. Cabalín, J. J. Laserna, *Laser-induced breakdown spectroscopy*, Anal. Chem. 85 (2013) 640–669.

2 D. A. Cremers, R. C. Chinni, *Laser-induced breakdown spectroscopy—capabilities and limitations*, Appl. Spectrosc. Rev. 44 (2009) 457–506.

3 T. H. Maiman, *Stimulated optical radiation in ruby*, Nature 187 (1960) 493–494.

4 F. Brech, L. Cross, *Optical microemission stimulated by a ruby laser*, Appl. Spectrosc. 16 (1962) 59.

5 J. Debras Guédon, N. Liodec, *De l'utilisation du faisceau d'un amplificateur a ondes lumineuses par émission induite de rayonnement (laser á rubis), comme source énergetique pour l'excitation des spectres d'émission des elements*, C.R. Acad. Sci. 257 (1963) 3336–3339.

6 E. F. Runge, R. W. Minck, F. R. Bryan, *Spectrochemical analysis using a pulsed laser source*, Spectrochim. Acta 20 (1964) 733–735.

7 P. D. Maker, R. W. Terhune, C. M. Savage,. *Optical third harmonic generation*, Proceedings of the 3rd International Conference on Quantum Electronics, Paris, Columbia University Press, New York (1964), Vol. 2: 1559.

8 A. A. Buzukov, Y. A. Popov, V. S. Teslenko, *Experimental study of explosion caused by focusing monopulse laser radiation in water*, Zhurnal Prikladnoi Makhaniki i Tekhnicheskoi Fiziki, 10 (1969) 17–22.

9 T. R. Loree, L. J. Radziemski, *Laser-induced breakdown spectroscopy: time-integrated applications*. Plasma Chem. Plasma Proc. 1 (1981) 271–280.

10 L. J. Radziemski T. R. Loree, *Laser-induced breakdown spectroscopy: time-resolved spectrochemical applicatio*ns, Plasma Chem. Plasma Proc. 1 (1981) 281–293.

11 V. I. Babushok, F .C. De Lucia, Jr., J. L. Gottfried, C. A. Munson, A. W. Miziolek, *Double pulse laser ablation and plasma: Laser induced breakdown spectroscopy signal enhancement*, Spectrochim. Acta Part B, 61 (2006) 999–1014.

12 S. Y. Chan, N. H. Cheung, *Analysis of solids by laser ablation and resonance-enhanced laser-induced breakdown spectroscopy*, Anal. Chem. 72 (2000) 2087–2092.

13 J. D. Wu, N. H. Cheung, *Resonant-enhanced laser-induced breakdown spectroscopy for multielement analysis in laser ablative sampling*, Appl. Spectrosc. 55 (2001) 366–370.

14 S. L. Lui, N. H. Cheung, *Resonance-enhanced laser-induced plasma spectroscopy for sensitive elemental analysis: Elucidation of enhancement mechanisms*, Appl. Phys. Lett. 81 (2002) 5114.

15 L. M. Cabalín, A. González, V. Lazic, J. J. Laserna, *Deep ablation and depth profiling by laser-induced breakdown spectroscopy (LIBS) employing multi-pulse laser excitation: Application to galvanized steel*, Appl. Spectrosc. 65 (2011) 797–805.

16 B. Le Drogoff, J. Margot, M. Chaker, M. Sabsabi, O. Barthélemy, T. W. Johnston, S. Laville, F. Vidal, Y. Von Kaenel, *Temporal characterization of femtosecond laser pulses induced plasma for spectrochemical analysis of aluminum alloys*, Spectrochim. Acta Part B 56 (2001) 987–1002.

17 F. J. Fortes, J. J. Laserna, *The development of fieldable laser-induced breakdown spectrometer: No limits on the horizon*, Spectrochim. Acta Part B 65 (2010) 975–990.

18 B. Sallé, P. Mauchien, S. Maurice, *Laser-induced breakdown spectroscopy in open-path configuration for the analysis of distant objects*, Spectrochim. Acta Part B 62 (2007) 739–768.

19 S. Guirado, F. J. Fortes, V. Lazic, J. J. Laserna, *Chemical analysis of archeological materials in submarine environments using laser-induced breakdown spectroscopy. On-site trials in the Mediterranean Sea*, Spectrochim. Acta Part B 74–75 (2012) 137–143.

20 R. C. Wiens, S. Maurice, & The ChemCam Team, *The ChemCam instrument suite on the Mars Science Laboratory rover Curiosity: remote sensing by laser-induced plasmas*, Geochem. News 145 (2011) 41–48.

21 R. Noll, C. Fricke-Begemann, M. Brunk, S. Connemann, C. Meinhardt, M. Scharun, V. Sturm, J. Makowe, C. Gehlen, *Laser-induced breakdown spectroscopy expands into industrial applications*, Spectrochim. Acta Part B 93 (2014) 41–51.

22 Q. Q. Wang, K. Liu, H. Zhao, C. H. Ge, Z. W. Huang, *Detection of explosives with laser-induced breakdown spectroscopy*, Front. Phys. 7 (2012) 701–707.

23 J. L. Gottfried, F. C. De Lucia Jr., C. A. Munson, A. W. Miziolek, *Laser-induced breakdown spectroscopy for detection of explosives residues: A review of recent advances, challenges, and future prospects*, Anal. Bioanal. Chem. 395 (2009) 283–300.

24 R. S. Harmon, J. Remus, N. J. McMillan, C. McManus, L. Collins, J. L. Gottfried, F.C. De Lucia Jr., A. W. Miziolek, *LIBS analysis of geomaterials: Geochemical fingerprinting for the rapid analysis and discrimination of minerals*, Appl. Geochem. 24 (2009) 1125–1141.

25 J. L. Gottfried, R. S. Harmon, F. C. De Lucia Jr., A. W. Miziolek, *Multivariate analysis of laser-induced breakdown spectroscopy chemical signatures for geomaterial classification*, Spectrochim. Acta Part B, 64 (2009) 1009–1019.

26 V. K. Singh, A. K. Rai, *Prospects for laser-induced breakdown spectroscopy for biomedical applications: A review*, Lasers Med. Sci. 26 (2011) 673–687.

27 R. Gaudiuso, M. Dell'Aglio, O. De Pascale, G. S. Senesi, A. De Giacomo, *Laser-induced breakdown spectroscopy for elemental analysis in environmental, cultural heritage and space applications: A review of methods and results*, Sensors 10 (2010) 7434–7468.

28 R. C. Wiens, S. Maurice, B. Barraclough, M. Saccoccio, W. C. Barkley, J. F. Bell III, S. Bender, J. Bernardin, D. Blaney, J. Blank, M. Bouyé, N. Bridges, N. Bultman, P. Caïs, R. C. Clanton, B. Clark, S. Clegg, A. Cousin, D. Cremers, A. Cros, L. DeFlores, D. Delapp, R. Dingler, C. D'Uston, M. D. Dyar, T. Elliott, D. Enemark, C. Fabre, M. Flores, O. Forni, O. Gasnault, T. Hale, C. Hays, K. Herkenhoff, E. Kan, L. Kirkland, D. Kouach, D. Landis, Y. Langevin, N. Lanza, F. LaRocca, J. Lasue, J. Latino, D. Limonadi, C. Lindensmith, C. Little, N. Mangold, G. Manhes, P. Mauchien, C. McKay, E. Miller, J. Mooney, R. V. Morris, L. Morrison, T. Nelson, H. Newsom, A. Ollila, M. Ott, L. Pares, R. Perez, F. Poitrasson, C. Provost, J. W. Reiter, T. Roberts, F. Romero, V. Sautter, S. Salazar, J. J. Simmonds, R. Stiglich, S. Storms, N. Striebig, J.J. Thocaven, T. Trujillo, M. Ulibarri, D. Vaniman, N. Warner, R. Waterbury, R. Whitaker, J. Witt, B. Wong-Swanson, *The ChemCam instrument suite on the Mars Science Laboratory (MSL) rover: Body unit and combined system tests*, Space Sci. Rev. 170 (2012) 167–227.

29 S. Maurice, R. C. Wiens, M. Saccoccio, B. Barraclough, O. Gasnault, O. Forni, N. Mangold, D. Baratoux, S. Bender, G. Berger, J. Bernardin, M. Berthé, N. Bridges, D. Blaney, M. Bouyé, P. Caïs, B. Clark, S. Clegg, A. Cousin, D. Cremers, A. Cros, L. DeFlores, C. Derycke, B. Dingler, G. Dromart, B. Dubois, M. Dupieux, E. Durand, L. d'Uston, C. Fabre, B. Faure, A. Gaboriaud, T. Gharsa, K. Herkenhoff, E. Kan, L. Kirkland, D. Kouach, J. L. Lacour, Y. Langevin, J. Lasue, S. Le Mouélic, M. Lescure, E. Lewin, D. Limonadi, G. Manhès, P. Mauchien, C. McKay, P. Y. Meslin, Y. Michel, E. Miller, H. E. Newsom, G. Orttner, A. Paillet, L. Parès, Y. Parot, R. Pérez, P. Pinet, F. Poitrasson, B. Quertier, B. Sallé, C. Sotin, V. Sautter, H. Séran, J. J. Simmonds, J. B. Sirven, R. Stiglich, N. Striebig, J. J. Thocaven, M. J. Toplis, D. Vaniman, *The ChemCam instrument suite on the Mars Science Laboratory (MSL) rover: Science objectives and mast unit description*, Space Sci. Rev. 170 (2012) 95–166.

30 D. W. Hahn, N. Omenetto, *Laser-induced breakdown spectroscopy (LIBS), part II: Review of instrumental and methodological approaches to material analysis and applications to different fields*, Appl. Spectrosc. 66 (2012) 347–419.

31 D. W. Hahn, N. Omenetto, *Laser-induced breakdown spectroscopy (LIBS), part I: Review of basic diagnostics and plasma particle interactions: Still-challenging issues within the analytical plasma community*, Appl. Spectrosc. 64 (2010) 335–366.

32 L. St-Onge, R. Sing, S. Béchard, M. Sabsabi, *Carbon emissions following 1:064 nm laser ablation of graphite and organic samples in ambient air*, Appl. Phys. A 69 (1999) S913–S916.

33 V. I. Babushok, F. C. De Lucia Jr., P. J. Dagdigian, J. L. Gottfried, C. A. Munson, M. J. Nusca, A. W. Miziolek, *Kinetic modeling study of the laser-induced plasma plume of cyclotrimethylenetrinitramine (RDX)*, Spectrochim. Acta Part B 62 (2007) 1321–1328.

34 M. Baudelet, M. Boueri, J. Yu, S. S. Mao, V. Piscitelli, X. Mao, R. E. Russo, *Time-resolved ultraviolet laser-induced breakdown spectroscopy for organic material analysis*, Spectrochim. Acta Part B 62 (2007) 1329–1334.

35 J. J. Camacho, L. Díaz, M. Santos, L. J. Juan, J. M. L. Poyato, *Temporal evolution of the laser-induced plasma generated by IR CO_2 pulsed laser on carbon targets*, J. Appl. Phys. 106 (2009) 033306.

36 P. J. Dagdigian, A. Khachatrian, V. I. Babushok, *Kinetic model of C/H/N/O emissions in laser-induced breakdown spectroscopy of organic compounds*, Appl. Opt. 49 (2010) C58–C66

37 K. Sovová, K. Dryahina, P. Španěl, M. Kyncl, S. Civiš, *A study of the composition of the products of laser-induced breakdown of hexogen, octogen, pentrite and trinitrotoluene using selected ion flow tube mass spectrometry and UV-Vis spectrometry*, Analyst 135 (2010) 1106–1114.

38 P. Lucena, A. Doña, L. M. Tobaria, J. J. Laserna, *New challenges and insights in the detection and spectral identification of organic explosives by laser induced breakdown spectroscopy*, Spectrochim. Acta Part B 66 (2011) 12−20.

39 S. Grégoire, V. Motto-Ros, Q. L. Ma, W. Q. Lei, X. C. Wang, F. Pelascini. F. Surma, V. Detalle, J. Yu, *Correlation between native bonds in a polymeric material and molecular emissions from the laser-induced plasma observed with space and time resolved imaging*, Spectrochim. Acta Part B 74–75 (2012) 31–37.

40 R. E. Russo, X. Mao, J. J. Gonzalez, V. Zorba, J. Yoo, *Laser ablation in analytical chemistry*, Anal. Chem. 85 (2013) 6162–6177.

41 S. S. Harilal, R. C. Issac, C. V. Bindhu, V. P. N. Nampoori, C. P. G. Vallabhan, *Optical emission studies of C_2 species in laser-produced plasma from carbon*, J. Phys. D. Appl. Phys. 30 (1997) 1703–1709.

42 D. A. Cremers, L. J. Radmziemski, *Handbook of laser-induced breakdown spectroscopy*, Wiley, Chichester (2006).

43 J. Yu, Q. Ma, V. Motto-Ros, W. Lei, X. Wang, X. Bai, *Generation and expansion of laser-induced plasma as a spectroscopic emission source*, Front. Phys. 7 (2012) 649–669.

44 R. Noll, *Laser-induced breakdown spectroscopy (LIBS). Fundamentals and applications*, Springer-Verlag, Berlin (2012).

45 G. Cristoforetti, S. Legnaioli V. Palleschi, A. Salvetti, E. Tognoni, *Characterization of a collinear double pulse laser-induced plasma at several ambient gas pressures by spectrally- and time-resolved imaging*, Appl. Phys. B 80 (2005) 559–568.

46 P. K. Diwakar, S. Groh, K. Niemax, D. W. Hahn, *Study of analyte dissociation and diffusion in laser-induced plasmas: implications for laser-induced breakdown spectroscopy*, J. Anal. At. Spectrom. 25 (2010) 1921–1930.

47 G. Galbács, N. Jedlinszki, K. Herrera, N. Omenetto, B. W. Smith, J. D. Winefordner, *A study of ablation, spatial, and temporal characteristics of laser-induced plasmas generated by multiple collinear pulses*, Appl. Spectrosc. 64 (2010) 161–172.

48 M. Hauer, D. J. Funk, T. Lippert, A. Wokaun, *Time resolved study of the laser ablation induced shockwave*, Thin Solid Films 453–454 (2004) 584–588.

49 X. Zeng, X. L. Mao, R. Greif, R. E. Russo, *Experimental investigation of ablation efficiency and plasma expansion during femtosecond and nanosecond laser ablation of silicon*, Appl. Phys. A 80 (2005) 237–241.

50 M. Boueri, M. Baudelet, J. Yu, X. Mao, S. S. Mao, R. Russo, *Early stage expansion and time-resolved spectral emission of laser-induced plasma from polymer*, Appl. Surf. Sci. 255 (2009) 9566–9571.

51 B. Pokrzywka, A. Mendys, K. Dzierżęga, M. Grabiec, S. Pellerin, *Laser light scattering in a laser-induced argon plasma: Investigations of the shock wave*, Spectrochim. Acta Part B 74–75 (2012) 24–30.

52 B. Sallé, C. Chaléard, V. Detalle, J. L. Lacour, P. Mauchien, C. Nouvellon, A. Semerok, *Laser ablation efficiency of metal samples with UV laser nanosecond pulses*, Appl. Surf. Sci. 138–139 (1999) 302–305.

53 A. Semerok, C. Chaléard, V. Detalle, J. L. Lacour, P. Mauchien, P. Meynadier, C. Nouvellon, B. Sallé, P. Palianov, M. Perdrix, G. Petite, *Experimental investigations of laser ablation efficiency of pure metals with femto, pico and nanosecond pulses*, Appl. Surf. Sci. 138–139 (1999) 311–314.

54 A. De Giacomo, M. Dell'Aglio, R. Gaudiuso, S. Amoruso, O. De Pascale, *Effects of the background environment on formation, evolution and emission spectra of laser-induced plasmas*, Spectrochim. Acta Part B 78 (2012) 1–19.

55 L. V. Zhigilei, Z. Lin, D. S. Ivanov, *Atomistic modeling of short pulse laser ablation of metals: connections between melting, spallation, and phase explosion*, J. Phys. Chem. C 113 (2009) 11892–11906.

56 N. M. Bulgakova, R. Stoian, A. Rosenfeld, I. V. Hertel, W. Marine, E. E. B. Campbell, *A general continuum approach to describe fast electronic transport in pulsed laser irradiated materials: the problem of Coulomb explosion*, Appl. Phys. A 81 (2005) 345–356.

57 R. G. Root, *Modeling of post-breakdown phenomena in laser-induced plasmas and applications*, Ch. 2, edited by L. J. Radziemski and D. A. Cremers, New York: Dekker (1989).

58 D. D. Vallejo, *Spectroscopic investigations of plasma emission induced during laser material processing*, epubli GmbH, Berlin (2013).

59 M. Milan, J. J. Laserna, *Diagnostics of silicon plasmas produced by visible nanosecond laser ablation*, Spectrochim. Acta Part B 56 (2001) 275–288.

60 R. Rozman, I. Grabec, E. Govekar, *Influence of absorption mechanisms on laser-induced plasma plume*, Appl. Surf. Sci. 254 (2008) 3295–3305.

61 G. Bekfi, *Principles of laser plasmas*, Wiley, New York (1976).

62 Y. B. Zel'dovich, Y. P. Reizer, *Physics of shock waves and high temperature dynamics phenomena,* Dover publications, Inc., Mineola, New York, Academic (2002).

63 J. J. Chang and B. E. Warner, *Laser-plasma interaction during visible-laser ablation of metals*, Appl. Phys. Lett. 69 (1996) 473–475.

64 C. Porneala, D. A. Willis, *Observation of nanosecond laser-induced phase explosion in aluminum*, Appl. Phys. Lett. 89 (2006) 211121.

65 E. Leveugle, D.S. Ivanov, L.V. Zhigilei, *Photomechanical spallation of molecular and metal targets: Molecular dynamics study,* Appl Phys A-Mater. 79 (2004) 1643–1655.

66 A. A. Ionin, S. I. Kudryashov, L. V. Seleznev, *Near-critical phase explosion promoting breakdown plasma ignition during laser ablation of graphite*, Phys. Rev. E 82 (2010) 016404.

67 S. S. Harilal, A. Hassanein, M. Polek, *Late-time particle emission from laser-produced graphite plasma*, J. Appl. Phys. 110 (2011) 053301.

68 F. Capitelli, F. Colao, M. R. Provenzano, R. Fantoni, G. Brunetti, N. Senesi, *Determination of heavy metals in soils by laser induced breakdown spectroscopy*, Geoderma 106 (2002) 45−62.

69 I. B. Gornushkin, A. Ya. Kazakov, N. Omenetto, B. W. Smith, J. D. Winefordner, *Experimental verification of a radiative model of laser-induced plasma expanding into vacuum*, Spectrochim. Acta Part B 60 (2005) 215−230.

70 G. Cristoforetti, E. Tognoni, L. A. Gizzi, *Thermodynamic equilibrium states in laser-induced plasmas: From the general case to laser-induced breakdown spectroscopy plasmas*, Spectrochim. Acta Part B 90 (2013) 1–22

71 H. R. Griem, *Plasma spectroscopy*, McGraw-Hill, Inc., New York (1964).

72 J. A. Aguilera, C. Aragón, *Multi-element, Saha–Boltzmann and Boltzmann plots in laser-induced plasmas*, Spectrochim. Acta Part B 62 (2007) 378–385.

73 S. Rai, A. K. Rai and S. N. Thakur, *Identification of nitrocompounds with LIBS*, Appl. Phys. B: Lasers Opt. 91 (2008) 645–650.

74 M. Dong, X. Mao, J. J. González, J. Lu, R. E. Russo, *Time-resolved LIBS of atomic and molecular carbon from coal in air, argon and helium*, J. Anal. At. Spectrom. 27 (2012) 2066–2075.

75 D. A. Rusak, B. C. Castle, B. W. Smith, J. D. Winefordner, *Excitational, vibrational, and rotational temperatures in Nd:YAG and XeCl laser-induced plasmas*, Spectrochim. Acta Part B 52 (1997) 1929–1935.

76 C. Aragón, J. A. Aguilera, *Characterization of laser induced plasmas by optical emission spectroscopy: A review of experiments and methods*, Spectrochim. Acta Part B 63 (2008) 893–916.

77 J. Luque and D. R. Crosley, *LIFBASE: database and spectral simulation (version 2.1.1), SRI International Report MP 99– 009*, 1999.

78 G. Cristoforetti, A. De Giacomo, M. Dell'Aglio, S. Legnaioli, E. Tognoni, V. Palleschi, N. Omenetto, *Local Thermodynamic Equilibrium in Laser-Induced Breakdown Spectroscopy: Beyond the McWhirter criterion*, Spectrochim. Acta Part B 65 (2010) 86–95.

79 C. Tendero, C. Tixier, P. Tristant, J. Desmaison, P. Leprince, *Atmospheric pressure plasmas: A review*, Spectrochim. Acta Part B 61 (2006) 2–30.

80 R. W. P. McWhirter, in: Eds. R.H. Huddlestone, S.L. Leonard, *Plasma diagnostic techniques*, Academic Press, New York (1965) pp. 201–264.

81 A. Bogaerts, Z. Chen, *Effect of laser parameters on laser ablation and laser-induced plasma formation: A numerical modeling investigation*, Spectrochim. Acta Part B 60 (2005) 1280–1307.

82 J. M. Vadillo, J. M. Fernández Romero, C. Rodríguez, J. J. Laserna, *Effect of plasma shielding on laser ablation rate of pure metals at reduced pressure*, Surf. Interface Anal. 27 (1999) 1009–1015.

83 G. Cristoforetti, S. Legnaioli, V. Palleschi, E. Tognoni, P. A. Benedetti, *Observation of different mass removal regimes during the laser ablation of an aluminum target in air*, J. Anal. At. Spectrom. 23 (2008) 1518–1528.

84 X. Bai, Q. Ma, M. Perrier, V. Motto-Ros, D. Sabourdy, L. Nguyen, A. Jalocha, J. Yu *Experimental study of laser-induced plasma: Influence of laser fluence and pulse duration*, Spectrochim. Acta Part B 87 (2013) 27–35.

85 S. S. Harilal, C. V. Bindhu, Riju C. Issac, V. P. N. Nampoori, and C. P. G. Vallabhan, *Electron density and temperature measurements in a laser produced carbon plasma*, J. Appl. Phys. 82 (1997) 2140–2146.

86 M. Akram, S. Bashir, A. Hayat, K. Mahmood, R. Ahmad, M. Khaleeq-U-Rahaman, *Effect of laser irradiance on the surface morphology and laser induced plasma parameters of zinc*, Laser Part. Beams 32 (2014) 119–128.

87 A. E. Hussein, P. K. Diwakar, S. S. Harilal, A. Hassanein, *The role of laser wavelength on plasma generation and expansion of ablation plumes in air*, J. Appl. Phys. 113 (2013) 143305.

88 M. P. Mateo, G. Nicolás, A. Yañez, *Characterization of inorganic species in coal by laser-induced breakdown spectroscopy using UV and IR radiations*, Appl. Surf. Sci. 254 (2007) 868–872.

89 C. Barnett, E. Cahoon, J. R. Almirall, *Wavelength dependence on the elemental analysis of glass by laser induced breakdown spectroscopy*, Spectrochim. Acta Part B 63 (2008) 1016–1023.

90 W. Q. Lei, Q. L. Ma, V. Motto-Ros, X. S. Bai, L. J. Zheng, H. P. Zeng, J. Yu, *Effect of ablation photon energy on the distribution of molecular species in laser-induced plasma from polymer in air*, Spectrochim. Acta Part B 73 (2012) 7–12.

91 N. M. Shaikh, M. S. Kalhoro, A. Hussain, M. A. Baig, *Spectroscopic study of a lead plasma produced by the 1064 nm, 532 nm and 355 nm of a Nd:YAG laser*, Spectrochim. Acta Part B 88 (2013) 198–202.

92 T. Moscicki, J. Hoffman, Z. Szymanski, *The effect of laser wavelength on laser-induced carbon plasma*, J. Appl. Phys. 114 (2013) 083306.

93 V. Morel, A. Bultel, *Theoretical study of the formation mechanism of laser-induced aluminum plasmas using Nd:YAG fundamental, second or third harmonics*, Spectrochim. Acta Part B 94–95 (2014) 63–70.

94 Q. Wang, P. Jander, C. Fricke-Begemann, R. Noll, *Comparison of 1064 nm and 266 nm excitation of laser-induced plasmas for several types of plastics and one explosive*, Spectrochim. Acta Part B 63 (2008) 1011–1015.

95 N. S. Allen, *Photochemistry and photophysics of polymers materials, Ch. 14; Photoablation of polymers materials*, John Wiley and Sons, Inc.; New Jersey (2010).

96 S. Lazare, V. Granier, *Ultraviolet laser photoablation of polymers: a review and recent results*, Laser Chem. 10 (1989) 25–40.

97 E. Sutcliffe, R. Srinivasan, *Dynamics of UV laser ablation of organic polymer surfaces*, J. Appl. Phys. 60 (1986) 3315–3322.

98 G. D. Mahan, H. S. Cole, Y. S. Liu, H. R. Philipp, *Theory of polymer ablation*, Appl. Phys. Lett. 53 (1988) 2377–2379.

99 S. R. Cain, F. C. Burns, C. E. Otis, *On single-photon ultraviolet ablation of polymeric materials*, J. Appl. Phys. 71 (1992) 4107–4117.

100 S. R. Cain, *A photothermal model for polymer ablation: chemical modification*, J. Phys. Chem. 97 (1993) 7572–7577.

101 B. Luk'yanchuk, N. Bityurin, M. Himmelbauer, N. Arnold, *UV-laser ablation of polyimide: from long to ultra-short laser pulses*, Nucl. Instrum. Methods Phys. Res. B 122 (1997) 347–355.

102 V. Srinivasan, M. A. Smrtic, S. V. Babu, *Excimer laser etching of polymers*, J. Appl. Phys. 59 (1986) 3861–3867.

103 H. Schmidt, J. Ihlemann, B. Wolff-Rottke, K. Luther, J. Troe, *Ultraviolet laser ablation of polymers: Spot size, pulse duration, and plume attenuation effects explained*, J. Appl. Phys. 83 (1998) 5458–5468.

104 B. Luk'yanchuk, N. Bityurin, S. Anisimov, D. Bauerle, *The role of excited species in UV-laser materials ablation - Part I: Photophysical ablation of organic polymers*, Appl. Phys. A: Mater. Sci. Process. 57 (1993) 367–374.

105 B. Luk'yanchuk, N. Bityurin, S. Anisimov, N. Arnold, D. Bauerle, *The role of excited species in ultraviolet-laser materials ablation III*. Non-stationary ablation of organic polymers, Appl. Phys. A: Mater. Sci. Process. 62 (1996) 397–401.

106 R. E. Russo, X. Mao, J. J. González, J. Yoo, *Femtosecond vs. Nanosecond laser pulse duration for laser ablation chemical analysis*, Spectroscopy 28 (2013) 24–35.

107 T. A. Labutin, V. N. Lednev, A. A. Ilyin, A. M. Popov, *Femtosecond laser-induced breakdown spectroscopy*, J. Anal. At. Spectrom. 31 (2016) 90–118.

108 M. D. Shirk, P. A. Molian, *A review of ultrashort pulsed laser ablation of materials*, J. Laser Appl. 10 (1998) 18–28.

109 J. B. Sirven, B. Bousquet, L. Canioni, L. Sarger, *Time-resolved and time-integrated single-shot laser-induced plasma experiments using nanosecond and femtosecond laser pulses*, Spectrochim. Acta Part B 59 (2004) 1033–1039.

110 J. R. Freeman, S. S. Harilal, P. K. Diwakar, B. Verhoff, A. Hassanein, *Comparison of optical emission from nanosecond and femtosecond laser produced plasma in atmosphere and vacuum conditions*, Spectrochim. Acta Part B 87 (2013) 43-50.

111 B. N. Chichkov, C. Momma, S. Nolte, F. von Alvensleben, A. Tünnermann, *Femtosecond, picosecond and nanosecond laser ablation of solids*, Appl. Phys. A, 63 (1996) 109-115.

112 M. Baudelet, L. Guyon, J. Yu, J. P. Wolf, T. Amodeo, E. Frejafon, P. Laloi, *Femtosecond time-resolved laser-induced breakdown spectroscopy for detection and identification of bacteria: A comparison to the nanosecond regime*, J. Appl. Phys. 99 (2006) 084701.

113 B. Verhoff, S. S. Harilal, J. Freeman, P. K. Diwakar, A. Hassanein, *Dynamics of femto- and nanosecond laser ablation plumes investigated using optical emission spectroscopy*, J. Appl. Phys. 112 (2012) 093303.

114 K. H. Leitz, B. Redlingshofer, Y. Reg, A. Otto, M. Schmidt, *Metal ablation with short and ultrashort laser pulses*, Phys. Proc. 12 (2011) 230–238.

115 G. M. Fuge, M. N. R. Ashfold, S. J. Henley, *Studies of the plume emission during the femtosecond and nanosecond ablation of graphite in nitrogen*, J. Appl. Phys. 99 (2006) 014309.

116 J. R. Scott, A. J. Effenberger Jr., J. J. Hatch, *Influence of Atmospheric Pressure and Composition on LIBS*, in: S. Musazzi, U. Perini (Eds.), *Laser-induced breakdown spectroscopy*, Springer-Verlag, Berlin (2014) pp. 91–116.

117 Z. Chen, D. Bleiner, A. Bogaerts, *Effect of ambient pressure on laser ablation and plume expansion dynamics: A numerical simulation*, J. Appl. Phys. 99 (2006) 063304.

118 S. Mehrabian, M. Aghaei, S. H. Tavassoli, *Effect of background gas pressure and laser pulse intensity on laser induced plasma radiation of copper samples*, Phys. Plasmas 17 (2010) 043301.

119 K. R. Chen, J. N. Leboeuf, R. F. Wood, D. B. Geohegan, J. M. Donato, C. L. Liu, A. A. Puretzky, *Modeling of dynamical processes in laser ablation*, Appl. Surf. Sci. 96–98 (1996) 14–23.

120 T. Delgado, J. M. Vadillo, J. J. Laserna, *Pressure effects in laser-induced plasmas of trinitrotoluene and pyrene by laser-induced breakdown spectroscopy (LIBS)*, Appl. Spectrosc. 68 (2014) 33–38.

121 S. Yalçin, Y. Y. Tsui, R. Fedosejevs, *Pressure dependence of emission intensity in femtosecond laser-induced breakdown spectroscopy*, J. Anal. At. Spectrom. 19 (2004) 1295–1301.

122 N. Farid, S. S. Harilal, H. Ding, A. Hassanein, *Emission features and expansion dynamics of nanosecond laser ablation plumes at different ambient pressures*, J. Appl. Phys. 115 (2014) 033107.

123 A. J. Effenberger Jr., J. R. Scott, *Effect of atmospheric conditions on LIBS spectra*, Sensors 10 (2010) 4907–4925.

124 Y. I. Lee, K. Song, H. K. Cha, J. M. Lee, M. C. Park, G. H. Lee, J. Sneddon, *Influence of atmosphere and irradiation wavelength on copper plasma emission induced by excimer and Q-switched Nd:YAG laser ablation*, Appl. Spectrosc. 51 (1997) 959–964.

125 C. Colón, A. Alonso-Medina, *Application of a laser produced plasma: Experimental Stark widths of single ionized lead lines*, Spectrochim. Acta Part B. 61 (2006) 856–863.

126 N. Konjević, M. Ivković, S. Jovićević, *Spectroscopic diagnostics of laser-induced plasmas*, Spectrochim. Acta Part B. 65 (2010) 593–602.

127 Y. Iida, *Effects of atmosphere on laser vaporization an excitation processes of solid samples,* Spectrochim. Acta Part B 45 (1990) 1353–1367.

128 J. A. Aguilera, C. A. Aragón, *Comparison of the temperatures and electron densities of laser-produced plasmas obtained in air, argon, and helium at atmospheric pressure*, Appl. Phys. A Mater. 69 (1999) S475–S478.

129 E. Vors, C. Gallou, L. Salmon, *Laser-induced breakdown spectroscopy of carbon in helium and nitrogen at high pressure*, Spectrochim. Acta Part B 63 (2008) 1198–1204.

130 W. Sdorra, K. Niemax, *Basic investigations for laser microanalysis. III. Application of different buffer gases for laser-produced sample plumes*, Mikrochim. Acta 107 (1992) 319–327.

131 M. Kuzuya, H. Matsumoto, H. Takechi, O. Mikami, *Effect of laser energy and atmosphere on the emission characteristics of laser-induced plasmas*, Appl. Spectrosc. 47 (1993) 1659–1664.

132 H. H. Telle, A. González Ureña, R. J. Donovan, *Laser chemistry: spectroscopy, dynamics and applications*, John Wiley & Sons; Chichester (2007).

133 W. Koechner, *Solid-state laser engineering*, Springer Series in Optical Sciences, New York (2006).

134 D. Strickland, G. Mourou, *Compression of amplified chirped optical pulses*, Opt. Commun. 56 (1985) 219–221.

135 A. Dubietis, G. Jonusauskas, A. Piskarskas, *Powerful femtosecond pulse generation by chirped and stretched pulse parametric amplification in BBO crystal*, Opt. Commun. 88 (1992) 437–440.

136 S. Yefet, A. Pe'er, *A review of cavity design for Kerr lens mode-locked solid-state lasers*, Appl. Sci. 3 (2013) 694–724.

137 D. E. Spence, P. N. Kean, W. Sibbett, *60-fs Pulse generation from a self-mode-locked Ti:sapphire Laser*, Opt. Lett. 16 (1991) 42–44.

138 M. Wollenhaupt, A. Assion, T. Baumert, *Short and ultrashort laser pulses*. Chapter 12 in Springer *Handbook of lasers and optics*, F. Träger (Ed.), Springer, Berlin (2012) pp 1047–1094.

139 W. M. Steen, J. Mazumder, *Laser material processing*, 4th Edition, Springer, London (2010).

140 C. E. Webb, J. D. C. Jones, *Handbook of laser technology and applications*: Applications, Taylor & Francis; UK (2003).

141 H. Becker-Ross, S. V. Florek, *Echelle spectrometers and charge-coupled devices*, Spectrochim. Acta Part B 52 (1997) 1367–1375

142 C. Pasquini, J. Cortez, L. M. C. Silva, F. B. Gonzaga, *Laser induced breakdown spectroscopy*, J. Braz. Chem. Soc. 18 (2007) 463–512.

143 S. Musazzi, U. Perini, *LIBS instrumental techniques*, in: S. Musazzi, U. Perini (Eds.), *Laser-Induced breakdown spectroscopy*, Springer-Verlag, Berlin (2014) pp. 59-89.

144 S. Laville, M. Sabsabi, F. R. Doucet, *Multi-elemental analysis of solidified mineral melt samples by laser-induced breakdown spectroscopy coupled with a linear multivariate calibration*, Spectrochim. Acta Part B 62 (2007) 1557–1566.

145 D. L. Death, A. P. Cunningham, L. J. Pollard, *Multi-element analysis of iron ore pellets by laser-induced breakdown spectroscopy and principal components regression*, Spectrochim. Acta Part B 63 (2008) 763–769.

146 S. Yao, J. Lu, J. Li, K. Chen, J. Li, M. Dong, *Multi-elemental analysis of fertilizer using laser-induced breakdown spectroscopy coupled with partial least squares regression*, J. Anal. At. Spectrom. 25 (2010) 1733–1738.

147 J. M. Anzano, C. Bello-Gálvez, R. J. Lasheras, *Identification of polymers by means of LIBS*, in: S. Musazzi, U. Perini (Eds.), *Laser-Induced breakdown spectroscopy*, Springer-Verlag, Berlin (2014) pp. 421–438.

148 S. Morel, N. Leone, P. Adama, J. Amouroux, *Detection of bacteria by time-resolved laser-induced breakdown spectroscopy*, Appl. Optics 42 (2003) 6184–6191.

149 M. Baudelet, J. Yu, M. Bossu, J. Jovelet, J. P. Wolf, *Discrimination of microbiological samples using femtosecond laser-induced breakdown spectroscopy*, Appl. Phys. Letters 89 (2006) 163903.

150 S. J. Rehse, N. Jeyasingham, J. Diedrich, S. Palchaudhuri, *A membrane basis for bacterial identification and discrimination using laser-induced breakdown spectroscopy*, J. Appl. Phys. 105 (2009) 102034.

151 D. Marcos-Martínez, J. A. Ayala, R. C. Izquierdo-Hornillos, F. J. M De Villena, J. O. Cáceres, *Identification and discrimination of bacterial strains by laser induced breakdown spectroscopy and neural networks*, Talanta 84 (2011) 730–737.

152 S. Manzoor, S. Moncayo, F. Navarro-Villoslada, J. A. Ayala, R. Izquierdo-Hornillos, F. J. Manuel de Villena, J. O. Cáceres, *Rapid identification and discrimination of bacterial strains by laser induced breakdown spectroscopy and neural networks*, Talanta 121 (2014) 65–70.

153 R. Srinivasan, W. J. Leigh, *Ablative photodecomposition: action of far-ultraviolet (193 nm) laser radiation on poly (ethylene terephthalate) films*, J. Am. Chem. Soc. 104 (1982) 6784–6785.

154 Y. Iida, E. S. Yeung, *Optical monitoring of laser-induced plasma derived from graphite and characterization of the deposited carbon film*, Appl. Spectrosc. 48 (1994) 945–950.

155 S. Acquaviva, M. L. Giorgi, *Temporal and spatial analysis of plasmas during graphite laser ablation in low-pressure N_2*, Appl. Surf. Sci. 197-198 (2002) 21–26.

156 S. Amoruso, G. Ausanio, M. Vitiello, X. Wang, *Infrared femtosecond laser ablation of graphite in high vacuum probed by optical emission spectroscopy*, Appl. Phys. A 81 (2005) 981–986.

157 K. F. Al-Shboul, S. S. Harilal, A. Hassanein, *Spatio-temporal mapping of ablated species in ultrafast laser-produced graphite plasmas*, Appl. Phys. Lett. 100 (2012) 221106.

158 A. Portnov, S. Rosenwaks, I. Bar, *Emission following laser-induced breakdown spectroscopy of organic compounds in ambient air*, Appl. Optics 42 (2003) 2835–2842.

159 A. Portnov, S. Rosenwaks, I. Bar, *Identification of organic compounds in ambient air via characteristic emission following laser ablation*, J. Lumin. 102 (2003) 408–413.

160 R. K. Thareja, R. K. Dwivedi, K. Ebihara, *Interaction of ambient nitrogen gas and laser ablated carbon plume: Formation of CN*, Nucl. Instrum. Meth. B 192 (2002) 301–310.

161 M. Tran, Q. Sun, B. W. Smith, J. D. Winefordner, *Determination of C:H:O:N ratios in solid organic compounds by laser-induced plasma spectroscopy*, J. Anal. At. Spectrom. 16 (2001) 628–632.

162 E. A. P. Cheng, R. D. Fraser, J. G. Eden, *Detection of trace concentrations of column III and V hydrides by laser-induced breakdown spectroscop*y, Appl. Spectrosc. 45 (1991) 949–952.

163 L. Dudragne, Ph. Adam, J. Amouroux, *Time-resolved laser-induced breakdown spectroscopy: application for qualitative and quantitative detection of fluorine, chlorine, sulfur, and carbon in air*, Appl. Spectrosc. 52 (1998) 1321–1327.

164 M. Tran, Q. Sun, B. W. Smith, J. D. Winefordner, *Determination of F, Cl, and Br in solid organic compounds by laser-induced plasma spectroscopy*, Appl. Spectrosc. 55 (2001) 739–744.

165 S. Kaski, H. Häkkänen, J. Korppi-Tommola, *Determination of Cl/C and Br/C ratios in pure organic solids using laser-induced plasma spectroscopy in near vacuum ultraviolet*, J. Anal. At. Spectrom. 19 (2004) 474–478.

166 R. B. King, *Relative transition probabilities of the Swan bands of carbon*, Astrophys. J. 108 (1948) 429–433.

167 L. L. Danylewych, R. W. Nicholls, *Intensity measurements on the C_2 ($d^3\Pi_g$-$a^3\Pi_u$) Swan band system. I. Intercept and partial band methods*, Proceedings of the Royal Society of London. Series A, Mathematical and Physical Sciences 339 (1974) 197–212.

168 W. Weltner Jr., R. J. Van Zee, *Carbon molecules, ions, and clusters*, Chem. Rev. 89 (1989) 1713–1747.

169 S. Pellerin, K. Musiol, O. Motret, B. Pokrzywka, J. Chapelle, *Application of the (0,0) Swan band spectrum for temperature measurements*, J. Phys. D: Appl. Phys. 29 (1996) 2850–2865.

170 S. Acquaviva, *Simulation of emission molecular spectra by a semi-automatic program package: the case of C_2 and CN diatomic molecules emitting during laser ablation of a graphite target in nitrogen environment*, Spectrochim. Acta Part A, 60 (2004) 2079–2086.

171 J. O. Hornkohl, C. Parigger, J. W. L. lewis, *Temperature measurements from CN spectra in a laser-induced plasma*, J. Quant. Spectrosc. Radiat. Transfer, 46 (1991) 405–411.

172 S. S. Harilal, R. C. Issac, C. V. Bindhu, P. Gopinath, V. P. N. Nampoori, C. P. G. Vallabhan, *Time resolved study of CN band emission from plasma generated by laser irradiation of graphite*, Spectrochim. Acta Part A 53 (1997) 1527–1536.

173 B. Német, K. Musiol, I. Sánta, J. Zachorowski, *Time-resolved vibrational and rotational emission analysis of laser-produced plasma of carbon and polymers*, J. Mol. Struct. 511–512 (1999) 259–270.

174 J. J. Camacho, L. Díaz, J. P. Cid, J. M. L. Poyato, *Time-resolved spectroscopic diagnostic of the CO_2 plasma induced by a high-power CO_2 pulsed laser*, Spectrochim. Acta Part B 66 (2011) 698–705.

175 T. Delgado, J. M. Vadillo, J. J. Laserna, *Laser-induced plasma spectroscopy of organic compounds. Understanding fragmentation processes using ion-photon coincidence measurements*, J. Anal. Atom. Spectrom. 28 (2013) 1377–1384.

176 M. Civiš, S. Civiš, K. Sovová, K. Dryahina, P. Španěl, M. Kyncl, *Laser Ablation of FOX-7: Proposed mechanism of decomposition*, Anal. Chem. 83 (2011) 1069–1077.

177 L. Wallace, *Band-head wavelengths of C_2, CH, CN, CO, NH, NO, O_2, OH, and their ions*, Astrophys. J. Suppl. S. 7 (1962) 165–290.

178 M. Dong, G. C.Y. Chan, X. Mao, J. J. Gonzalez, J. Lu, R. E. Russo, *Elucidation of C_2 and CN formation mechanisms in laser-induced plasmas through correlation analysis of carbon isotopic ratio*, Spectrochim. Acta Part B 100 (2014) 62–69.

179 R. Glaus, J. Riedel, I. Gornushkin, *Insight into the formation of molecular species in laser-induced plasma of isotopically labeled organic samples*, Anal. Chem. 87 (2015) 10131–10137.

180 T. Delgado, J. M. Vadillo, J. J. Laserna, *Primary and recombined emitting species in laser-induced plasmas of organic explosives in controlled atmospheres*, J. Anal. At. Spectrom. 29 (2014) 1675–1685.

181 S. S. Harilal, R. C. Issac, C. V. Bindhu, V. P. N. Nampoori, C. P. G. Vallabhan, *Spatial analysis of C_2 band emission from laser produced plasma*, Plasma Sources Sci. Technol. 6 (1997) 317–322.

182 M. W. Slack, *Kinetics and thermodynamics of the CN molecule. III. Shocktube measurements of CN dissociation rates*, J. Chem. Phys. 64 (1976) 228–236.

183 T. Kruse, P. Roth, *Kinetics of C_2 reactions during high-temperature pyrolysis of acetylene*, J. Phys. Chem. A 101 (1997) 2138–2146.

184 S. Zhang, X. Wang, M. He, Y. Jiang, B. Zhang, W. Hang, B. Huang, *Laser-induced plasma temperature*, Spectrochim. Acta Part B 97 (2014) 13–33.

185 http://people.chem.umass.edu/botch/Chem122S08/Chapters/Ch6/BondEnthalpy/BondEnthalpy.html

186 B. de B. Darwent, Bond dissociation energies in simple molecules, http://www.nist.gov/data/nsrds/NSRDS-NBS31.pdf.

187 C. Vivien, J. Hermann, A. Perrone, C. Boulmer-Leborgne, A. Luches, *A study of molecule formation during laser ablation of graphite in low-pressure nitrogen*, J. Phys. D: Appl. Phys. 31 (1998) 1263–1272.

188 S. Abdelli-Messaci, T. Kerdja, A. Bendib, S. Malek, *Emission study of C_2 and CN in laser created carbon plasma under nitrogen environment*, J. Phys. D: Appl. Phys. 35 (2002) 2772–2778.

189 M. Baudelet, L. Guyon, J. Yu, J. P. Wolf, T. Amodeo, E. Fréjafon, P. Laloi, *Spectral signature of native CN bonds for bacterium detection and identification using femtosecond laser-induced breakdown spectroscopy*, Appl. Phys. Lett. 88 (2006) 063901.

190 N. A. Zakorina, G. S. Lazeeva, A. A. Petrov, *Spectroscopic determination of the isotopic composition of boron trifluoride*, J. Nucl. Energy 21 (1967) 309–313.

191 G. S. Lazeeva, V. M. Nemets, A. A. Petrov, *Spectral-isotopic method of determination of gas-forming elements in organic and inorganic substances*, Spectrochim. Acta Part B 36 (1981) 1233–1242.

192 R. E. Russo, A. A. Bol'shakov, X. Mao, C. P. McKay, D. L. Perry, O. Sorkhabi, *Laser ablation molecular isotopic spectrometry*, Spectrochim. Acta Part B 66 (2011) 99–104.

193 A. A. Bol'shakov, X. Mao, J. J. Gonzalez, R. E. Russo, *Laser ablation molecular isotopic spectrometry (LAMIS): current state of the art*, J. Anal. At. Spectrom. 31 (2016) 119–134.

194 C. R. Burnet, *Isotope shift in the atomic spectrum of carbon*, Phys. Rev., 80 (1950) 494.

195 J. P. Nicklas, *Isotope shift in neutral carbon*, Phys. Rev., 95 (1954) 1469–1471.

196 K. H. Kurniawan, T. J. Lie, M. M. Suliyanti, R. Hedwig, M. Pardede, D. P. Kurniawan, *Quantitative analysis of deuterium using laser-induced plasma at low pressure of helium*, Anal. Chem. 78 (2006) 5768–5773.

197 J. R. Holmes, *Isotope shift in some lines of nitrogen*, Phys. Rev. 63 (1942) 41–46.

198 L. W. Parker, J. R. Holmes, *Isotope Shift in Neutral Oxygen*, J. Opt. Soc. Am., 43 (1953) 103–109.

199 M. Dong, X. Mao, J. J. Gonzalez, J. Lu, R. E. Russo, *Carbon isotope separation and molecular formation in laser-induced plasmas by laser ablation molecular isotopic spectrometry*, Anal. Chem. 85 (2013) 2899–2906.

200 A. Sarkar, X. Mao, G. C. Y. Chan, R. E. Russo, *Laser ablation molecular isotopic spectrometry of water for* $_1D^2/_1H^1$ *ratio analysis*, Spectrochim. Acta Part B 88 (2013) 46–53.

201 P. Bollmark, I. Kopp, B. Rydh, *Rotational analysis of the ND* $A^3\pi_i$-$X^3\Sigma^-$ *(0,0) band*, J. Mol. Spectrosc. 34 (1970) 487–499.

202 M. Zachwieja, W. Szajna, R. Hakalla, *The* $A^2\Delta$–$X^2\pi$ *band system of the CD radical*, J. Mol. Spectrosc. 275 (2012) 53–60.

203 A. A. Bol'shakov, X. Mao, J. Jain, D. L. McIntyre, R. E. Russo, *Laser ablation molecular isotopic spectrometry of carbon isotopes*, Spectrochim. Acta Part B 113 (2015) 106–112.

204 H. Hou, G. C.Y. Chan, X. Mao, V. Zorba, R. Zheng, R. E. Russo, *Femtosecond laser ablation molecular isotopic spectrometry for zirconium isotope analysis*, Anal. Chem. 87 (2015) 4788–4796.

205. X. Mao, A. A. Bol'shakov, D. L. Perry, O. Sorkhabi, R. E. Russo, *Laser ablation molecular isotopic spectrometry: parameter influence on boron isotope measurement*s, Spectrochim. Acta Part B 66 (2011) 604–609.

206 X. Mao, A. A. Bol'shakov, I. Choi, C. P. McKay, D. L. Perry, O. Sorkhabi, R. E. Russo, *Laser ablation molecular isotopic spectrometry: strontium and its isotopes*, Spectrochim. Acta Part B 66 (2011) 767–775.

207 A. K. Jain, R. P. W. Duin, J. Mao, *Statistical pattern recognition: A review*, IEEE Transactions on Pattern Analysis and Machine Intelligence 22 (2000) pp. 4–37.

208 A. Ferrero, P. Lucena, R. G. Herrera, A. Doña, R. Fernández-Reyes, J. J. Laserna, *Libraries for spectrum identification: Method of normalized coordinates versus linear correlation*, Spectrochim. Acta Part B 63 (2008) 383–388.

209 J. B. Sirven, B. Sallé, P. Mauchien, J. L. Lacour, S. Maurice, G. Manhès, *Feasibility study of rock identification at the surface of Mars by remote laser-induced breakdown spectroscopy and three chemometric methods*, J. Anal. At. Spectrom. 22 (2007) 1471–1480.

210 M. J. C. Pontes, J. Cortez, R. K. H. Galvão, C. Pasquini, M. C. U. Araújo, R. M. Coelho, M. K. Chiba, M. F de Abreu, B. E. Madari, *Classification of Brazilian soils by using LIBS and variable selection in the wavelet domain*, Anal. Chim. Acta 642 (2009) 12–18.

211 J. L. Gottfried, F. C. De Lucia Jr., A. W. Miziolek, *Discrimination of explosive residues on organic and inorganic substrates using laser-induced breakdown spectroscopy*, J. Anal. At. Spectrom. 24 (2009) 288–296.

212 F-Y. Yueh, H. Zheng, J. P. Singh, S. Burgess, *Preliminary evaluation of laser-induced breakdown spectroscopy for tissue classification*, Spectrochim. Acta Part B 64 (2009) 1059–1067.

213 M. Boueri, V. Motto-Ros, W. Q. Lei, Q. L. Ma, L. J. Zheng, H. P. Zeng, J. Yu, *Identification of polymer materials using laser-induced breakdown spectroscopy combined with artificial neural networks*, Appl. Spectrosc. 65 (2011) 307–314.

214 S. Moncayo, S. Manzoor, F. Navarro-Villoslada, J. O. Cáceres*, Evaluation of supervised chemometric methods for sample classification by laser induced breakdown spectroscopy*, Chemometr. Intell. Lab. 146 (2015) 354–364.

215 M. J. Adams, Chemometrics in Analytical Spectroscopy, 2nd Edition, The Royal Society of Chemistry, Thomas Graham House, Science Park, Milton Road, Cambridge CB4 OWF, UK (2004).

216 J. Yinon, *Counterterrorist Detection Techniques of Explosives*, Amsterdam, The Netherland (2007).

217 S. Singh, *Sensors-An effective approach for the detection of explosives*, J. Hazard Mater. 144 (2007) 15–28.

218 C. López-Moreno, S. Palanco, J. J. Laserna, F. De Lucia Jr., A. W. Miziolek, J. Rose, R. A. Walters, A. I. Whitehouse, *Test of a stand-off laser-induced breakdown spectroscopy sensor for the detection of explosive residues on solid surfaces*, J. Anal. At. Spectrom. 21 (2006) 55–60.

219 J. Moros, F. J. Fortes, J. M. Vadillo, J. J. Laserna, *LIBS detection of explosives in traces*, in: S. Musazzi, U. Perini (Eds.), *Laser-induced breakdown spectroscopy*, Springer-Verlag, Berlin (2014) pp. 349–375.

220 P. Lucena, I. Gaona, J. Moros, J. J. Laserna, *Location and detection of explosive-contaminated human fingerprints on distant targets using standoff laser-induced breakdown spectroscopy*, Spectrochim. Acta Part B 85 (2013) 71–77.

221 M. I. Gaona Fernández, (2014) *Standoff sensing technology based on laser-induced breakdown spectroscopy: advanced targeting, surveillance and reconnaissance in security and architectural heritage applications*. Unpublished PhD thesis. University of Málaga. Retrieved from the institutional repository of the University of Málaga at https://riuma.uma.es/xmlui/handle/10630/8213.

222 F. C. De Lucia Jr., J. L. Gottfried, C. A. Munson, A. W. Miziolek, *Double pulse laser-induced breakdown spectroscopy of explosives: Initial study towards improved discrimination,* Spectrochim. Acta Part B 62 (2007) 1399–1404.

223 J. L. Gottfried, F. C. De Lucia Jr., C. A. Munson, A. W. Miziolek, *Double-pulse standoff laser-induced breakdown spectroscopy for versatile hazardous materials detection*, Spectrochim. Acta Part B 62 (2007) 1405–1411.

224 J. L. Gottfried, F. C. De Lucia Jr., C. A. Munson, A. W. Miziolek, *Strategies for residue explosives detection using laser-induced breakdown spectroscopy*, J. Anal. At. Spectrom., 23 (2008) 205–216.

225 Y. Dikmelik, C. McEnnis, J. B. Spicer, *Femtosecond and nanosecond laser-induced breakdown spectroscopy of trinitrotoluene*, Opt. Express 16 (2008) 5332–5337.

226 F. C. De Lucia Jr., J. L. Gottfried, A. W. Miziolek, *Evaluation of femtosecond laser-induced breakdown spectroscopy for explosive residue detection*, Opt. Express 17 (2009) 419–425.

227 S. Sunku, M. K. Gundawar, A. K. Myakalwar, P. P. Kiran, S. P. Tewari, S. V. Rao, *Femtosecond and nanosecond laser induced breakdown spectroscopic studies of NTO, HMX, and RDX*, Spectrochim. Acta Part B 79-80 (2013) 31–38.

228 S. Sreedhar, E. N. Rao, G. M. Kumar, S. P. Tewari, S. V. Rao, *Molecular formation dynamics of 5-nitro-2,4-dihydro-3H-1,2, 4-triazol-3-one,1,3,5-trinitroperhydro-1,3,5-triazine, and 2,4,6-trinitrotoluene in air, nitrogen, and argon atmospheres studied using femtosecond laser induced breakdown spectroscopy*, Spectrochim. Acta Part B 87 (2013) 121–129.

229 V. Lazic, A. Palucci, S. Jovicevic, C. Poggi, E. Buono, *Analysis of explosive and other organic residues by laser induced breakdown spectroscopy*, Spectrochim. Acta Part B 64 (2009) 1028–1039.

230 Á. Fernández-Bravo, P. Lucena, J. J. Laserna, *Selective sampling and laser-induced breakdown spectroscopy (LIBS) analysis of organic explosive residues on polymer surfaces*, Appl. Spectrosc. 66 (2012) 1197–1203.

231 I. Gaona, J. Serrano, J. Moros, J. J. Laserna, *Range-adaptive standoff recognition of explosive fingerprints on solid surfaces using a supervised learning method and laser-induced breakdown spectroscopy*, Anal. Chem. 86 (2014) 5045–5052.

232 R. J. Lasheras, C. Bello-Gálvez, J. Anzano, *Identification of polymers by LIBS using methods of correlation and normalized coordinates*, Polym. Test. 29 (2010) 1057–1064.

233 M. A. Gondal, M. N. Siddiqui, *Identification of different kinds of plastics using laser-induced breakdown spectroscopy for waste management*, J. Environ. Sci. Heal. A 42 (2007) 1989–1997.

234 S. Grégoire, M. Boudinet, F. Pelascini, F. Surma, V. Detalle, Y. Holl, *Laser-induced breakdown spectroscopy for polymer identification*, Anal. Bioanal. Chem. 400 (2011) 3331–3340.

235 R. Sattmannlop, I. Monch, H. Krause, R. Noll, S. Couris, A. Hatziapostolou, A. Mavromanolakis, C. Fotakis, E. Larrauri, R. Miguel, *Laser-induced breakdown spectroscopy for polymer identification*, Appl. Spectrosc. 52 (1998) 456–461.

236 N. Huber, S. Eschlböck-Fuchs, H. Scherndl, A. Freimund, J. Heitz, J. D. Pedarnig, *In-line measurements of chlorine containing polymers in an industrial waste sorting plant by laser-induced breakdown spectroscopy*, Appl. Surf. Sci. 302 (2014) 280–285.

237 D. A. Rusak, K. D. Weaver, B. L. Taroli, *Laser-induced breakdown spectroscopy for analysis of chemically etched polytetrafluoroethylene*, Appl. Spectrosc. 62 (2008) 773–777.

238 R. Viskup, B. Praher, T. Linsmeyer, H. Scherndl, J. D. Pedarnig, J. Heitz, *Influence of pulse-to-pulse delay for 532 nm double-pulse laser-induced breakdown spectroscopy of technical polymers*, Spectrochim. Acta Part B 65 (2010) 935–942.

239 Q. Godoi, D. Santos Jr., L. C. Nunes, F. O. Leme, I. A. Rufini, J. A. M. Agnelli, L. C. Trevizan, F. J. Krug, *Preliminary studies of laser-induced breakdown spectrometry for the determination of Ba, Cd, Cr and Pb in toys*, Spectrochim. Acta Part B 64 (2009) 573–581.

240 S. Barbier, S. Perrie, P. Freyermuth, D. Perrin, B. Gallard, N. Gilon, *Plastic identification based on molecular and elemental information from laser induced breakdown spectra: a comparison of plasma conditions in view of efficient sorting*, Spectrochim. Acta Part B 88 (2013) 167–173

241 F. W. B. Aquino, E. R. Pereira-Filho, *Analysis of the polymeric fractions of scrap from mobile phones using laser-induced breakdown spectroscopy: Chemometric applications for better data interpretation*, Talanta 134 (2015) 65–73.

242 C. A. Munson, F. C. De Lucia Jr., T. Piehler, K. L. McNesby, A. W. Miziolek, *Investigation of statistics strategies for improving the discriminating power of laser-induced breakdown spectroscopy for chemical and biological warfare agent simulants*, Spectrochim. Acta Part B 60 (2005) 1217–1224.

243 J. L. Gottfried, F. C. De Lucia Jr., C. A. Munson, A. W. Miziolek, *Standoff detection of chemical and biological threats using laser-induced breakdown spectroscopy*, Appl. Spectrosc. 62 (2008) 353–363.

244 R. A. Putnam, Q. I. Mohaidat, A. Daabous, S. J. Rehse, A *comparison of multivariate analysis techniques and variable selection strategies in a laser-induced breakdown spectroscopy bacterial classification*, Spectrochim. Acta Part B 87 (2013) 161–167.

245 A. C. Samuels, F. C. DeLucia, K. L. McNesby, A. W. Miziolek, *Laser-induced breakdown spectroscopy of bacterial spores, molds, pollens, and protein: initial studies of discrimination potential*, Appl. Optics 42 (2003) 6205–6209.

246 R. A. Multari, D. A. Cremers, J. A. M. Dupre, J. E. Gustafson, *Detection of biological contaminants on foods and food surfaces using laser-induced breakdown spectroscopy (LIBS)*, J. Agric. Food Chem. 61 (2013) 8687–8694.

247 J. O. Cáceres, S. Moncayo, J. D. Rosales, F. J. M. de Villena, F. C. Alvira, G. M. Bilmes, *Application of laser-induced breakdown spectroscopy (LIBS) and neural networks to olive oils analysis*, Appl. Spectrosc. 67(9) (2013) 1064–1072.

248 Y. G. Mbesse Kongbonga, H. Ghalila, M. Boyomo Onana, Z. Ben Lakhdar, *Classification of vegetable oils based on their concentration of saturated fatty acids using laser induced breakdown spectroscopy (LIBS)*, Food Chem. 147 (2014) 327–331.

249 M. Pardede, R. Hedwig, S. N. Abdulmadjid, K. Lahna, N. Idris, E. Jobiliong, H. Suyanto, A. M. Marpaung, M. M. Suliyanti, M. Ramli, M. O. Tjia, T. J. Lie, Z. S. Lie, D. P. Kurniawan, K. H. Kurniawan, K. Kagawa, *Quantitative and sensitive analysis of CN molecules using laser induced low pressure He plasma*, J. Appl. Phys. 117 (2015) 113302.

250 Z. Abdel-Salam, J. Al Sharnoubi, M. A. Harith, *Qualitative evaluation of maternal milk and commercial infant formulas via LIBS*, Talanta 115 (2013) 422–426.

251 F. Ma, D. Dong, *A measurement method on pesticide residues of apple surface based on laser-induced breakdown spectroscopy*, Food Anal. Method. 7 (2014) 1858–1865.

252 L. St-Onge, E. Kwong, M. Sabsabi , E. B. Vadas, *Quantitative analysis of pharmaceutical products by laser-induced breakdown spectroscopy*, Spectrochim. Acta Part B 57 (2002) 1131–1140.

253 J. Anzano, B. Bonilla, B. Montull-Ibor, J. Casas-González, *Rapid characterization of analgesic pills by laser-induced breakdown spectroscopy (LIBS)*, Med. Chem. Res. 18 (2009) 656–664.

254 A. K. Myakalwar, S. Sreedhar, I. Barman, N. C. Dingari, S. Venugopal Rao, P. Prem Kiran, S. P. Tewari, G. Manoj Kumar, *Laser-induced breakdown spectroscopy-based investigation and classification of pharmaceutical tablets using multivariate chemometric analysis*, Talanta 87 (2011) 53–59.

255 N. C. Dingari, I. Barman, A. K. Myakalwar, S. P. Tewari, M. Kumar Gundawar, *Incorporation of support vector machines in the LIBS toolbox for sensitive and robust classification amidst unexpected sample and system variability*, Anal. Chem. 84 (2012) 2686–2694.

256 A. Dubey, G. Keyvan, R. Hsia, K. Saranteas, D. Brone, T. Misra, F. J. Muzzio, *Analysis of pharmaceutical tablet coating uniformity by laser-induced breakdown spectroscopy (LIBS)*, J. Pharm. Innov. 6 (2011) 77–87.

257 M. D. Mowery, R. Sing, J. Kirsch, A. Razaghi, S. Béchard, R. A. Reed, *Rapid at-line analysis of coating thickness and uniformity on tablets using laser induced breakdown spectroscopy*, J. Pharmaceut. Biomed. 28 (2002) 935–943.

258 F. Ferioli, S. G. Buckley, *Measurements of hydrocarbons using laser-induced breakdown spectroscopy*, Combust. Flame 144 (2006) 435–447.

259 T. X. Phuoc, F. P. White, *Laser induced spark for measurements of the fuel-to-air ratio of a combustible mixture*, Fuel 81 (2002) 1761–1765.

260 P. Stavropoulos, A. Michalakou, G. Skevis, S. Couris, *Quantitative local equivalence ratio determination in laminar premixed methane–air flames by laser induced breakdown spectroscopy (LIBS)*, Chem. Phys. Lett. 404 (2005) 309–314.

261 P. Stavropoulos, A. Michalakou, G. Skevis, S. Couris, *Laser-induced breakdown spectroscopy as an analytical tool for equivalence ratio measurement in methane–air premixed flames*, Spectrochim. Acta Part B 60 (2005) 1092–1097.

262 K. E. Eseller, F. Y. Yueh, J. P. Singh, *Laser-induced breakdown spectroscopy measurement in methane and biodiesel flames using an ungated detector*, Appl. Optics 47 (2008) G144–G148.

263 M. Mansour, H. Imam, K. A. Elsayed, A. M. Elbaz, W. Abbass, *Quantitative mixture fraction measurements in combustion system via laser induced breakdown spectroscopy*, Opt. Laser Technol. 65 (2015) 43–49.

264 M. Kotzagianni, S. Couris, *Femtosecond laser induced breakdown for combustion diagnostics*, Appl. Phys. Lett. 100 (2012) 264104.

265 M. Kotzagianni, S. Couris, *Femtosecond laser induced breakdown spectroscopy of air–methane mixtures*, Chem. Phys. Lett. 561–562 (2013) 36–41.

CHAPTERS

Chapter 1

Sensing signatures mediated by chemical structure of molecular solids in laser-induced plasmas

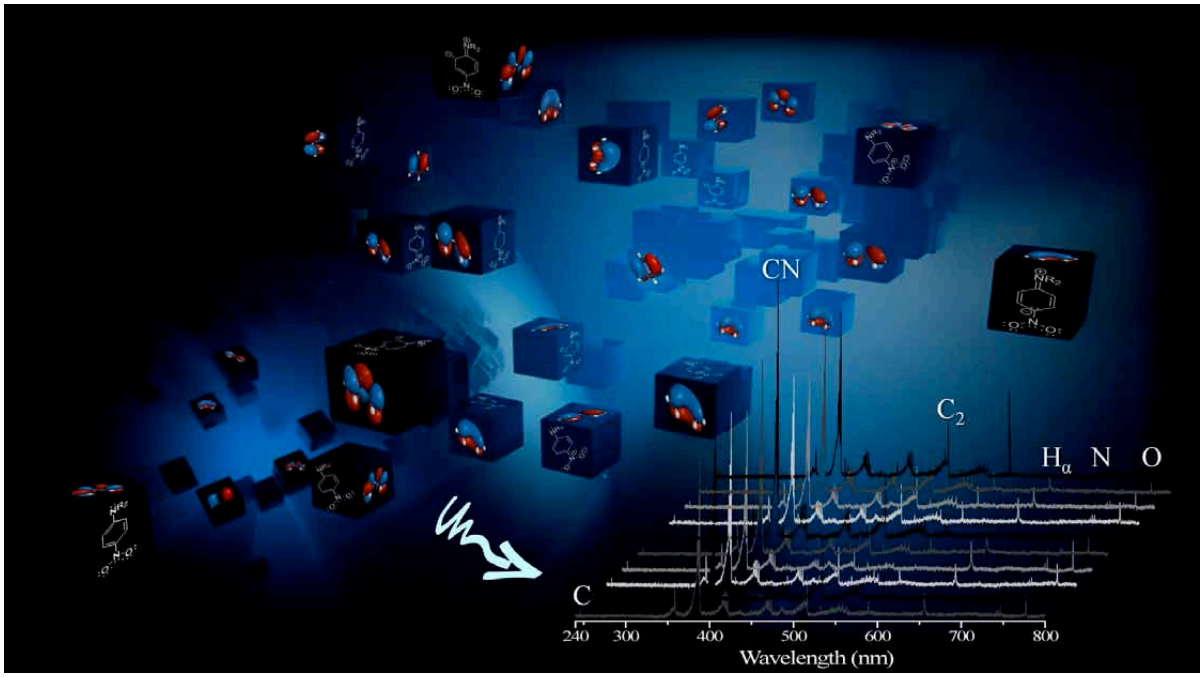

analytical chemistry

Article

pubs.acs.org/ac

Sensing Signatures Mediated by Chemical Structure of Molecular Solids in Laser-Induced Plasmas

Jorge Serrano, Javier Moros, and J. Javier Laserna*

Universidad de Málaga, Departamento de Química Analítica, 29071 Málaga, España

ABSTRACT: Laser ablation of organic compounds has been investigated for almost 30 years now, either in the framework of pulse laser deposition for the assembling of new materials or in the context of chemical sensing. Various monitoring techniques such as atomic and molecular fluorescence, time-of-flight mass spectrometry, and optical emission spectroscopy have been used for plasma diagnostics in an attempt to understand the spectral signature and potential origin of gas-phase ions and fragments from organic plasmas. Photochemical and photophysical processes occurring within these systems are generally much more complex than those suggested by observation of optical emission features. Together with laser ablation parameters, the structural and chemical−physical properties of molecules seem to be closely tied to the observed phenomena. The present manuscript, for the first time, discusses the role of molecular structure in the optical emission of organic plasmas. Factors altering the electronic distribution within the organic molecule have been found to have a direct impact on its ensuing optical emissions. The electron structure of an organic molecule, resulting from the presence, nature, and position of its atoms, governs the breakage of the molecule and, as a result, determines the extent of atomization and fragmentation that has proved to directly impact the emissions of CN radicals and C_2 dimers. Particular properties of the molecule respond more positively depending on the laser irradiation wavelength, thereby redirecting the ablation process through photochemical or photothermal decomposition pathways. It is of paramount significance for chemical identification purposes how, despite the large energy stored and dissipated by the plasma and the considerable number of transient species formed, the emissions observed never lose sight of the original molecule.

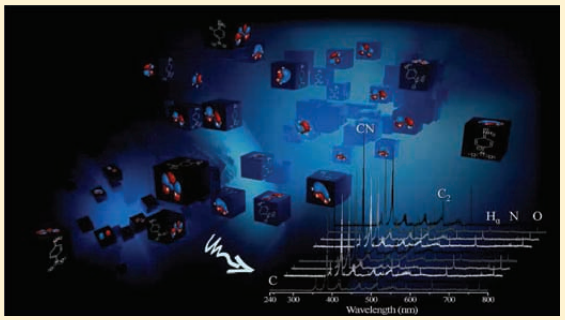

DOI: 10.1021/acs.analchem.5b00212
Anal. Chem. 2015, 87, 2794−2801

Received: November 7, 2014
Accepted: February 10, 2015
Published: February 10, 2015

Chapter 2

Exploring the formation routes of diatomic hydrogenated radicals using fs laser-induced breakdown spectroscopy of deuterated molecular solids

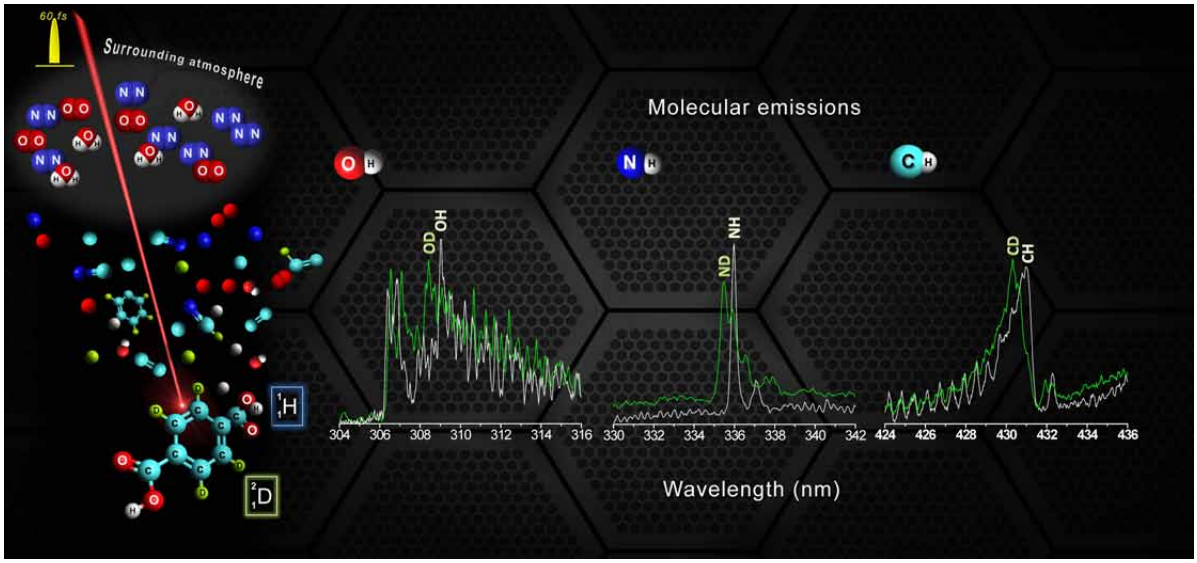

JAAS

PAPER

View Article Online
View Journal | View Issue

Exploring the formation routes of diatomic hydrogenated radicals using femtosecond laser-induced breakdown spectroscopy of deuterated molecular solids

Jorge Serrano, Javier Moros and J. Javier Laserna*

In recent years, laser-induced breakdown spectroscopy (LIBS) has expanded beyond multielemental analysis capability by exploring molecular solids and optical emissions from diatomic radicals. Despite many efforts to this end, the greatest emphasis has been placed on the study of the dynamics and the optical and temporal behavior of CN and C_2 emissions in order to elucidate the main chemical reactions occurring in the plasma. Other diatomic species, whose emission bands also appear in the visible and near-ultraviolet regions of the LIBS spectrum, remain virtually unexplored. This research focuses, for the first time, on elucidating the formation pathways of CH, NH, and OH radicals in femtosecond laser-produced plasmas of molecular solids. As the origin of diatomic species is not easily traceable to a single formation route due to the occurrence of primary and secondary processes within the plasma plume, isotopic labeling of some molecules has been used as a diagnostic tool. Deuterated isotopologues of urea, terephthalic acid and anthracene have been evaluated. The dominant routes have been identified through a comparison of the observed isotopic patterns. The findings reveal the direct release of native molecular bonds as a significant source that populates femtosecond laser-produced plasmas with NH radicals. Additional reactions of native hydrogen from molecules and atmospheric nitrogen also contribute to form such species. Oxygen from the atmosphere competes with nitrogen in these reactions to populate plasmas with OH radicals. Alternatively, the direct connection between C_2 and CH emissions verify that this radical derives from diatomic carbon fragments as precursors. These new findings entail a further step towards the use of molecular emissions as diagnostic tools in the analytical applications of laser-induced plasmas of organic compounds.

J. Anal. At. Spectrom., 2015, **30**, 2343–2352

Received 25th May 2015

Accepted 25th September 2015

DOI: 10.1039/c5ja00192g

www.rsc.org/jaas

Chapter 3

Molecular signatures in femtosecond laser-induced organic plasmas: comparison with nanosecond laser ablation

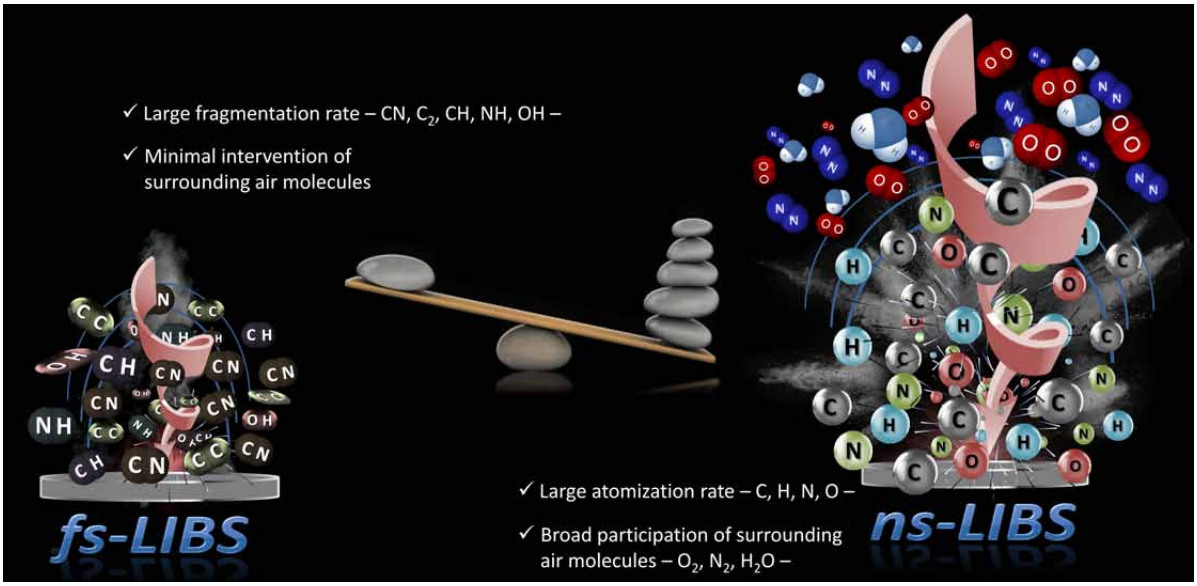

PCCP

PAPER

Cite this: *Phys. Chem. Chem. Phys.*, 2016, **18**, 2398

Molecular signatures in femtosecond laser-induced organic plasmas: comparison with nanosecond laser ablation

Jorge Serrano, Javier Moros and J. Javier Laserna*

During the last few years, laser-induced breakdown spectroscopy (LIBS) has evolved significantly in the molecular sensing area through the optical monitoring of emissions from organic plasmas. Large efforts have been made to study the formation pathways of diatomic radicals as well as their connections with the bonding framework of molecular solids. Together with the structural and chemical–physical properties of molecules, laser ablation parameters seem to be closely tied to the observed spectral signatures. This research focuses on evaluating the impact of laser pulse duration on the production of diatomic species that populate plasmas of organic materials. Differences in relative intensities of spectral signatures from the plasmas of several organic molecules induced in femtosecond (fs) and nanosecond (ns) ablation regimes have been studied. Beyond the abundance and origin of diatomic radicals that seed the plasma, findings reveal the crucial role of the ablation regime in the breakage pattern of the molecule. The laser pulse duration dictates the fragments and atoms resulting from the vaporized molecules, promoting some formation routes at the expense of other paths. The larger amount of fragments formed by fs pulses advocates a direct release of native bonds and a subsequent seeding of the plasma with diatomic species. In contrast, in the ns ablation regime, the atomic recombinations and single displacement processes dominate the contribution to diatomic radicals, as long as atomization of molecules prevails over their progressive decomposition. Consequently, fs-LIBS better reflects correlations between strengths of emissions from diatomic species and molecular structure as compared to ns-LIBS. These new results entail a further step towards the specificity in the analysis of molecular solids by fs-LIBS.

Phys. Chem. Chem. Phys., 2016, **18**, 2398-2408

Received 23rd October 2015

Accepted 27th November 2015

DOI: 10.1039/c5cp06456b

www.rsc.org/pccp

Chapter 4

Potential of laser-induced breakdown spectroscopy for discrimination of nano-sized carbon materials. Insights on the optical characterization of graphene

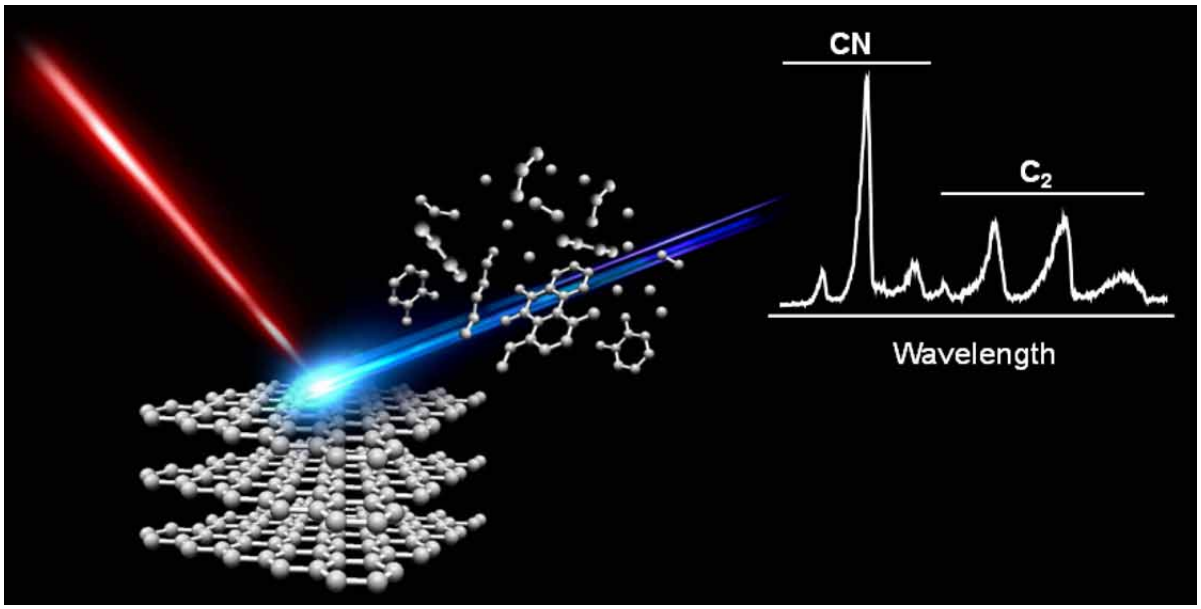

Spectrochimica Acta Part B 97 (2014) 105–112

Contents lists available at ScienceDirect

Spectrochimica Acta Part B

journal homepage: www.elsevier.com/locate/sab

Potential of laser-induced breakdown spectroscopy for discrimination of nano-sized carbon materials. Insights on the optical characterization of graphene ☆

J. Serrano, L.M. Cabalín, J. Moros, J.J. Laserna *

Universidad de Málaga, Departamento de Química Analítica, E-29071 Málaga, Spain

A B S T R A C T

Since its invention in 2004, graphene has attracted considerable interest worldwide. Advances in the use of graphene in materials science and engineering require important increases in the quality of the final product for integration in photonic and electronic devices. To meet this demand, which will become increasingly strict in the future, analytical techniques capable of differentiating between the starting materials and graphene need to be developed. The interest in the use of laser-induced breakdown spectroscopy (LIBS) for this application rests on the rapid progress experienced by this technology for identification of carbon-based materials of close chemical composition. The potential of LIBS has been explored here by a careful investigation of the spectral properties of both multi-layer and few-layer graphene, graphite and graphene oxide. Results reveal significant differences in the specific optical emission responses of these materials, expressly reflected on the behavior of CN and C_2 molecular emissions. These differences result from the particularities of the materials, such as the number of carbon layers and the carbon hybridization in the bonding structure, together with the post-ablation evolution of the concerned plasma plume. In short, this interconnection between ablation and emission events generated from each material allows its characterization and its differentiation from other materials with highly similar chemical composition.

Spectrochimica Acta Part B 97 (2014) 105–112

Article history:
Received 22 October 2013
Accepted 1 May 2014
Available online 19 May 2014

http://dx.doi.org/10.1016/j.sab.2014.05.003
0584-8547/

Chapter 5

New chemometrics in laser-induced breakdown spectroscopy for recognizing explosive residues

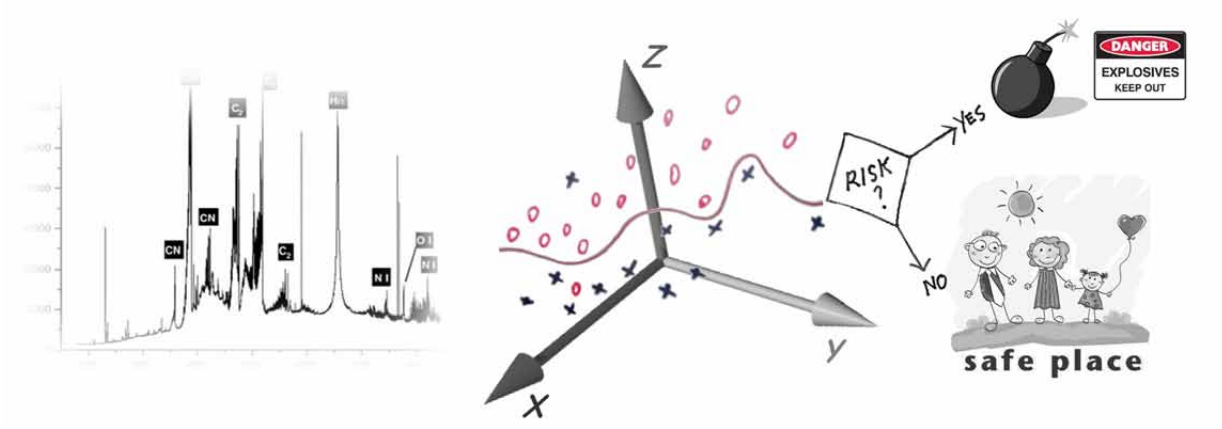

JAAS

J. Anal. At. Spectrom., 2012, **27**, 2111–2122

www.rsc.org/jaas

PAPER

New chemometrics in laser-induced breakdown spectroscopy for recognizing explosive residues

J. Moros,[a] J. Serrano,[a] C. Sánchez,[b] J. Macías[b] and J. J. Laserna*[a]

Received 3rd August 2012, Accepted 10th October 2012
DOI: 10.1039/c2ja30230f

Detection of explosives in traces is an important area for preventing terrorist attacks and for anticipating their disastrous consequences. Laser-induced breakdown spectroscopy (LIBS) has been demonstrated to be an effective analytical technique for the detection and characterization of energetic materials. However, the major obstacle in the identification of explosives is their elevated spectral similarity with those compounds that share an analogous elemental composition. Despite that a number of different chemometric methods have been developed in the past for the detection of explosives, this hurdle remains latent today. Our recent efforts have been focused on the use of an alternative chemometric approach for improving the sensitivity and selectivity of LIBS for residue explosives identification. Through the survey of the spectral responses from the analysis of a variety of organic residues (either explosive or potential confusant materials) located on the surface of a support, relationships between the optical emission behaviors of residues and their corresponding hazardous nature have been extracted. By using the original intensities of the most relevant emission signals (C : CN : C_2 : H : N : O) properly projected onto 2D subspaces, different machine learning classifiers have been designed and trained. This approach has been demonstrated to be capable for the identification of organic explosive residues against several potential confusant materials when they are placed on the surface of an aluminum support. False positive and false negative rates better than 5% are achieved. These results evidence a great stride in solving this particular problem, enabling the LIBS technology as a practical tool in complex applications related to homeland security.

[a]*Department of Analytical Chemistry, University of Malaga, E-29071 Malaga, Spain. E-mail: laserna@uma.es; Fax: +34 952 13 2000; Tel: +34 952 13 1881*
[b]*Department of Mathematical Analysis, University of Malaga, E-29071 Malaga, Spain*

Chapter 6

Advanced recognition of explosives in traces on polymer surfaces using LIBS and supervised learning classifiers

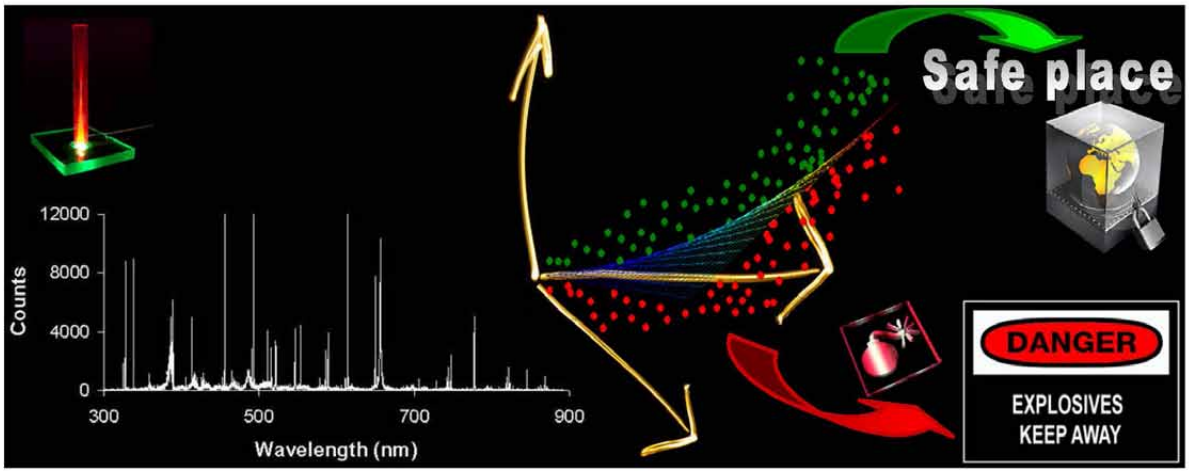

Analytica Chimica Acta 806 (2014) 107–116

Contents lists available at ScienceDirect

Analytica Chimica Acta

journal homepage: www.elsevier.com/locate/aca

Advanced recognition of explosives in traces on polymer surfaces using LIBS and supervised learning classifiers

Jorge Serrano[a], Javier Moros[a], Carlos Sánchez[b], Jorge Macías[b], J. Javier Laserna[a,*]

[a] Department of Analytical Chemistry, University of Málaga, E-29071 Málaga, Spain
[b] Department of Mathematical Analysis, University of Málaga, E-29071 Málaga, Spain

HIGHLIGHTS

- Supervised learning lets LIBS identify organic traces located on polymer surfaces.
- Classifiers capture nonlinear relationships between emissions and target nature.
- False negative rate of 2% and false positive rate of 1% are reached.
- Proposed approach offers better understanding than other chemometric alternatives.

GRAPHICAL ABSTRACT

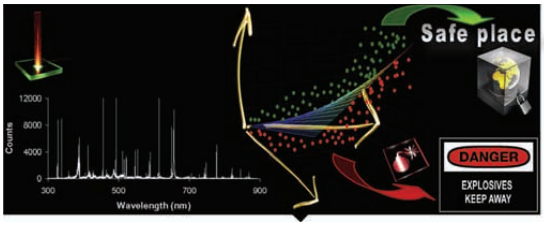

ARTICLE INFO

Article history:
Received 5 September 2013
Received in revised form
11 November 2013
Accepted 14 November 2013
Available online 22 November 2013

Keywords:
Laser-induced breakdown spectroscopy
Explosives
Confusants
Polymer surfaces
Machine learning classifiers

ABSTRACT

The large similarity existing in the spectral emissions collected from organic compounds by laser-induced breakdown spectroscopy (LIBS) is a limiting factor for the use of this technology in the real world. Specifically, among the most ambitious challenges of today's LIBS involves the recognition of an organic residue when neglected on the surface of an object of identical nature. Under these circumstances, the development of an efficient algorithm to disclose the minute differences within this highly complex spectral information is crucial for a realistic application of LIBS in countering explosive threats. An approach cemented on scatter plots of characteristic emission features has been developed to identify organic explosives when located on polymeric surfaces (*teflon*, *nylon* and *polyethylene*). By using selected spectral variables, the approach allows to design a concise classifier for alerting when one of four explosives (*DNT*, *TNT*, *RDX* and *PETN*) is present on the surface of the polymer. Ordinary products (*butter*, *fuel oil*, *hand cream*, *olive oil* and *motor oil*) cause no confusion in the decisions taken by the classifier. With rates of false negatives and false positives below 5%, results demonstrate that the classification algorithm enables to label residues according to their harmful nature in the most demanding scenario for a LIBS sensor.

* Corresponding author. Tel.: +34 952 13 1881; fax: +34 952 13 2000.

E-mail address: laserna@uma.es (J.J. Laserna).

0003-2670/$ – see front matter © 2013 Elsevier B.V. All rights reserved.
http://dx.doi.org/10.1016/j.aca.2013.11.035

Chapter 7

Recognition of explosives fingerprints on objects for courier services using machine learning methods and laser-induced breakdown spectroscopy

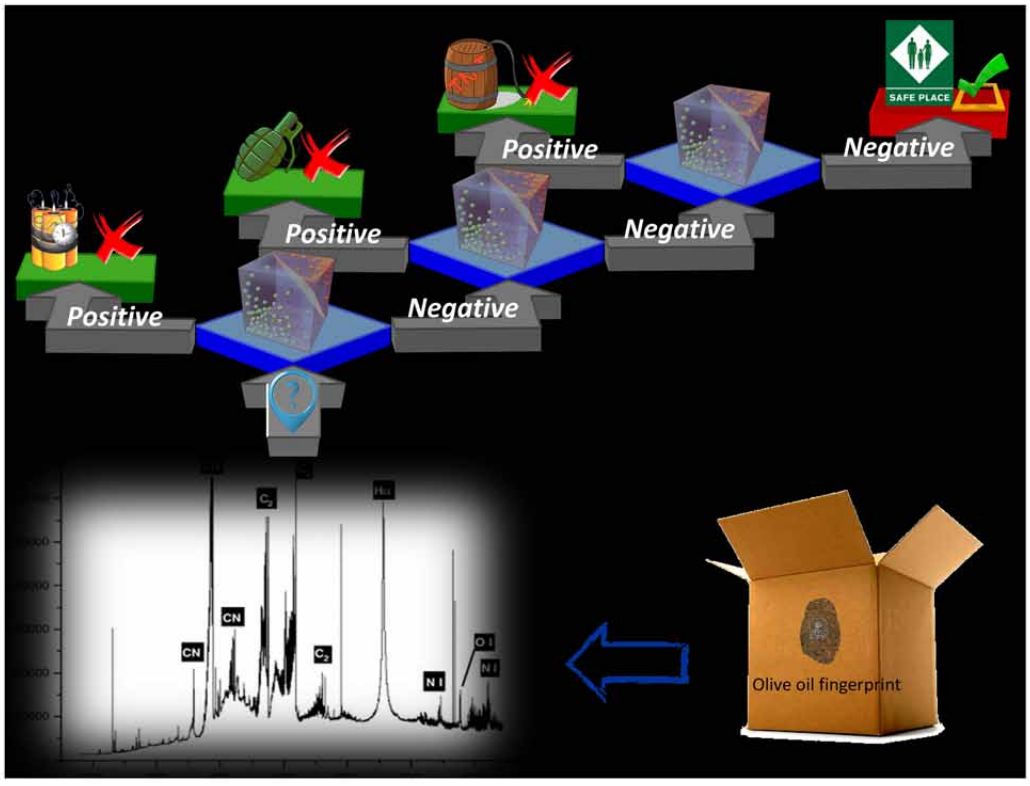

Talanta 110 (2013) 108–117

Contents lists available at SciVerse ScienceDirect

Talanta

journal homepage: www.elsevier.com/locate/talanta

Recognition of explosives fingerprints on objects for courier services using machine learning methods and laser-induced breakdown spectroscopy

J. Moros [a], J. Serrano [a], F.J. Gallego [b], J. Macías [b], J.J. Laserna [a,*]

[a] Department of Analytical Chemistry, University of Malaga, E-29071 Malaga, Spain
[b] Department of Mathematical Analysis, University of Malaga, E-29071 Malaga, Spain

ARTICLE INFO

Article history:
Received 7 November 2012
Received in revised form 1 February 2013
Accepted 11 February 2013
Available online 19 February 2013

Keywords:
LIBS
Fingerprints
Home-made explosives Harmless
Machine learning Decision tree

ABSTRACT

During recent years laser-induced breakdown spectroscopy (LIBS) has been considered one of the techniques with larger ability for trace detection of explosives. However, despite of the high sensitivity exhibited for this application, LIBS suffers from a limited selectivity due to difficulties in assigning the molecular origin of the spectral emissions observed. This circumstance makes the recognition of fingerprints a latent challenging problem. In the present manuscript the sorting of six explosives (*chloratite*, *ammonal*, *DNT*, *TNT*, *RDX* and *PETN*) against a broad list of potential harmless interferents (butter, fuel oil, hand cream, olive oil, …), all of them in the form of fingerprints deposited on the surfaces of objects for courier services, has been carried out. When LIBS information is processed through a multi-stage architecture algorithm built from a suitable combination of 3 learning classifiers, an unknown fingerprint may be labeled into a particular class. Neural network classifiers trained by the *Levenberg–Marquardt* rule were decided within *3D* scatter plots projected onto the subspace of the most useful features extracted from the LIBS spectra. Experimental results demonstrate that the presented algorithm sorts fingerprints according to their hazardous character, although its spectral information is virtually identical in appearance, with rates of false negatives and false positives not beyond of 10%. These reported achievements mean a step forward in the technology readiness level of LIBS for this complex application related to defense, homeland security and force protection.

* Corresponding author. Tel.: +34 952 13 1881; fax: +34 952 13 2000.
E-mail address: laserna@uma.es (J.J. Laserna).

0039-9140/$ - see front matter © 2013 Elsevier B.V. All rights reserved.

http://dx.doi.org/10.1016/j.talanta.2013.02.026

CONCLUSIONS

Investigations within the present Doctoral Thesis have been devoted to elucidate several questions raised on laser-induced breakdown spectroscopy of molecular solids. In turn, the ability of this spectroscopic technique to solve analytical problems in different application fields involving organic materials has been exploited. This section summarizes the most relevant conclusions drawn from this research work. Some future avenues for work in this area are also suggested.

In particular, the appraisal of the studies covering **fundamental aspects about laser-induced plasmas of organics** leads to the following conclusions:

❖ Findings herein have demonstrated that the chemical structure of a molecular solid and, consequently, its properties –aromaticity, presence of inductive and resonance effects as well as geometric and steric factors–, is one of the cornerstones of its emission final response. Notably, these properties have proved to have an special influence on the CN-to-C_2 signals intensity ratio that reflects the degree of atomization in connection with the partial fragmentation of the compound when breaks. That is, a high value of the CN-to-C_2 ratio indicates a large atomization of the molecules, whereas a low value suggests the release of variably sized fragments during their rupture.

❖ An in-depth analysis of emission signals from plasmas in air at atmospheric pressure of a wide set of organics with a variant elementary composition and some structural particularities has allowed unveiling the dominant formation pathways of different diatomic species –CN, C_2, NH, CH and OH.

❖ The detailed examination of the spectral features from plasmas of organics has also allowed inferring their relationships with the molecular structure of the ablated compounds. It has been proved that such connections are hardly identified and may be distorted because of a severe atomization of the target or by plasma-atmosphere interactions; phenomena mainly occurring when nanosecond laser pulses are used for targets ablation.

❖ Findings have corroborated that changing operational parameters like the laser pulse duration severely affects optical emission responses from plasmas of organics. Research has revealed that *fs*-LIBS data manifest a correspondence with the molecular structure of organic compounds better than those gathered from *ns*-LIBS. The lesser atomization of molecules, the preferential direct release of diatomic species, as well as the lower interference of the surrounding atmosphere have been judged as the causes responsible of this coherence when using ultrashort laser pulses. Hence, results herein dictate that *fs*-LIBS may provide a larger selectivity than conventional *ns*-LIBS to the analysis and identification of organic targets.

❖ To summarize, findings from this research throw more light to the complex chemistry involving laser-induced plasma spectroscopy of organics and anticipate a future usefulness of molecular emissions as diagnostic tool in different analytical applications with an improved selectivity.

On the other hand, regarding on the **application of LIBS to the characterization of carbon-based nanosized materials and to the recognition of explosive residues** the main conclusions extracted from the research performed during this Doctoral Thesis are outlined as follows:

❖ The choosing of appropriate operational conditions for both the laser ablation process and the emission signal collection, has shown to allow differentiating graphitic lattices with different stacking and carbon bonding nature because of the different temporal behavior revealed by their optical responses, mainly that of molecular emissions CN and C_2.

❖ The combination of LIBS data with advanced chemometric strategies like the machine learning methods has demonstrated to be an accurate analytical tool for the recognition of explosive residues left over surfaces of different nature. Results reached suggest that LIBS sensors may become a valuable tool to be used in applications related to defense and homeland security in order to anticipate and respond to potential terrorist attacks.

❖ The most informative spectral features that are extracted to build the classification algorithms depend significantly on the nature not only of the residues but also of the supports where those may be located. Although any possibility of designing a universal algorithm capable of effectively meeting all expected scenarios is still far from being achieved; the rigorous implementation of particular strategies has proven its effectiveness on solving well-defined situations.

❖ Although specific classifiers need to be designed, constructed, and tested, findings here have corroborated the goodness of this sensing control approach to identify explosive residues at fingerprint level regardless the nature of the supports.

❖ Finally, the chemometric approach based on the use of classifiers has also proved to be useful when facing to a much more complex identification process. A sequential evaluation of LIBS information into a decision tree involving specific classifiers has demonstrated an accurate recognition between a broad set of residues of a very different nature. In summary, a solution that allows to better exploit the ability of LIBS sensors.

❖ It must be pointed out that despite the inherent limitations of LIBS, principally related to its low selectivity because of its multielemental character, its combination with advanced chemometric tools not only minimizes its shortcomings, but also places it at the forefront of analytical techniques intended to security and defense applications.

FUTURE PROSPECTS

Despite that investigations performed have allowed to discover critical aspects in laser ablation and spectroscopy of molecular solids, further work needs to be done to disclose more information to this matter. As an example, to improve knowledge on the influence of the molecular structure on the emission spectrum and to corroborate the conclusions drawn here, a broader database of organic compounds should be assessed. In the light of the results obtained from the analysis of deuterated organic compounds, the examination of molecular emissions from plasmas of molecular solids labeled with other isotopes (e.g. ^{13}C-, ^{15}N-, ^{17}O-) may reveal much more faithful information on the formation routes of diatomic species as well as on potential connections between the optical emissions and the molecular structures. Furthermore, this same approach also may open a new window to LIBS on its application as a valuable tool for isotope ratios determination.

On the other hand, experimental findings have suggested that the analysis of molecular solids by LIBS is benefited from the improved selectivity provided by the fs excitation regime. In such a way, the action of ultrashort laser pulses to enhance the analytical potential of LIBS on the recognition, identification, characterization, and even quantification of different organic compounds – explosives, polymers, drugs…– in several application areas should be critically evaluated.

Finally, any research revealing further understanding about the influence of operational parameters –features of the laser pulses, focusing conditions, surrounding atmosphere…– into the chemistry of laser-induced organic plasmas are also welcome investigations for contributing to develop future applications of LIBS.